

https://dspace.org/

Treatment of acid mine drainage using silica sodalite infused polysulfone composite membrane

Ntshangase, Nobuhle C

2021

https://hdl.handle.net/10539/32965

Downloaded from a DSpace repository. https://dspace.org/



Treatment of Acid Mine Drainage Using Silica Sodalite Infused Polysulfone Composite Membrane

MSc RESEARCH

Prepared by

Nobuhle C. Ntshangase

(876791)

A dissertation submitted to the Faculty of Engineering and the Built Environment, University of the Witwatersrand, Johannesburg, in fulfilment of the requirements for the degree of Master of Science in Engineering.

Supervisor: Prof M.O Daramola

30 July, 2021

Declaration

I, Nobuhle Ntshangase, solemnly declare that this dissertation is my unaided work. It is being submitted for the degree of Master of Science in Engineering at the University of the Witwatersrand Johannesburg, South Africa. It has not been submitted before for any other degree or examination at any other university.

_____ 30th Day of July, 2021

Nobuhle Cecilia Ntshangase Date

Abstract

Water contamination by Acid Mine Drainage (AMD) has been a challenge in the mining and water treatment industry. This is due to the acidity, alkalinity, high salinity, conductivity and heavy metal toxicity associated with AMD contaminated water. The quality of affected water bodies has negative impacts on the agricultural land, aquatic ecosystem, and on the health of nearby communities. Studies have been conducted on the treatment of AMD using different methods, but there is currently no successful method which has the required combination of scale, resources, affordability, and performance.

Conventional treatment methods which have been explored in the treatment of AMD include but are not limited to wetlands, limestone drains, ion exchange, absorption/adsorption, density sludge plants and membranes. The application of some of these methods is limited by economic viability, effectiveness, and time consuming or sludge production. Membrane technology has drawn the interest of many researchers because of its flexibility, efficiency, selectivity, and reliability. The incorporation of nanoparticles into membranes have improved their mechanical properties and surface chemistry resulting in better performing membranes. Nanoparticles like carbon nanotubes, chitosan, and zeolites have been explored on the treatment of wastewater.

Hydroxy sodalite (HSOD) and silica sodalite (SSOD) are types of zeolites which are explored in this study for the treatment of AMD. HSOD and SSOD synthesized by hydrothermal synthesis and topotactic conversion, respectively, were successfully employed in composite polysulfone (Psf) membrane for the treatment of AMD. SEM analysis revealed that synthesized HSOD nanoparticles possess a thread-ball like morphology with a touch of cubic structures while textural properties show a BET pore volume and surface area of 0.115 cm^3/g and 201 m^2/g, respectively. The morphology of SSOD nanoparticles shows a plate-like structure similar to that of its mother silicate RUB-15, indicating successful topotactic conversion without

structural collapse. A BET pore volume and surface area of 0.242 cm^3/g and 200 m^2/g was obtained for SSOD. The XRD patterns showed a crystalline structure for all the nanoparticles and it matched to that of simulated patterns from the DIFFRAC.EVA software. The SSOD nanoparticles showed high thermal stability with 6% weight loss when compared to 8% and 19% weight loss from fSSOD and HSOD nanoparticles, respectively, on the TGA. The high weight loss from HSOD confirmed the presence of pore occluded with water molecules as described in literature. SSOD nanoparticles were further functionalized to introduce carboxylic functional groups. The functionalization process was able to preserve the physical and chemical structure of SSOD with a slight decrease in BET surface area and pore volume (i.e. 188 m^2/g for BET area and 0.240 cm^3/g for the pore volume).

The synthesized nanoparticles were infused into the Psf at 5wt.% and 10wt.% loadings (10%HSOD/Psf, 10%SSOD/Psf, 5%HSOD/Psf, 5%SSOD/Psf and 10%fSSOD/Psf) and membranes were formed by phase inversion. The SEM images of membranes loaded with HSOD and SSOD show formation of agglomerates, while SEM image of 10%fSSOD/Psf membrane reveals a uniform dispersion of nanoparticles in the polymer matrix. The successful infusion of nanoparticles into Psf enhanced the membrane thermal stability as Psf had 27% residual while 10%HSOD/Psf, 10%SSOD/Psf, 5%HSOD/Psf and 5%SSOD/Psf membranes had 43%, 33%, 32%, and 28% residuals, respectively, after calcination of up to 800°C. The infusion of nanoparticles was also able to improve the membranes mechanical strength from 67 MPa Young modulus for Psf to a maximum of 92 MPa for 5%HSOD/Psf membrane. Nevertheless, the nanoparticles agglomeration at higher loading reduced the membranes mechanical strength.

The performance of the as-produced membranes was evaluated in the treatment of AMD by investigating the membranes permeability and selectivity. The SSOD infused membranes showed good permeability with 10%SSOD/Psf reaching a maximum pure water flux of 2.1

L/m^2.h while 10%HSOD/Psf membranes showed poor permeability of 0.6 L/m^2.h. The fSSOD loaded membrane had negligible effect on the pure water flux as it showed a maximum flux of 2.2 L/m^2. h. HSOD loaded membrane showing poor permeability, was able to produce selectivity above 50% for most metal ions. This indicates a trade-off between membrane selectivity and permeability as the SSOD loaded membranes with high pure water flux presented very poor rejections (2.3-13.3%) which was attributed to nanoparticles agglomeration. Agglomeration reduces the quality of the membrane as it forms sites of nanoparticles concentration, hence increases the surface pore size of the membranes.

The 10%SSOD/Psf membrane was then selected to be evaluated further by modification of SSOD surface chemistry to fSSOD as it presented good permeability. The 10%fSSOD/Psf membrane presented reduced fouling rate with 78.7% reduction in flux over time while the 10%SSOD/Psf membrane showed 90.8% which is even higher than that of pure Psf (87.7%). Functionalization of the SSOD nanoparticles to fSSOD was also able to enhance the membranes selectivity, with most rejections in the range of 51.5%-74.2%, indicating enhanced nanoparticles dispersion.

The successful coating of the membranes was confirmed by the improved reduction of flux over time. The initial flux of 10%fSSOD/Psf/PVA membranes was 4 L/m^2.h, while that of 10%SSOD/Psf/PVA was 3.5 L/m^2.h. This reduced to 1.1 L/m^2.h for both PVA coated membranes after operating for 3 hours, which translate to 68.2% reduction in flux. This indicated an improved reduction in flux when compared to 90.8%, 87.8% and 78.7% for 10%SSOD/Psf, Psf and 10%fSSOD/Psf membranes, respectively. After cleaning the PVA coated membranes with deionized water, a flux of 3.25 L/m^2.h and 1.95 L/m^2.h was obtained, translating to a flux recovery ratio of 81.3% and 55.5% for 10%fSSOD/Psf/PVA and 10%SSOD/Psf/PVA, respectively. The performance shown by the 10%fSSOD/Psf/PVA membrane shows that this membrane can be applied in the treatment of AMD as it was able to

present good selectivity (>50%), membrane flux (4 $L/m^2.h$), reduced flux decline (68%) and it is able to recover 81% of its initial flux after a simple cleaning process

Acknowledgements

I would like to express the deepest appreciation to my supervisor, Prof Michael Daramola. Without his guidance and persistent help this dissertation would not have been possible. I am extremely grateful to my loving husband Mr Nkosinathi Nyembe for his support, words of encouragement and prayers towards my study.

I would like to thank the University of the Witwatersrand, and the lab technicians form the School of Chemical and Metallurgical Engineering for their support. Members of Sustainable Energy and Environment Research Unit (SEERU) who were always readily available to assist me in this journey. The Council of Scientific and Industrial Research (CSIR) for their financial support.

Last but not least, I would like to thank my family and friend for their social support.

Table of contents

Declaration II

Abstract III

Acknowledgements VII

Table of contents VIII

List of Figures XIII

List of Tables XVI

List of Abbreviations 1

Publication from the study 2

1. Background and Motivation 3

1.1. Introduction 3

1.2. Problem statement 4

1.3. Research aim, questions and objectives 5

1.4. Project scope 6

1.5. References 7

2. Literature review 10

2.1. Introduction 10

2.2. Acid Mine Drainage (AMD) 11

2.2.1. Fundamentals of AMD 11

2.2.2. Acid mine drainage Impacts 14

2.2.3. AMD treatment technologies 15
2.3. Membrane technology 18
2.3.1. Fundamentals of membrane technology 18
2.3.2. Classification of membranes 19
2.3.3. Mixed matrix membranes (MMMs) fundamentals 26
2.3.4. Filler particles for heavy metals removal in wastewater 28
2.3.5. Membranes configuration & flow regime 32
2.3.5. Membranes applications 34
2.5. Membrane fouling 36
2.6. Summary 38
2.7. References 39
3. Materials and Experimental Procedures 47
3.1. Introduction 47
3.2. Materials and equipment 47
3.3. Experimental procedure 49
3.3.1. Synthesis of sodalite nanoparticles 50
3.3.2. Functionalization of SSOD nanoparticles 52
3.3.3. Membrane preparation 52
3.3.4. Membrane coating 53
3.4. Characterization of nanoparticles and membranes 53
3.4.1. Scanning electron microscopy (SEM) 53

3.4.1. Nitrogen physisorption experiment for surface area 53
3.4.2. X-ray diffraction (XRD) 54
3.4.3. Fourier transform infrared (FTIR) 54
3.4.4. Thermo-gravimetric analysis (TGA) 54
3.4.5. Atomic force microscopy (AFM) 55
3.4.6. Porosity and mean pore size 55
3.4.7. Contact angle 55
3.4.8. Mechanical strength (young modulus and tensile strength) 56
3.5. Membrane performance evaluation 56
3.6. References 59
4. Sodalite-Infused Polysulfone Membranes: Characterization and Performance Evaluation 61
4.1. Introduction 61
4.2. Nanoparticles characterization 61
4.2.1. Preparation of sodalite nanoparticles 61
4.2.2. Morphology and textural properties of synthesized nanoparticles 62
4.2.3. Crystallinity and purity of synthesized nanoparticles 64
4.2.4. Thermal behaviour of nanoparticles (TGA) 67
4.3. Membrane characterization 69
4.3.1. Morphology (SEM) and topology of membrane 69
4.3.2. Membrane thermostability (TGA) 72
4.3.3. Porosity, mean pore size and contact angle 74

4.3.4. Mechanical strength (young modulus and tensile strength) 76
4.3.5. Surface chemistry (FTIR) 77
4.4. Performance evaluation of membrane 78
4.4.1. Pure water flux 78
4.4.2. Separation performance 79
4.4.2.1. Membrane flux 79
4.4.2.2. Membrane selectivity 80
4.5. Summary 84
4.6. References 85
5. Functionalized Silica-Sodalite Infused Polysulfone Composite Membrane 90
5.1. Introduction 90
5.2. Experimental 91
5.2.1. Functionalization techniques 91
5.2.2. Characterization of the functionalized nanoparticles 92
5.2.3. Membrane morphology (SEM) and topology (AFM) 96
5.2.4. Mechanical strength of the membranes 98
5.2.5. Membranes hydrophilicity (contact angle and porosity) 99
5.3. Performance evaluation of fSSOD infused membrane 100
5.3.1. Membrane permeability 100
5.3.2. Membrane selectivity 103
5.4. Summary 104

5.5. References 105

6. Investigation of the Fouling Behaviour of Poly(Vinyl Alcohol) Coated Psf/SSOD and Psf/f-SSOD Membranes 109

6.1. Introduction 109

6.2. Membrane coating 110

6.3. Physico-chemical characterization of membrane (SEM & Contact angle) 110

6.4. Performance evaluation of fSSOD/Psf/PVA membrane 112

6.4.1. Membranes selectivity 112

6.4.2. Effects of transmembrane pressure on the selectivity 113

6.4.3. Fouling behaviour of fSSOD/Psf/PVA membrane 114

6.5. Summary 116

References 117

7. Conclusions and Recommendations 120

7.1. Conclusions 120

7.2. Recommendations 122

APPENDIX i

A.1. Water characteristics i

Copyright Permissions iii

List of Figures

Figure 2.1: Classification of membranes (Theresa et al., 2011) 22

Figure 2.2: Schematic presentation of a mixed matrix membranes (Used with permission from Chung et al., 2007).....26

Figure 2.3: β-cage (left) and hydroxyl sodalite framework (right) (Used with permission from Khajavi et al., 2009).....31

Figure 2.4: Representation of feed flow in dead end and cross flow filtration (Used with permission from Zena-Membranes http://www.zena-membranes.cz/images/mgallery/other/Dead%20end%20vs%20cross%20flow%20filtration.jpg) 34

Figure 2.5: Hermia model fouling mechanism (a) pore blocking, (b) standard blocking, (c)intermediate blocking, and (d) complete pore blocking (Used with permission from Choobar et al., 2019) 37

Figure 3.1: Summary of experimental procedure 49

Figure 3.2: Schematic illustration of the synthesis of hydroxy sodalite nanoparticles.....50

Figure 3.3: Schematic illustration of the synthesis of silica sodalite nanoparticles.....51

Figure 3.4: Dead-end filtration cell schematic set-up.....57

Figure 4.1: SEM images of (a) HSOD, (b) RUB-15 and (c) SSOD 63

Figure 4.2: XRD patterns for (a) HSOD and (b) RUB-15 and SSOD nanoparticles 65

Figure 4.3: FTIR spectra of RUB-15, SSOD, and HSOD nanoparticles.....66

Figure 4.4: SSOD and HSOD Thermo gravimetric weight loss analysis 68

Figure 4.5: Cross sectional SEM images of (a) Psf, (b) 5%HSOD/Psf, (c) 5%SSOD/Psf, (d) 10%HSOD/Psf, and 10%SSOD/Psf.....70

Figure 4.6: AFM images of (a) 5%HSOD/Psf, (b) 10%HSOD/Psf, (c) 5%SSOD/Psf and (d) 10%SSOD/Psf.....71

Figure 4.7: Membranes surface roughness evaluation....72
Figure 4.8: Thermogravimetric analysis curve for the sodalite loaded membranes....73
Figure 4.9: Contact angles of sodalite infused polysulfone composite....75
Figure 4.10: Tensile strengths and Young Modulus of the sodalite infused polysulfone membranes....76
Figure 4.11: FTIR spectra of the synthesized membranes....77
Figure 4.12: Membranes pure water flux at different transmembrane pressures....78
Figure 4.13: Water flux from different membranes....80
Figure 4.14: Heavy metal rejection from the different membranes....83
Figure 5.1: SEM images of SSOD (left) and the functionalized SSOD (right) nanoparticles.93
Figure 5.2: FTIR spectra of SSOD and fSSOD nanoparticles....94
Figure 5.3: TG analysis of fSSOD and SSOD nanoparticles....95
Figure 5.4: XRD pattern of SSOD and fSSOD....96
Figure 5.5: SEM cross sectional images 10%SSOD/Psf (left) and 10%fSSOD/Psf (right)....97
Figure 5.6: AFM images of 10%SSOD/Psf (left) and 10%fSSOD/Psf (right)....97
Figure 5.7: Surface roughness measurements of 10%SSOD/Psf and 10%fSSOD/Psf membranes....98
Figure 5.8: Comparison of mechanical strength measures of Psf, 10%fSSOD/Psf and 10%SSOD/Psf....99
Figure 5.9: Membranes contact angle....100
Figure 5.10: Membranes water flux with increasing transmembrane pressure....101
Figure 5.11: Comparison of permeate flux for Psf, 10%fSSOD/Psf and 10%SSOD/Psf membranes....103
Figure 5.12: Metal rejections from Psf, 10%fSSOD/Psf and 10%SSOD/Psf....104

Figure 6.1: Cross sectional images of (a) 10%fSSOD/Psf/PVA and (b) 10%fSSOD/Psf membranes 111
Figure 6.2: Membranes water contact angle (left) and surface roughness measurement (right) 111
Figure 6.3: Mechanical strength of the PVA coated and the uncoated membranes 112
Figure 6.4: Comparison of heavy metal rejection between PVA coated and uncoated membranes 113
Figure 6.5: Heavy metal rejection of PVA coated membranes at different transmembrane pressures (a) 2 bar, (b) 4 bar, and (c) 5 bar 114
Figure 6.6: Membranes flux reduction over time 115
Figure 6.7: Flux recovery ratio of PVA coated membranes 116

List of Tables

Table 2.1: SANS 241 water standards compared to AMD composition from different sources 13

Table 2.2: Classification of AMD treatment technologies (Taylor et al., 2005) 17

Table 2.3: Membrane characterization by pore size (Theresa et al., 2011) 18

Table 2.4: Comparison of the performance of ceramic and polymeric membranes (Daramola et al., 2010; Daramola et al., 2012; Fard, et al., 2018) 19

Table 2.5: Structural categories of membranes (Fard et al., 2018).....20

Table 2.6: Comparison of types of membranes (Theresa et al., 2011; Fard, et al., 2018).....23

Table 2.7: Comparison of common membrane polymers in wastewater treatment (Olaru et al., 2010) 27

Table 3.1: Metal composition of synthetic AMD 57

Table 4.1: BET data of SSOD and HSOD nanoparticles.....64

Table 4.2: Porosity (%) and EWC (%) of the membranes.....74

Table 5.1: Comparison of functionalization methods (grafting and co-condensation) (Sae-ung & Boonamnuayvitaya, 2008; Yokoi et al., 2012; Da'na, 2017).....92

Table 5.2: fSSOD and SSOD BET analysis data.....93

Table 5.3: EWC and porosity.....100

List of Abbreviations

AFM	Atomic Force Microscopy
AMD	Acid mine drainage
BET	Branauer-Emmett-Teller
CA	Cellulose acetate
EC	Electrical conductivity
fSSOD	Functionalized silica sodalite
FTIR	Fourier Transform Infrared spectroscopy
HSOD	Hydroxy sodalite
MF	Microfiltration
MMMs	Mixed matrix membranes
NF	Nano Filtration
PES	Polyethersulfone
Psf	Polysulfone
PVA	Poly(vinyl alcohol)
RO	Reverse osmosis
SEM	Scanning electron microscopy
SOD	Sodalite
SSOD	Silica sodalite
TDS	Total dissolved solids
TEOS	Tetraethyl orthosilicate
TGA	Thermo-gravimetric analysis
TMAOH	Tetramethylammonium hydroxide
UF	Ultrafiltration
XRD	X-ray driffraction

Publication from the study

Nobuhle C. Ntshangase, Olawumi O. Sadare, Michael O. Daramola (2021) Effect of silica sodalite functionalization and PVA coating on performance of sodalite infused PSF membrane during treatment of acid mine drainage, Membranes, 11(5), 315. doi: 10.3390/membranes11050315 (published).

1. Background and Motivation

1.1. Introduction

Water has become scarce in most parts of the world including South Africa due to factors like the ever-changing climate. Water is critical for sustaining ecosystems; it plays a fundamental role in the climate regulation cycle and is also the primary requirement for human and socio-economic development (Masindi et al., 2018). Hence, water sources affected by acid mine drainage (AMD) also known as acid rock drainage has become the focus of most wastewater treatment research to ensure water reclamation. AMD is characterised by high concentrations of sulphates, low pH, high salinity, and high heavy metal toxicity (Moodley et al., 2018). The challenge with AMD is that it is a threat to surface water and underground water quality.

Methods to prevent AMD formation have proven not to be practical, hence research on treatment methods instead of prevention has expanded over the years (Moodley et al., 2018). It is understood that AMD problems are unique for each case since they depend on the source of pollution and other environmental factors, hence there is no distinctive technology which applies to all cases. Treatment methods are classified in three mechanisms which are physical, chemical, and biological, these methods are further classified as either active or passive treatment methods (Taylor et al., 2005). According to Kefeni et al (2017), passive methods are more appropriate for application in abondoned mines as they have a potential of low operational cost and maintenance. They are usually less effective than active methods and they require longer process time for effective remediation of AMD. Some of the passive methods that are used to treat AMD include wetlands, permeable reactive barriers and chemical neutralising agents while active methods include ion exchange and membranes amongst others (Masindi et al., 2018).

More research has been focused on membrane technology for the treatment of industrial water because of its effectiveness, simplicity, energy saving and low costs (Daramola et al., 2015). According to Fard et al (2018), recent financial reports indicated that the global demand for membranes and membrane modules reached 15.6 million USD and is expected to grow annually by 8% in the future. This implies that membrane technology is becoming more competitive, hence more effort must be applied on the development and improvement of membranes to meet market demand.

Nanoparticles have been incorporated in conventional membranes (ceramic and polymeric) to improve the performance of the membranes. These nanotechnology-based membranes include mixed matrix membranes (MMMs) that are infused with zeolite material within the polymer membrane (Theresa et al., 2011). MMMs have the advantage of reducing plant footprint, reduced sludge production, enhanced flexibility and lower energy consumption (Daramola et al., 2015).

1.2. Problem statement

The performance and commercialisation of membranes is limited by fouling, and the trade-off between selectivity and membrane flux. Membrane fouling is described as a process where particles in the feed are deposited on the membrane surface resulting into the reduction of active pores (Abbasi et al., 2012). In AMD treatment, this fouling is due to the susceptibility of membrane systems to low pH and exposure to dissolved solids. This results in additional cost of maintenance of the membrane. Another challenge in membrane application has been the trade-off between selectivity and flux of the membrane. To obtain high flux, the membrane must be more porous of which in turn will allow unwanted particles to pass through, and this will decrease the selectivity of the membrane (Werber et al., 2016). As a result, further investigations are required to improve these aspects of the membrane system.

Recent study on the application of sodalite-infused polymer membrane for AMD treatment was first reported by Daramola et al. (2015). The authors reported metal rejections ranging from 1-57% for divalent metal ions (e.g. Mn^{2+}, Pb^{2+}, Cu^{2+}, Mg^{2+}) at different hydroxy sodalite (HSOD) loadings. A maximum rejection of 57% for Pb^{2+} was obtained at maximum HSOD loading (15 wt.%). The authors attributed this limited performance to the micropores of the sodalite that they have not been used effectively because guest species (water molecules) which were acquired during hydrothermal synthesis were trapped in the cages. This project is expected to overcome the presence of the water molecules acquired during hydrothermal synthesis of HSOD by using SSOD which can be synthesized by topotactic conversion. According to Moteki et al. (2011), SSOD synthesised by topotactic conversion has accessible micropores, which allow very tiny molecules to pass through, thereby enhancing the selectivity of the membrane. It is well understood that this proposed sodalite has less hydrophilicity when compared to HSOD, hence functionalization by the condensation method of the SSOD crystals is to be introduced to enhance the reactivity of SSOD. To limit membrane fouling, polyvinyl alcohol (PVA) is to be coated over the SSOD infused polysulfone (Psf) membrane by the dip coating method as PVA is said to have anti-fouling property (Bolto et al., 2009).

1.3. Research aim, questions and objectives

The aim of this project is to develop and evaluate a silica sodalite infused polysulfone composite membrane for AMD treatment. To achieve this aim, the underlisted questions were considered:

i. What will be the separation performance of SSOD infused Psf (SSOD/Psf) membrane during AMD treatment?

ii. Can the functionalization of SSOD crystals enhance the dispersion of the SSOD particles in polysulfone, and consequently the membrane performance?

iii. Will coating the SSOD infused Psf membrane with a PVA layer enhance hydrophilicity and anti-fouling property?

iv. What will be the fouling behaviour of the membranes in (ii) and (iii)?

To answer the above questions, the following objectives were considered:

i. Fabricate SSOD/Psf membrane and HSOD/Psf membrane using similar conditions and evaluate their performance during AMD treatment.

ii. Functionalize the SSOD particles, fabricate functionalized SSOD/Psf membranes and evaluate its performance during AMD treatment

iii. Fabricate SSOD/Psf membrane, coat it with PVA and evaluate its performance during AMD treatment.

iv. Investigate the fouling behaviours of the SSOD/Psf/PVA and fSSOD/Psf/PVA membranes during AMD treatment.

1.4. Project scope

As per the objectives, the planned activities of this project are as follows:

i. Fabricate SSOD/Psf membrane and HSOD/Psf membrane

   a. Synthesize HSOD nanoparticles by hydrothermal synthesis.

   b. Synthesize SSOD nanoparticles by topotactic conversion method.

   c. Infuse HSOD into Psf in 5 and 10 wt.% to form HSOD/Psf membranes.

   d. Infuse SSOD into Psf in 5, 10 and 15 wt.% to form SSOD/Psf membranes.

   e. Compare HSOD/Psf and SSOD/Psf membrane performance based on metal rejection and membrane flux using synthetic AMD.

f. Select the best performing membrane.

ii. Functionalize the SSOD particles using the post grafting method.

a. Infuse the functionalized SSOD (fSSOD) particles into Psf in loadings corresponding to the best performing SSOD/Psf or HSOD/Psf membrane.

b. Compare this membrane performance with that of the selected membrane in (i) using synthetic AMD.

iii. Coat membranes with PVA.

a. Coat the best performing SSOD/Psf and fSSOD/Psf membranes with PVA

b. Compare their performance based on water flux and heavy metal rejection using synthetic AMD.

c. Evaluate the fouling behaviour and the effectiveness of a simple membrane cleaning method.

1.5. References

1. Abbasi, M., Sebzari, M. R., Salahi, A., & Mirza, B. (2012). Modelling of Membrane Fouling and Flux Decline in Microfiltration of Oily Wastewater using Ceramic Membranes. *Chemical Engineering Communications*, 78-93. doi:10.1080/00986445.2011.570391

2. Bolto, B., Tran, T., Hoang, M., & Xie, Z. (2009). Crosslinked Poly(Vinyl Alcohol) Membranes. *Progress in Polymer Science*, 969–981. doi:10.1016/j.progpolymsci.2009.05.003

3. Daramola, M. O., Silinda, B., Masondo, S., & Oluwasina, O. O. (2015). Polyethersulphone-Sodalite (PES-SOD) Mixed-Matrix Membranes: Prospects for Acid

Mine Drainage (AMD) Treatment. *Journal of the Southern African Institute of Mining and Metallurgy, 115*(12), 1221-1228. doi:10.17159/2411-9717/2015/v115n12a11

4. Fard, A. K., McKay, G., Buekenhoudt, A., Sulaiti, H. A., Motmans, F., & Atieh, M. (2018). Inorganic Membranes: Preparation and Application for Water Treatment and Desalinaton. *Materials, 11*(74). doi:10.3390/ma11010074

5. Kefeni, K. K., Msagati, T. A., & Mamba, B. B. (2017). Acid Mine Drainage: Prevention, Treatment Options, and Resource Recovery: A Review. *Journal of Cleaner Production, 151*, 475-493. doi:10.1016/j.jclepro.2017.03.082

6. Masindi, V., Chatzisymeon, E., Kortidis, I., & Foteinis, S. (2018). Assessing the Sustainability of Acid Mine Drainage (AMD) Treatment in South Africa. *Science of the Total Environment, 635*, 793-802. doi:10.1016/j.scitotenv.2018.04.108

7. Moodley, I., Sheridan, C. M., Kappelmeyer, U., & Akcil, A. (2018). Environmentally Sustainable Acid Mine Drainage Remediation: Research Developments with a Focus on Waste/By-Products. *Minerals Engineering*, 207-220. doi:10.1016/j.mineng.2017.08.008

8. Moteki, T., Chaikittsilp, W., Sakamoto, Y., Shimojima, A., & Okubo, T. (2011). Role of Acidic Pre-treatment of Layered Silicate RUB-15 in its Topotactic Conversion into Pure Silica Sodalite. *Chemistry of Materials*, 3564–3570. doi:10.1021/cm201480x

9. Taylor, J., Pape, S., & Murphy, N. (2005). A Summary of Passive and Active Treatment Technologies for Acid and Metalliferous Drainage (AMD). *Fifth Australian Workshop on Acid Drainage*. [PDF]Fremantle, Western Australia: Earth Systems Pty Ltd. Retrieved from https://earthsystems.com.au/wp-content/uploads/2012/02/AMD_Treatment_Technologies_06.pdf

10. Theresa, M., Pendergast, M., & Hoek, E. M. (2011). A Review of Water Treatment Membrane Nanotechnologies. *Energy and Environmental Science* (6), 1946-1971. doi:10.1039/C0EE00541J

11. Werber, J. R., Deshmukh, A., & Elimelech, M. (2016). The Critical Need for Increased Selectivity, Not Increased Water Permeability, for Desalination Membranes. *Environmental Science and Technology*, 112−120. doi:10.1021/acs.estlett.6b00050

2. Literature review

2.1. Introduction

The South African economy is very driven by both the mining and agricultural sectors amongst others. These industries interfere with each other in their water usage as the pollution of water by mining activities negatively impacts on the production of the agricultural sector. When raw mine water containing sulphide, minerals is exposed to atmospheric oxygen and water-borne bacteria they form AMD (Masindi et al., 2018). The sulphide minerals are oxidised and produce sulphuric acid which then leaches other metals from the rocks (Daramola et al., 2015). This problem occurs in both operating and abandoned sites which may be underground or open pit mines. This impacts underground and surface water sources and the terrestrial land, hence the agricultural activities.

AMD characteristics vary from one source to another because of environmental factors and source characteristics, hence there is no defined treatment methods that fits all AMD cases. AMD is treated by passive or active methods. Passive treatment includes biological treatment by constructed wetlands, chemical treatment by limestone drains and sulphate reducing bioreactor (Kefeni et al., 2017). Active treatment includes techniques like adsorption, ion exchange, membrane technology, and the use of alkaline chemicals to precipitate metals (Kefeni et al., 2017). Passive methods are mostly associated with treating AMD from abandoned mines as they are effective in treating AMD with low acidity, low flowrate, and low acidity loads (Taylor et al., 2005). Although Ion exchange and adsorption technologies have proven to be effective, their application is limited by their economic viability (Taylor et al., 2005).

This Chapter will look at the formation of AMD, its impact and frequently used treatment technologies. It will further look at membrane technology and its application in industry. The challenges in the membrane technology application will also be outlined.

2.2. Acid Mine Drainage (AMD)

2.2.1. Fundamentals of AMD

AMD is formed in both gold and coal mines when sulphide bearing minerals are exposed to oxidizing bacteria, water, and oxygen (Moodley et al., 2018). This is a common problem mostly at abandoned mines where the water collecting inside the mine is no longer being pumped to the surface. AMD is commonly explained by the oxidation of pyrite since it is the most common sulphide in mining rocks. There are four well known reactions associated with the formation of AMD (Moodley et al., 2018; Tutu et al., 2008; Masindi et al., 2018; Kefeni et al., 2017).

$$FeS_2 + \frac{7}{2}O_2 + H_2O \rightarrow Fe^{2+} + 2SO_4^{2-} + 2H^+ \quad (2.1)$$

$$Fe^{2+} + \frac{1}{4}O_2 + H^+ \rightarrow Fe^{3+} + \frac{1}{2}H_2O \quad (2.2)$$

$$Fe^{3+} + 3H_2O \rightarrow Fe(OH)_3 + 3H^+ \quad (2.3)$$

$$FeS_2 + 14Fe^{3+} + 8H_2O \rightarrow 15Fe^{2+} + 2SO_4^{2-} + 16H^+ \quad (2.4)$$

Pyrite is oxidised to ferrous iron and sulphate when exposed to water and oxygen (2.1). In the presence of iron-oxidizing bacteria, the formed ferrous iron is oxidised to ferric iron (2.2), according to Taylor et al (2005), this reaction is rate-determining as the reaction rate is pH dependent and proceeds slowly under acidic conditions. When the pH of the affected water is increased through contact with fresh water (pH>3.5), the formed ferric iron reacts with water and forms ferric hydroxide (2.3) which is the orange-red precipitate also called the ‘yellow

boy' in affected water. The acidity increases the mobility and toxicity of metals, and the iron hydroxide precipitation produces co-precipitation and adsorption of metals in solution (Tutu et al., 2008). If the ferric iron is in excess and pH is lower (pH<3.5) it reduces the pyrite to ferrous iron and sulphuric acid (2.4) which results in the water being acidic. The overall reaction (2.5) from reaction (2.1), (2.3), and (2.4) results in sulphuric acid and ferric hydroxide being produced, releasing high acidity into the water (Moodley et al., 2018).

$$FeS_2 + 3.5O_2 + 3.5H_2O \leftrightarrow FeOH_3 + 2SO_4^{2-} + 4H^+ \quad (2.5)$$

AMD water characteristics differ according to their source as shown in Table 2.1. They generally have low pH and alkalinity, and high salinity, acidity, conductivity and heavy metal toxicity (Moodley et al., 2018; Taylor et al., 2005) (terms defined in Appendix A.1). Taylor et al (2005) describes five factors which affect the rate of oxidation of pyrite, namely:

- Morphology of the sulphides
- Oxygen concentration
- Wetting and drying cycles
- Presence of bacteria and acid consuming material
- Geological (thermal and tectonic) history of the sulphides

Table 2.1: SANS 241 water standards compared to AMD composition from different sources

Parameter	SANS 241 (Masindi et al., 2017)	Coal mine AMD (Westholm et al., 2014)	Coal mine AMD (Westholm et al., 2014)	Coal mine AMD (Masindi et al., 2017)	Coal mine AMD (Masindi et al., 2018)	Unkown AMD (Daramola et al., 2015)	Middleburg abandoned coal mine AMD (Bell et al., 2001)	Witbank abandoned coal mine AMD (Bell et al., 2001)
pH	≥5 to ≤9.7	2.8	2.4	2	2	2.28	2.8	2.7
EC (mS/m [25°C])	300			-	600	-	348	396
TDS	-			-	3500	-	4691	3201
Hardness (mg/L) as CaCO	≤650			3131	2000	-	296	134
Mg (mg/L)	≤400			480	300	848.8	160	15
Mn (mg/L)	≤2	96	235	125	75	51.58	29	5
Na (mg/L)	≤200			30	≤0.01	-	223	688
SO_4^- (mg/L)	≤500	25 000	12 200	18 000	30 000	-	2337	1108
Cu (mg/L)	≤2000	7.1		0.05	-	15.98	-	-
Pb (mg/L)	≤10	0.46		0.05	-	4.3	-	-
Zn (mg/L)	≤5	16	80	0.2	-	86.47	-	-
Al (mg/L)	≤1	450	1110	500	-	1370	58	84
Fe (mg/L)	≤2	6600	6400	6000	-	833	196	111
Ca (mg/L)	≤300			500	-	-	297	41

2.2.2. Acid mine drainage Impacts

The economy of the mining industry is affected by the AMD problem as AMD corrodes the infrastructure and equipment, it limits the recycling of water in the process, and the mines also incur costs associated with overseeing the problem once the mine is closed. The concern for AMD arises from the high concentration of heavy metals as they pose danger to the surrounding environment and human due to their bioaccumulation and non-biodegradability. According to Kefeni et al. (2017), if AMD is not managed properly it causes considerable environmental degradation, water and soil contamination, severe health impact on nearby communities, biodiversity and aquatic ecosystem loss.

Water is critical for sustaining ecosystems, it plays a fundamental role in the climate regulation cycle and is also a primary requirement for human survival and socioeconomic development (Masindi et al., 2018). Since there are rural areas in South Africa which still depend on river water, contamination of water sources can also be dangerous to human as heavy metals are known to be carcinogenetic and cannot be decomposed or biodegraded. A large portion of coalfields lie in the upper catchment of the Vaal River which is the most important river in South Africa (McCarthy, 2011). Downstream water sources usage becomes limited as metals can be mobilised to hazardous levels hence affecting the aquatic ecosystem and human health. If the mining activities are in the proximity of human settlements, municipal waters can be contaminated resulting in potential consumption by human. Consumption of Fe^{3+} as low as 60 mg/kg of body weight is said to be fatal, with an excessive iron in the blood causing damage to the cells of gastrointestinal tract (Habiba et al., 2017). The intake of copper leads to necrotic changes in the liver and kidney, mucosal irritation, widespread capillary damage, depression, gastrointestinal irritation and lung cancer (Abu-Saied, et al., 2017).

In some parts of the world like Northeast India, the impact of AMD from coal mining was investigated. Choudhury et al (2017) found that the AMD has acidified the soil, contaminated it with heavy metals and left the soil depleted in potassium and zinc. This resulted in the affected soil being less productive with an average yield of 1.21 tonne/hectare while the unaffected soil had an average yield of 3.2 tonne/hectare. In a study by Bell et al (2001) on abandoned coal mines in Witbank South Africa, they found that the AMD affected land of about 3 hectares had no vegetation due to the low pH which restricted respiration and root uptake of mineral salts and water for the plants. These scenarios explain the negative impacts of AMD in our environment.

2.2.3. AMD treatment technologies

There is currently no successful method which has the required combination of scale, resources and affordability to deal with the AMD problem (Lopez et al., 2018). It is important to determine the end use of the treated water in selecting a treatment option as this will guide on the quality required. Most research focuses on the development of a cost effective and efficient treatment technology, but according to Taylor et al (2005), an appropriate treatment method must be based on the acidity, flow rate, and acidity load of the AMD to be treated.

Treatment methods are classified into three mechanisms which are physical, chemical and biological. These methods are further classified as passive, active, and integrated methods. Passive methods include wetlands and chemical treatment by limestone drains and sulphate reducing bioreactor where little resource input is required once in operation. Active treatment methods include techniques like adsorption, ion exchange, membrane technology, and the use of alkaline chemicals to precipitate metals (Kefeni et al., 2017). Lastly the integrated treatment methods entail the combination of both passive and active. The types of practiced treatment methods as studied by Taylor et al. (2005) are outlined in Table 2.2. According to Kefeni et al.

(2017), passive methods are more appropriate for application in abandoned mines as they have a potential of low operational cost and maintenance. They are usually less effective than active methods and they require longer process time for effective remediation of AMD. Passive treatment methods are also said to be effective in AMD with low acidity (<800 mg $CaCO_3$/L), low flowrates (< 50 L/s), and low acidity loads (<150 kg $CaCO_3$/day). While active treatment systems have higher limits of acidity (<10 000 mg $CaCO_3$/L) and acidity loads (<50 000 kg $CaCO_3$/day), their application is limited by their economic viability (Taylor et al., 2005).

Table 2.2: Classification of AMD treatment technologies (Taylor et al., 2005)

Treatment technology	Description
Passive methods	
Anaerobic wetland systems	Organic substrate strips the oxygen out of the AMD resulting in sulphate reduction by bacterial activity. The sulphate reducing bacteria activity generate alkalinity. Metal concentrations are decreased by precipitation of metal sulfides in the reduced organic layer of the wetland.
Aerobic wetland systems	Accepts alkaline water from an external source and provide residence time and aeration to allow certain metals whose solubility is dependent on the redox state of the water to precipitate. These precipitates are then kept at the surface of the plants, in the wetland or carried downstream.
Anoxic limestone drains (ALD)	Gentle slopes layered by limestone aggregate. Passing AMD through these layers raises the pH and alkalinity of the water. Aerobic wetlands are usually installed at the outflow. These are said to be more suitable for coal mine AMD.
Limestone diversion wells	A man-made well is fitted with crushed limestone aggregate. Part of the AMD stream is diverted to the well where it causes a partial grinding of the limestone. The limestone small particles are carried by the exiting stream to the concentrated AMD, resulting in the neutralisation of the AMD stream.
Permeable reactive barrier	Reactive materials are buried which promote the sulphate reduction when AMD is passed through them. The sulphide precipitates progressively fill the pores of the barrier
Reducing and alkalinity producing system	Construction is different but generally they contain a mixture of limestone and organic matter to reduce the sulphates and generate alkaline.
Active methods	
Ion exchange/Absorption or adsorption/ flocculation and filtration	Particles are separated according to their molecule charge, size, and/or physical properties like density. These methods are known to be effective but have limited use due to their economic infeasibility.
Density sludge plants	A neutralising agent thick aqueous solution is used to neutralise the AMD. This mixture is then sent to a clarifier or for flocculation where it is then separated by density, with the heavy metals remaining in the sludge.

2.3. Membrane technology

2.3.1. Fundamentals of membrane technology

Interest on membrane technology as a viable method of treating wastewater has increased because of its efficiency, selectivity, reliability, and adaptation to changes of flow volume (Daramola et al., 2015). Membranes are defined as selective barriers which allow target materials to pass through while others are retained. The separation of the particles in membranes occur by selectively sieving, adsorbing and exchanging molecules, particles and ions respectively (Julbe, 2007). These membranes are categorized according to the pore size as shown in Table 2.3. Low pressure membranes are fabricated to have a specific pore size of which only molecules of a specific molecular size can pass through by diffusion and this desired selected solution is called the permeate. Molecules having a size greater than that of the membrane pores are retained on the other side of the barrier and are called the retentate. Whereas separation in high pressure membrane depends on the difference in solubility between the solvent and the solute in membranes (Aly, 2015).

Table 2.3: Membrane characterization by pore size (Theresa et al., 2011)

Membrane type	**Pore size range (nm)**
Microfiltration (MF)	50 - 500
Ultrafiltration (UF)	2 - 50
Nanofiltration (NF)	≤2
Reverse osmosis (RO)	0.3 - 0.6

2.3.2. Classification of membranes

Membranes are conventionally divided into organic (polymeric) and inorganic (ceramic) depending on the material of fabrication (general performance comparison is given in Table 2.4. Organic membranes have an asymmetric structure with an open porous support layer beneath a relatively thin, less porous skin layer of the same material while inorganic membranes are with a dense region close to the support structure (Theresa et al., 2011).

Table 2.4: Comparison of the performance of ceramic and polymeric membranes (Daramola et al., 2010; Daramola et al., 2012; Fard, et al., 2018)

Ceramic membranes	**Polymeric membranes**
Do not swell	Do swell
Possibility of uniform, molecular-sized pores allowing for molecular sieving	Do not have uniform molecular sized pores
Chemically resistant to solvents and low pH	Not chemically stable, denatured at low pH
Thermally stable	Not thermally stable, denatured at high temperature
High cost of production	Lower cost of production
More brittle	Less brittle

Membranes are further categorised in terms of their structure, they can be anisotropic (asymmetric) or isotropic (symmetric), and these structures are compared in Table 2.5. Anisotropic membranes have a heterogeneous composition both in their chemical composition as well as in their structure while isotropic membranes have a homogenous composition where their structure is made up of a single material (Fard et al., 2018).

Table 2.5: Structural categories of membranes (Fard et al., 2018)

Membrane structure	**Characteristics**
Anisotropic	
Phase-separation membrane	They have homogenous chemical composition. Structure, pore size, porosity, and thickness across the membrane vary from one point to another.
Composite membrane (e.g thin film)	They have heterogeneous chemical composition and structure. Solute transport is governed by the thin film surface layer and its thickness, porosity, pore size etc.
Isotropic	
Macro-separation membrane (sieving membranes)	They filter out solutes based on their sizes and the size of the membrane pores.
Non-porous dense film membrane	Transport of solute occurs by applying a force such as pressure, concentration gradient, or electric field gradient. They are diffusion driven based on the concentration difference on each side of the membrane.
Electrically charged membrane (Ion exchange membranes)	Have surfaces enhanced by negative or positive ions. The transport mechanism is governed by the ion concentration and charge density of the solute.

The conventional membrane technology has evolved to incorporate nanoparticles to develop nanotechnology-based membranes, with the advancement of technology. The classification of membrane technology is outlined in Figure 2.1 and their characteristics are compared in Table 2.6. Nanotechnology based membranes have been developed over the years to enhance water

permeability and solute selectivity in wastewater treatment membranes. They are divided into nanostructured ceramic membranes, inorganic membranes, and biologically inspired membranes while conventional membranes are divided into organic and inorganic (Theresa et al., 2011).

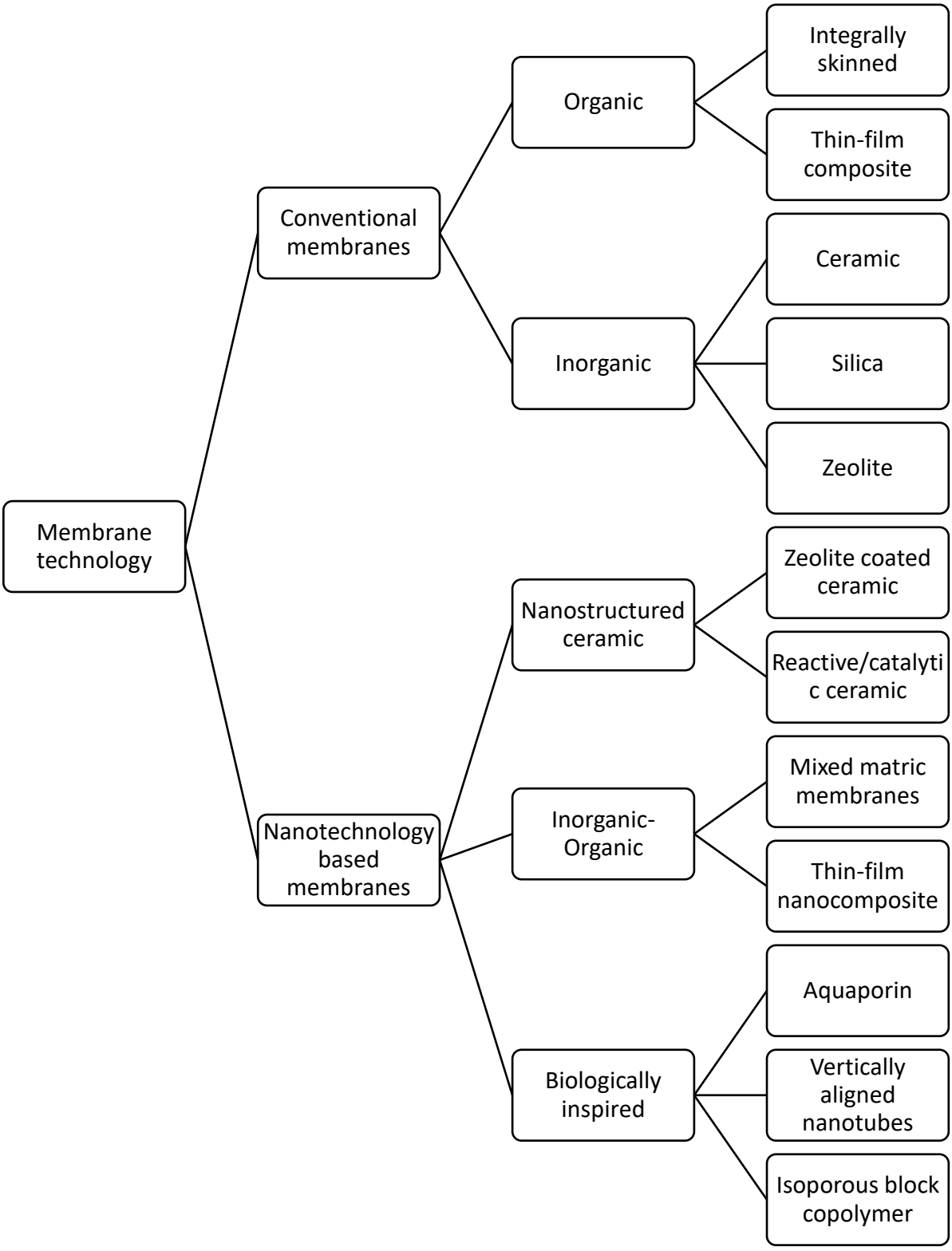


Figure 2.1: Classification of membranes (Theresa et al., 2011)

Table 2.6: Comparison of types of membranes (Theresa et al., 2011; Fard, et al., 2018)

Type of membrane	Advantages	Disadvantages
Inorganic Mesoporous ceramic	• Enhanced mechanical, thermal and chemical stability. • Suitable for oil/water separation, industrial and hazardous wastewater. • Extended lifetime even under extreme fouling and cleaning conditions.	• Too expensive for large scale e.g. municipal drinking water. • Limited to small industrial applications not suitable for polymeric membranes.
Silica	• High selectivity, temperature resistivity, and chemical resistance. • Less costly	• Structural degradation when exposed to water, resulting in loss of selectivity.
Zeolite	• Excellent thermal and mechanical stability • Good selectivity	• Expensive • Difficult to scale up • Less stable
Organic Integrally skinned (with reference to cellulose acetate (CA))	• Hydrophilic with surfaces having low fouling propensity. • Easy to manufacture and relatively inexpensive.	• Limited temperature range (≤30°C) and pH (4-6). • Chlorine intolerance. • Biodegradable, hence, can be consumed by the growing organisms in biofilms.
Thin-film composite (with reference to polyamide (PA))		• PA is even more less chlorine tolerant.

	• Selective layer and the porous support layer can be independently selected to optimize performance. • High salt selectivity and relatively high-water permeability for RO applications • PA can withstand higher temperatures and pH as compared to CA.	
Nanostructured ceramic Zeolite-coated ceramic	• Mechanical stability under high pressures. • Chemical stability to withstand disinfectants. • Fouling resistance. • Tuneable selectivity	• High manufacturing cost. • Low packing density relative to polymeric membranes
Reactive/catalytic ceramic	• Improved stability. • Enhanced hydrophilicity. • Self-cleaning capability	• Nano-catalyst recovery and regeneration. • Disposal of spent material. • High manufacturing cost. • Low packing density relative to polymeric membranes. • High energy demand for irradiating the surfaces. • Suitable for small scale.
Inorganic-organic Mixed matrix	• Low cost. • Ease of fabrication. • Improved chemical, mechanical and thermal stability. • Increased selectivity.	• Not capable of self-cleaning.
Thin film nano-composite	• Enhanced separation and performance • Reduced fouling and antimicrobial activity • Ease of fine tuning performance with addition of nanoparticles	• Nanoparticles (like zeolite) are expensive.

Biologically inspired Aquaporin	• Increased water permeability. • Full rejection of glucose, glycerol, salt, and urea. -	• Difficulties in attaining large quantities of proteins • Difficulties in producing large areas of membrane material • Complex fabrication.
Vertically aligned nanotube	• Fast mass transport. • Reduced hydraulic driving pressure. • Lower energy cost. • Longer lifetimes because of CNTs mechanical properties.	• Lack of scalability and cost.
Isoporous block copolymer	• Minimal external fields—electrical or shear—will impact the arrangement due to the soft nature. • Simple fabrication • High porosity	• Defects are easily formed. • Low permeability.

2.3.3. Mixed matrix membranes (MMMs) fundamentals

Conventional membranes have been developed to incorporate nanoparticles, creating a new set of membranes called nanotechnology-based membranes which include nanostructured ceramic, inorganic-organic, and biologically inspired membranes. They have been of interest because of their good mechanical properties, economic processability, unique structure of the dispersed inorganic phase, and good surface chemistry (Daramola et al., 2015). The MMMs consist of a polymer material to provide support and structure, and inorganic particles dispersed on the polymer phase to selectively sieve molecules as shown in Figure 2.2.

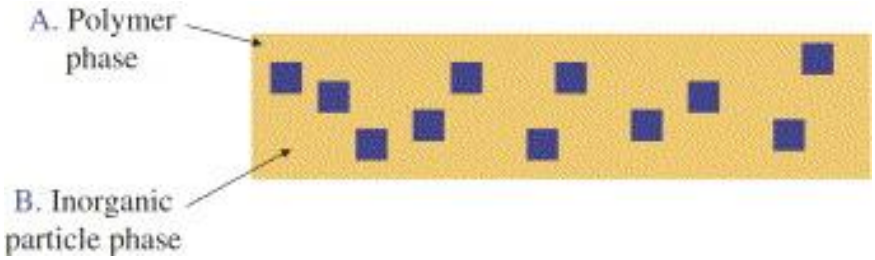


Figure 2.2: Schematic presentation of a mixed matrix membranes (Used with permission from Chung et al., 2007)

Some of the most used polymers in water treatment are cellulose acetate, polyamide and polysulfone as compared in Table 2.7. Several membranes have been fabricated using polysulfone (Psf) and polyethersulfone (PES) because of properties like good chemical resistance, high mechanical strength, easy processing and environmental endurance, tolerance of high temperatures and pH, easy to fabricate, commercially available and inexpensive (Ladewig & Al-Shaeli, 2017).

Table 2.7: Comparison of common membrane polymers in wastewater treatment (Olaru et al., 2010)

Polymer	**Properties**
Polysulfone (Psf)/ Polyethersulfone (PES)	- Applied in MF and UF - No swelling in aqueous solutions - Wide temperature limits (75°C for Psf and 120°C for PES) - Wide pH ranges (1-13) - Easy to fabricate in a wide variety of configurations and modules - Good chemical resistance - Wide range of pore size (10Å- 0.2 μm) - Low pressure limit and hydrophobicity, resulting in membrane fouling
Polyamide (PA)	- Applied in MF, UF, NF &RO - Moderate pH range (4-11) - High adsorption capacities - Resistance to hydrolysis and biological attack - Gradual loss of membrane properties under high temperature and pressure. - Subject to degradation by oxidants and biofouling.
Cellulose acetate (CA)	- Applied in MF, UF, NF, & RO - Nontoxic material - Easily available - Hydrophilic - Wide range of pore size - Narrow temperature limits (0-35°C) - Narrow pH range (3-8) - Susceptible to biodegradation and microbial attack - Gradual loss of membrane properties under high pressure over time.

According to Ladewig and Al-Shaeli (2017) the application of these polymers is limited by their high hydrophobicity which results in severe membrane fouling, leading to reduction in membrane performance and increase in costs of cleaning of the membrane. Nevertheless, Polysulfone and polyethersulfone remain a more practical choice for membrane filtration because of their robustness and ability to withstand strong acids and alkalis (Richards et al., 2012).

2.3.4. Filler particles for heavy metals removal in wastewater

2.4.1. Commonly used filler particles

Membranes have different types of filler materials as they have specific properties that define the separation mechanism and the morphology of the membrane. The material properties are defined by the structural features and chemical and physical nature. They are responsible for the different types of metal removal mechanisms, namely adsorption, ion exchange, sulphate reduction, and precipitation (Westholm et al., 2014). Metal ions can interact with the filler material by adhering to its surface by adsorption which is the most common phenomena in membrane technology.

According to literature, organic materials used in wastewater treatment include polymers, and peat and agricultural waste products while inorganic materials include minerals, rocks and industrial waste products (Westholm et al., 2014). Organic materials like chitin, chitosan, and rice husk are reported in a review paper by Westholm et al. (2014), showing that they are very effective in removing metals from wastewater. They have shown removal efficiencies above 90% for metals like Fe, Zn, Mn, Pb, and Cu at different experimental configurations. Fly ash, limestone, and zeolites are some of the commonly used inorganic materials in wastewater treatment because of their heavy metal removal efficiencies. While

other inorganic materials like limestone are mostly used in passive treatment methods, in membrane technology, zeolites dominate as a filler material.

2.4.2. Zeolites

Over thousands of zeolite materials have been prepared, which corresponds to 174 structural types of zeolites (Yu, 2007). According to (Mabilia et al., 1987), they are used in three commercial applications: catalysis, selective ion exchange, and molecular sieves and sorbents. Zeolites are tridimensional crystalline alluminosillicates constituted by Si and Al tetrahedral linked through bridging oxygen atoms giving rise to the so-called secondary binding units, constituted by rings and prisms of various sizes (Daramola et al., 2010; Daramola et al., 2012). They are said to be generally expressed according to equation 2.6 where *M* is the compensating cation (usually from group I or II) with valence *n*.

$$M_{x/n}[(AlO_2)_x.(SiO_2)_y]zH_2O \qquad (2.6)$$

The properties (hydrophobicity, acidity, adsorbent, catalytic, and ion-exchange) of this material are said to be determined by the Si/Al ratio in the structure. The Si/Al ratio results in a different structure which creates the different types of natural and artificial frameworks of zeolite. Zeolites occur naturally in basaltic rocks or volcanic tuffs, but they are mostly contaminated by other minerals (Jha & Singh, 2016).

In order to overcome the contamination, synthetic zeolites have been introduced as they are more uniform and purer. Zeolites synthesis is affected by the synthesis time, water molar content, zeolite seeds and the Si/Al ratio. In a study by Nabavi et al (2014), they found that when the synthesis time increases the particulate size also increased as this was promoting crystal growth. If zeolite seeds have been used, they should be uniformly small to synthesize uniform defect free zeolites and have high crystallinity to avoid non-zeolitic

pores. They also found that increasing the water molar content, reduced the crystal sizes. Zeolites are known for the below unique properties (Khajavi et al., 2010) [a]:

- High surface area
- Well defined microporosity
- Shape selectivity induced by their uniform pore size
- High hydrothermal stability
- High intrinsic acidity

Sodalite (SOD) is a type of zeolite that has a framework built from what is called a β-cage (Figure 2.3) which are connected through a 4- and 6- rings (Khajavi et al., 2009). This cage is the primary unit of other zeolitic material which differ in arrangement. The 4-rings are too small to allow permeation, hence permeation of water molecules (2.65 Å) can only pass through the 6-ring. The 6-ring is the bridges created by the connected oxygen atoms from each vertex of the cage and create a channel of diameter of 2-10Å, this allows for separation of molecules through molecular sieving (Nabavi et al., 2014; Jha & Singh, 2016). SOD's are characterised as a low silica because they have a Si/Al ratio less than two (Jha & Singh, 2016). This report will only look at the two types of sodalites (hydroxy sodalite and silica sodalite).

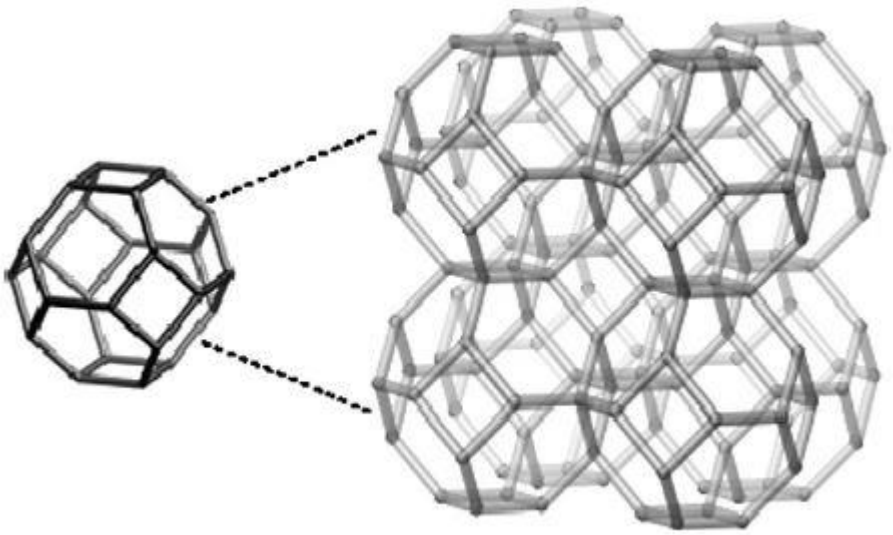


Figure 2.3: β-cage (left) and hydroxyl sodalite framework (right) (Used with permission from Khajavi et al., 2009)

2.3.4.2.1. Hydroxy Sodalite

Hydroxy sodalite (HSOD) is a type of zeolite that has the chemical formula $Na_8[AlSiO_4]_6(OH)_2.nH_2O$ where 0<n≤4 (Khajavi, 2010) [b] .It has been applied in different water separation processes including separation of water/alcohol (Khajavi et al., 2009), water/Pb^{2+} (Bobald et al., 2017), seawater (Khajavi et al., 2010)[a], and acid mine drainage (Daramola et al., 2015). The performance of the zeolite in some of these experiments was satisfactory with 100% methanol rejection, 98.1% rejection of Pb^{2+}, and more than 99.9% on salt rejection. This indicates the capability of HSOD in treating contaminated water.

Daramola et al (2015) varied the loading of HSOD in the polymer and evaluated its rejection and water flux capacity. They found that when the loading is increased, the flux and rejection were also increased. The highest rejected cation was Pb^{2+} with a rejection of 57.44% and the lowest rejected cation was Mn^{2+} with a rejection of 6%. Other cations which were evaluated were Mg^{2+}, Cu^{2+}, and Al^{3+}, which had moderate rejections.

According to the authors, this limited performance is attributed to the occlusion of the sodalite micropores by guest species (water). The guest species are trapped in the cages during hydrothermal synthesis. Moteki et al., (2008) indicated that if the guest species is to be removed, the framework structure would collapse, hence this project attempts silica sodalite as an alternative inorganic material to overcome the occlusion of the pores by water during synthesis.

2.3.4.2.2. Silica sodalite

Silica sodalite (SSOD) belong to the group of clathrasils, which are crystalline porous composite materials consisting of a pure and electrically neutral silica framework with a cage-like voids (host) (Werthmann et al., 2000). SSOD is a type of zeolite material with a chemical formula $M_2[Si_{12}O_{24}]$, where *M* is the organic template molecule (guest) which is enclosed into the β-cage of the sodalite structure during synthesis (Knorr et al., 2000). The structure of silica sodalite contains very small micropores surrounded by 4- and 6-membered ring silicates (Koike et al., 2017). This type of zeolite has been reported to be synthesized by solvothermal synthesis method where a structure directing agent (SDA) was added (Yang et al., 2007). Silica sodalite has been recently synthesized by topotactic conversion where a layered silicate RUB-15 ($[(CH_3)_4N]_8[H_8Si_{24}O_{56}].20H_2O$) consisting of crystalline 2D sheets composed of only SiO_4 units is converted by interlayer condensation by the formation of Si-O-Si bonds (Koike et al., 2017).

2.3.5. Membranes configuration & flow regime

Membranes are fabricated in configurations of flat sheet, hollow fibre, tubular, or spiral wound. Flat sheet membranes are usually used in research applications as they can be easily fabricated by casting. Hollow fibre and tubular membranes are prepared by spinning and are more common in industry than flat sheet membranes because they are cheaper to

fabricate and are effective in treatment as they have a large surface to volume ratio to resist pressure (Ladewig & Al-Shaeli 2017). These are also favoured because of their mechanical stability, and better capability to handle higher cross -flow velocities compared to flat sheet membranes (Samaei et al., 2018). Spiral wound membranes are used where pressure drop is to be considered but are not effective in counter current flow (Balster, 2013). Nevertheless, flat sheet membranes are easier to clean in case of fouling as compared to hollow fibre membranes.

Wastewater in membranes can flow in either a dead-end flow regime where the flow is perpendicular to the membrane, or it can flow in a cross-flow filtration regime where the flow is tangential to the membrane surface as shown in Figure 2.4 (Aly, 2015). The cake layer formation is said to be maximised on the dead-end flow as the feed is forced through the membrane hence the fluid is often stirred to create turbulence over the membrane (Tansel et al., 2006). On the cross-flow filtration, the residual particles are continuously swept by the feed from the membrane surface, hence, the cake layer formation is minimised.

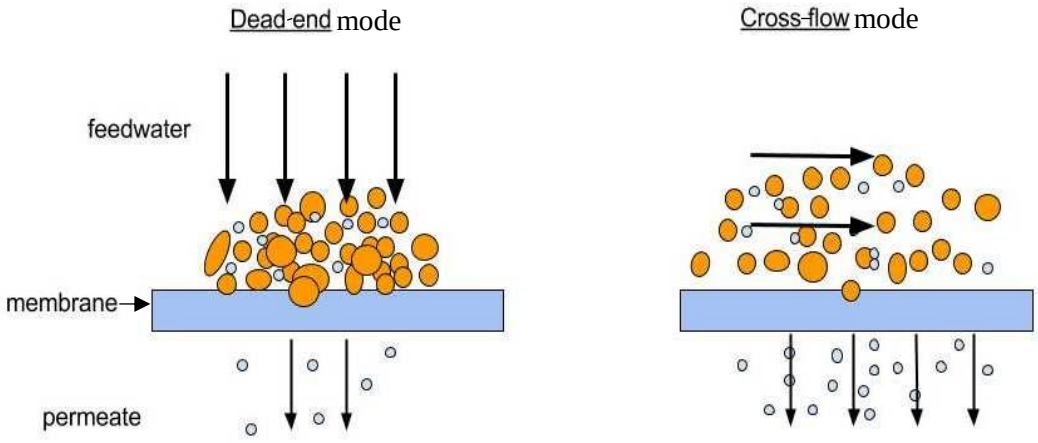


Figure 2.4: Representation of feed flow in dead end and cross flow filtration (Used with permission from Zena-Membranes http://www.zena-membranes.cz/images/mgallery/other/Dead%20end%20vs%20cross%20flow%20filtration.jpg)

2.3.5. Membranes applications

The application of membranes in large scale was witnessed more than 50 years ago, in the late 1980's where the large-scale application of emulsion liquid membranes for the removal of metals and organic matters from wastewater was commercialised (Khajavi, 2010). Researcher's interest is increasing in the membrane technology field because of the membranes potential to be the future of the separation processes. In inorganic membranes, industrially mesoporous ceramic membranes are used for MF and UF membranes as they are asymmetric in structure with a dense region close to the support structure (Theresa et al., 2011). For organic membranes, integrally skinned membranes also known as porous polymeric membranes are also used for MF and UF, where they act as pre-treatment for NF or RO membranes. Cellulose acetate (CA) is one of the polymers mostly used in these membranes but because of its limitations, other polymers including polysulfone (Psf), polyethersulfone (PES), and sulfonated Psf or PES are used (Theresa et al., 2011). Ceramic

membranes have attracted interest in the treatment of wastewater particularly industrial water, because of the advantages outlined in Table 2.4. Membrane application has been observed in industries like mining, pulp and paper, pharmaceutical, food, textile, and petrochemical.

The pulp and paper industry generates wastewater that is toxic, with suspended solids, and has pollutants which result in the water having high chemical oxygen demand and biochemical oxygen demand. Membrane technology has been evaluated in treating this water to remove particles of smaller diameter to be either suitable for reuse in the process or be discharged within the required limits. In the evaluation of UF and MF membranes, Neves et al (2017) found that the membranes are very efficient with an average removal of 84% and 75% of true colour and 84.3% and 80% of COD, respectively, from a pulp and paper wastewater. Industrial effluents have different types of pollutants depending on the activities of that specific industry. The complexity of the textile industry makes it difficult for treatment methods to be defined. Depending on the processes carried out, the industry produces wastewater of great chemical complexity and diversity including many dyes and chemicals containing trace and heavy metals such as Cr, As, Cu and Zn, non-biodegradable highly persistent organics and pesticides (Samaei et al., 2018). The performance of membranes in the textile industry is limited by biofouling, as evidenced from the work by Petrinic et al (2015) where they tested the effluents on RO, FO, NF, and UF membranes.

Most research in membrane technology focuses on the removal of metals which are found in different industries. In particular the treatment of mine waters using membranes has attracted researchers because the current treatment methods are either expensive or ineffective. Lopez et al (2018) fabricated a semi-aromatic polyimide (PI) and a sulfonated polyethersulfone (PES) membrane for the rejection of metals (Na_2SO_4, Fe^{2+}, Zn^{2+}, Cu^{2+}) from a specific AMD. Metal rejections higher than 90% for PI and between 60-70% for

PES were obtained, but the performance of these membranes decreased as the acidity of these samples was increased. Membrane application in mine effluents was also investigated by Daramola et al (2015) where they used a PES membrane infused with varying amounts of hydroxy sodalite for the rejection of heavy metals. The most rejected heavy metal was Pb^{2+} with a maximum rejection of 57%, while the least rejected metal was Mn^{2+} with a maximum rejection of 6%, both at maximum HSOD loadings. These indicate the vast application of membranes in different industries, and how they are shaping the wastewater treatment processes. Nevertheless, effort is still required to improve the performance of membranes as some cannot withstand the varying conditions of different processes.

2.5. Membrane fouling

Although the potential of membranes is realised in water treatment, their use is limited by disadvantages like fouling and the trade-off between selectivity and permeability. Fouling is a process where suspended or dissolved substances in feed solution deposit onto membrane surface in a way that causes water flux and quality decline and leads to the lower selectivity (Akbari et al., 2015). This is said to be often caused by reversible or irreversible deposition of organic or inorganic compounds in the feed solution on the hydrophobic surface. While reversible deposition can be cleared by physical backwashing, irreversible deposition requires chemical cleaning and often the membrane does not go back to its original form. Fouling is said to be influenced by the charge, roughness and the hydrophilicity of the membrane surface. The process of fouling occurs in four mechanisms namely, complete blocking of pores, intermediate blocking of pores, constriction of pores, and cake layer formation over the pores as shown in Figure 2.5, resulting in reduced water flux (Aly, 2015; Abbasi et al., 2012).

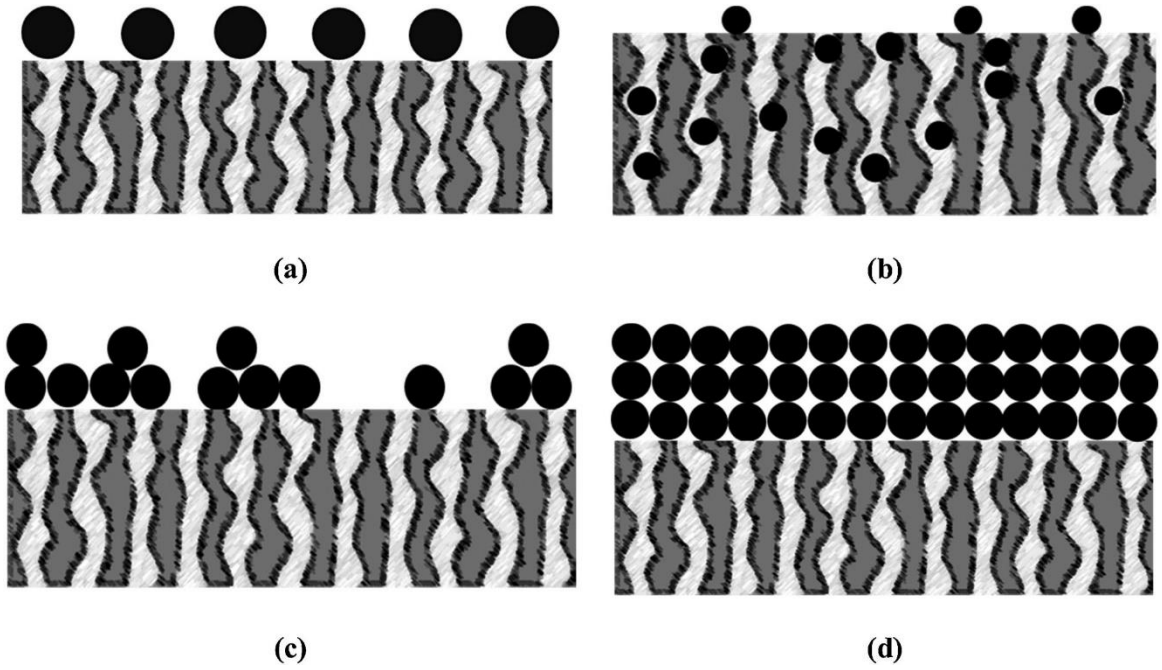


Figure 2.5: Hermia model fouling mechanism (a) pore blocking, (b) standard blocking, (c)intermediate blocking, and (d) complete pore blocking (Used with permission from Choobar et al., 2019)

These mechanisms are described by Abbasi et al (2012) in terms of the Hermia's model approach. The pore blocking mechanism occurs when the retained particles have a similar size to that of the membrane pores resulting in the blockage of the pores. The remaining particles are then diverted to the open pores, which also eventually get blocked hence the flux is reduced and the membrane resistance is increased. When some particles superimpose the already blocking particles, the intermediate blocking mechanism is observed. Constriction of pores (standard blocking) mechanism occurs when the particles are dimensionally smaller than the pores of the membrane and get attached to the inner surface of the membrane hence the pore diameters of the membrane are narrowed. The cake layer formation mechanism occurs when particles of a dimensionally larger size than the pores of the membrane block the membrane pores and accumulate of the blocked surface to form a layer. The Hermia's model is described mathematically according to equation 2.7- 2.10.

$$\frac{1}{J^2} = \frac{1}{J_o^2} + K_g t \qquad \text{pore blocking} \qquad (2.7)$$

$$\frac{1}{J^{1/2}} = \frac{1}{J_o^{1/2}} + K_s t \qquad \text{standard blocking} \qquad (2.8)$$

$$Ln(J) = Ln(J_o) - K_c t \qquad \text{complete pore blocking} \qquad (2.9)$$

$$\frac{1}{J} = \frac{1}{J_o} + K_i A t \qquad \text{intermediate pore blocking} \qquad (2.10)$$

Where J_o is the initial water flux of the membrane obtained by filtering clean water and J is the filtration flux at time t where the sample feed is passed through the membrane and volume collected over time is measured. A is the membrane area and K_i is the constant for model i.

To overcome the fouling problem, Akbari et al. (2015) suggests that the charge of the membrane should be lowered, surface must be less rough, and the hydrophilicity must be enhanced. The problem of fouling limits the performance of the membrane, leading to an increased demand for energy and higher cleaning frequency hence increased operational cost. Implementation of membrane plants at a larger scale is also limited by the costs associated with the operation of the plant in addition to the costs of maintenance.

2.6. Summary

This chapter provides information on the formation of AMD, its impact on the environment and human health and the current AMD treatment methods. It reviews membrane technology as one of the most promising treatment technologies for wastewater, and its application in industry was outlined. Filler particles commonly used in membrane technology and the challenge of membrane fouling which limits membrane application was outlined.

2.7. References

1. Abbasi, M., Sebzari, M. R., Salahi, A., & Mirza, B. (2012). Modelling of Membrane Fouling and Flux Decline in Microfiltration of Oily Wastewater using Ceramic Membranes. *Chemical Engineering Communications*, 78-93. doi:10.1080/00986445.2011.570391

2. Abu-Saied, M. A., Wycisk, R., Abbassy, M. M., El-Naim, G. A., El-Demerdash, F., Youssef, M. E., . . . Pintauro, P. N. (2017). Sulfated Chitosan/PVA Absorbent Membrane for Removal of Copper and Nickel Ions from Aqueous Solutions—Fabrication and Sorption Studies. *Carbohydrate Polymers*, 149-158. doi:10.1016/j.carbpol.2016.12.039

3. Akbari, A., Derikvandi, Z., & Rostami, S. M. (2015). Influence of Chitosan Coating on the Separation Performance, Morphology and Anti-Fouling Properties of the Polyamide Nanofiltration Membranes. *Journal of Industrial and Engineering Chemistry*, 268–276. doi:10.1016/j.jiec.2015.03.002

4. Aly, S. (2015). *PhD Thesis: Pre-Treatment Evaluation Prior to Ultrafiltration in Secondary Effluent Treatment for Water Reuse.* Waterloo: University of Waterloo.

5. Balster, J. (2013). Spiral Wound Membrane Module. *Encyclopedia Of Membranes*, 1-3. doi: 10.1007/978-3-642-40872-4_1586-1

6. Bell, F. G., Bullock, S. E., Halbich, T. F., & Lindsay, P. (2001). Environmental Impacts Associated with an Abandoned Mine in the Witbank Coalfield, South Africa. *International Journal of Coal Geology*, 195–216. doi:10.1016/50166-5162(00)00033-1

7. Choobar, B. G., Shahmirzadi, M. A. A., Kargari, A., Manouchehri, M. (2019). Fouling Mechanism Identification and Analysis in Microfiltration of Laundry Wastewater. *Journal of Environmental Chemical Engineering,*103030. doi:10.1016/j.jece.2019.1030300

8. Choudhury, B. U., Malang, A., Webster, R., Mohapatra, K. P., Verma, B. C., Kumar, M., Hazarika, S. (2017). Acid Drainage from Coal Mining: Effect on Paddy Soil and Productivity of Rice. *Science of the Total Environment*, 344-351. doi:10.1016/j.scitotenv.2017.01.074

9. Chung, T.S., Jiang, L. Y., & Kulprathipanja, S. (2007). Mixed Matrix Membranes (MMMs) Comprising Organic Polymers with Dispersed Inorganic Fillers for Gas Separation. *Progress in Polymer Science*, 483-507. doi:10.1016/j.progpolymsci.2007.01.008

10. Daramola, M. O., Aransiola, E. F., & Ojumu, T. V. (2012). Potential Application of Zeolite Membranes in Reaction Coupling Separation Processes. *Materials*, 2101-2136. doi:10.3390/ma5112101

11. Daramola, M. O., Burger, A. J., Pera-Titus, M., Giroir-Fendler, A., Miachon, S., Dalmon, J.A., & Lorenzen, L. (2010). Separation and Isomerization of Xylenes using Zeolite Membranes: A Short Overview. *Asia Parcific Journal of Chemical Engineering*, 815-837. doi:10.1002/apj.414

12. Daramola, M. O., Silinda, B., Masondo, S., & Oluwasina, O. O. (2015). Polyethersulphone-Sodalite (PES-SOD) Mixed-Matrix Membranes: Prospects for Acid Mine Drainage (AMD) Treatment. *Journal of the Southern African Institute of Mining and Metallurgy, 115*(12), 1221-1228. doi:10.17159/2411-9717/2015/v115n12a11

13. Fard, A. K., McKay, G., Buekenhoudt, A., Sulaiti, H. A., Motmans, F., & Atieh, M. (2018). Inorganic Membranes: Preparation and Application for Water Treatment and Desalinaton. *Materials, 11*(74). doi:10.3390/ma11010074

14. Habiba, U., Afifi, A. M., Salleh, A., & Ang, B. C. (2017). Chitosan/(Polyvinyl Alcohol)/Zeolite Electrospun Composite Nanofibrous Membrane for Adsorption of Cr6+, Fe3+ and Ni2+. *Journal of Hazardous Materials*, 182-194. doi:10.4102/sajs.v107i5/6.712

15. Jha, B., & Singh, D. N. (2016). Basics of Zeolites, *In: Fly Ash Zeolites* (1 ed., Vol. 78). Singapore: Springer. doi:10.1007/978-981-10-1404-8_2

16. Julbe, A. (2007). Zeolite Membranes Synthesis, Characterization and Application. In: J. Cejka, H. van Bekkum, A. Corma, & F. Schuth, *Introduction to Zeolite Science and Practice*, 181-210. doi:10.1007/978-3-662-44324-8_605

17. Kefeni, K. K., Msagati, T. A., & Mamba, B. B. (2017). Acid Mine Drainage: Prevention, Treatment Options, and Resource Recovery: A Review. *Journal of Cleaner Production, 151*, 475-493. doi:10.1016/j.jclepro.2017.03.082

18. Khajavi, S. (2010). *Separation of Process Water Using Hydroxy Sodalite Membrane.* Delft University of Technology. The Netherlands: Unpublished PhD thesis.

19. Khajavi, S., Jansen, J. C., & Kapteijn, F. (2009). Application of Hydroxy Sodalite Films as Novel Water Selective Membranes. *Journal of Membrane Science*, 153–160. doi:10.1016/j.memsci.2008.09.046

20. [a]Khajavi, S., Jansen, J. C., & Kapteijn, F. (2010). Production of Ultrapure Water by Desalination of Seawater using Hydroxy Sodalite Membrane. *Journal of Membrane Science*, 52-57. doi:10.1016/j.memsci.2010.03.026

21. [b]Khajavi, S., Sartipi, S., Gascon, J., Jansen, J. C., & Kapteijn, F. (2010). Thermostability of Hydroxy Sodalite in View of Membrane Applications. *Microporous and Mesoporous Materials*, 510-517. doi:10.1016/j.micromeso.2010.03.035

22. Knorr, K., Braunbarth, C. M., van de Goor, G., Behrens, P., Griewatsch, C., & Depmeier, W. (2000). High Pressure Study on Dioxolane Silica Sodalite (C3H6O2)2[Si12O24]-Neutron and X-ray Powder Diffraction Experiments. *Solid State Communications*, 503–507. doi:10.1016/S0038-1098(99)00516-5

23. Koike, M., Asakura, Y., Sugihara, M., Kuroda, Y., Tsuzura, H., Wada, H., & Kuronda, K. (2017). Topotactic Conversion of Layered Silicate RUB-15 to Silica Sodalite through Interlayer Condensation in N-methylformamide. *Royal Society of Chemistry*, 10232–10239. doi:10.1039/c7dt01287j

24. Ladewig, B., & Al-Shaeli, M. N. (2017). Fundamentals of Membrane Processes. *In: Fundamentals of Membrane Bioreactors* (pp.13-37). Singapore: Springer Transactions in Civil and Environmental Engineering. doi:10.1007/978-981-10-2014-8_2

25. Lopez, J., Reig, M., Gibert, O., Valderrama, C., & Cortina, J. L. (2018). Evaluation of NF Membrane as Treatment Technology of AMD: Metals and Sulfate Removal. *Desalination, 440*, 122–134. doi:10.1016/j.desal.2018.03.030

26. Mabilia, M., Pearlstein, R. A., & Hopfinger, A. J. (1987). Molecular Modelling of Zeolite Structure: Properties of the Zeolite Cage. *American Society*, *109*(26), 7960-7968. doi:10.1021/ja00260a005

27. Masindi V., Osman M.S., & Abu-Mahfouz A.M. (2017). Integrated Treatment of Acid Mine Drainage Using BOF Slag, Lime/Soda Ash and Reverse Osmosis (RO): Implication for the Production of Drinking Water. *Desalination*, 45-52. doi:10.1016/j.desal.2017.10.002

28. Masindi, V., Chatzisymeon, E., Kortidis, I., & Foteinis, S. (2018). Assessing the Sustainability of Acid Mine Drainage (AMD) Treatment in South Africa. *Science of the Total Environment, 635,* 793-802. doi:10.1016/j.scitotenv.2018.04.108

29. McCarthy, T. S. (2011). The Impact of Acid Mine Drainage in South Africa. *South African Journal of Science*, 1-7. doi:10.4102/sajs.v107i5/6.712

30. Moodley, I., Sheridan, C. M., Kappelmeyer, U., & Akcil, A. (2018). Environmentally Sustainable Acid Mine Drainage Remediation: Research Developments with a Focus on Waste/By-Products. *Minerals Engineering*, 207-220. doi:10.1016/j.mineng.2017.08.008

31. Moteki, T., Chaikittisilp, W., Shimojima, A., & Okubo, T. (2008). Silica Sodalite without Occluded Organic matters by Topotactic Conversion of Lamellar Precursor. *Journal of the American Chemical Society*,15780. doi:10.1021/ja806930h

32. Nabavi, M. S., Mohammadi, T., & Kazemimoghadam, M. (2014). Hydrothermal Synthesis of Hydroxy Sodalite Zeolite Membrane: Separation of H_2/CH_4. *Ceramics International*, 5889–5896. doi:10.1016/j.ceramint.2013.11.033

33. Neves, L. C., De Souza, J. B., De Sousa Vidal, C. M., Martins, K. G., & Manago, B. L. (2017). Pulp and Paper Mill Effluent Post-Treatment Using Microfiltration and Ultrafiltration Membranes. *Cellulose Chemistry and Technology*, 579-588.

34. Olaru, M., Bordianu, I., & Simionescu, B. C. (2010). Polymers in Membrane Science. *Systems Membrane*, 191-240. ISBN:978-606-521-526-9

35. Petrinic, I., Bajraktari, N., & Helix-Nielsen, C. (2015). Membrane Technologies for Water Treatment and Reuse in the Textile Industry. *Advances in Membrane Technologies for Water Treatment: Materials, Processes and Applications*, 537-550. doi:10.1016/B978-1-78242-121-4.00017-4

36. Richards, H. L., Baker, P. G., & Iwuoha, E. (2012). Metal Nanoparticle Modified Polysulfone Membrane for Use in Wastewater Treatment: A Critical Review. *Journal of Surface Engineered Materials and Advanced Technology*, 183-193. doi:10.4236/jsemat.2012.223029

37. Samaei, S. M., Gato-Trinidad, S., & Altaee, A. (2018). The Application of Pressure-Driven Ceramic Membrane Technology for the Treatment of Industrial Wastewaters- A Review. *Separation and Purification Technology*, 198-220. doi:10.1016/j.seppur.2018.02.041

38. Tansel, B., Sager, J., Rector, T., Garland, J., Strayer, R. F., Levine, L., . . . Bauer, J. (2006). Significance of Hydrated Radius and Hydration Shells on Ionic Permeability During Nanofiltration in Dead End and Cross Flow Modes. *Separation and Purification Technology*, 40-47. doi:10.1016/j.seppur.2005.12.020

39. Taylor, J., Pape, S., & Murphy, N. (2005). A Summary of Passive and Active Treatment Technologies for Acid and Metalliferous Drainage (AMD). *Fifth Australian Workshop on Acid Drainage*. [PDF]Fremantle, Western Australia: Earth Systems Pty Ltd. Retrieved from https://earthsystems.com.au/wp-content/uploads/2012/02/AMD_Treatment_Technologies_06.pdf

40. Theresa, M., Pendergast, M., & Hoek, E. M. (2011). A Review of Water Treatment Membrane Nanotechnologies. *Energy and Environmental Science*(6), 1946-1971. doi:10.1039/C0EE00541J

41. Tutu, H., McCarthy, T.S., Cukrowska, E. (2008). The Chemical Characteristics of Acid Mine Drainage with Particular Reference to Sources, Distribution and Remediation: The Witwatersrand Basin, South Africa as a Case Study. *Applied Geochemistry*, 3666-3684. doi:10.1016/j.geochem.2008.09.002

42. Werthmann, U., Marler, B., & Gies, H. (2000). Pyrrolidine Silica Sodalite and Ethylamine Silica Sodalite- Two New Silica Sodalite Materials Synthesized from Different Solid Silica Sources. *Microporous and Mesoporous Materials*, 549-562. doi:10.1016/S1387-1811(00)00230-4

43. Westholm, L. J., Repo, E., & Sillanpaa, M. (2014). Filter Mateials for Metal Removal from Mine Drainage- A Review. *Environmental Science and Pollution Research*, 9109-9128. doi:10.1007/s11356-014-2903-y

44. Yang, Y., Nie, C., Deng, Y., Cheng, C., He, C., Ma, L., & Zhao, C. (2016). Improving Antifouling and Antimicrobial Efficiency of Ultrafiltration Membranes with Functional Carbon Nanotubes. *RSC Advances*, 88265-88276. doi:10.1039/C6RA18706D

45. Yu, J. (2007). Synthesis of Zeolites. In J. Cejka, H. van Bekkum, A. Corma, & F. Scuth, *Introduction to Zeolite Science and Practice* (3rd ed., pp. 39-87). Elservier. ISBN:9780444530639

46. Dead End vs Cross Flow Scheme [online image]. Zena-Membranes. http://www.zena-

membranes.cz/images/mgallery/other/Dead%20end%20vs%20cross%20flow%20filtration.jpg

3. Materials and Experimental Procedures

3.1. Introduction

This section details the materials used to synthesize the nanoparticles (HSOD, SSOD and fSSOD). The synthesis procedure followed to fabricate the mixed matrix membranes is detailed in this section. This chapter also describes how the fabricated membranes were coated and how the synthetic AMD was prepared. The analytical equipment used to characterize the nanoparticles and the MMMs are also outlined together with the procedure of evaluating the performance of the fabricated membranes.

3.2. Materials and equipment

Sodium metasilicate (Na_2O_3Si), Sodium aluminate anhydrous technical grade [Al (as Al_2O_3):50-56%, Na (as Na_2O):40-45%], and sodium hydroxide anhydrous reagent grade ≥98% pellets were used for the synthesis of HSOD. Tetraethyl orthosilicate (TEOS) ($C_8H_{20}O_4Si$) reagent grade 98% and tetramethylammonium hydroxide (TMAOH) ($C_4H_{13}NO$) solution (25wt.% in H_2O) were used in the synthesis of RUB-15 which was then rinsed with acetone. Propionic acid purchased from CC Imelmann Pty Ltd was used for RUB-15 pre-treatment to form SSOD.

The SSOD particles were functionalized using nitric acid (55%) and sulphuric acid (98%). The membranes were fabricated with Polysulfone (average Mw= 22 000 g/mol) beads, dissolved in N,N-dimethylacetamide ≥99.9% (Mw=87.12 g/mol) as a solvent. Poly(vinyl alcohol) 87-90% hydrolysed (average Mw=30000-70000) was used for membrane coating.

Synthetic AMD was prepared using $MgCl_2$, $MnCl_2.4H_2O$, Na_2SO_4, $Al(NO_3)_3$, $Fe(NO_3)_3.9H_2O$, and Ca_2OH_2 where the pH was controlled by H_2SO_4 and NaOH. All

chemicals were purchased from Sigma Aldrich (Pty), South Africa and used with no further modification.

Membranes were hand cast on a glass plate using ‘Dr Blade’. Nanoparticles were synthesized using a 45 mL Teflon-lined autoclave from Parr company instrument. The dead-end filtration was performed using a “#memcon” filtration cell with a 400 mL holding volume, 10 bar max working pressure, and allowable working temperature in the range 5-80°C.

3.3. Experimental procedure

The experiments were carried out as summarised in Figure 3.1.

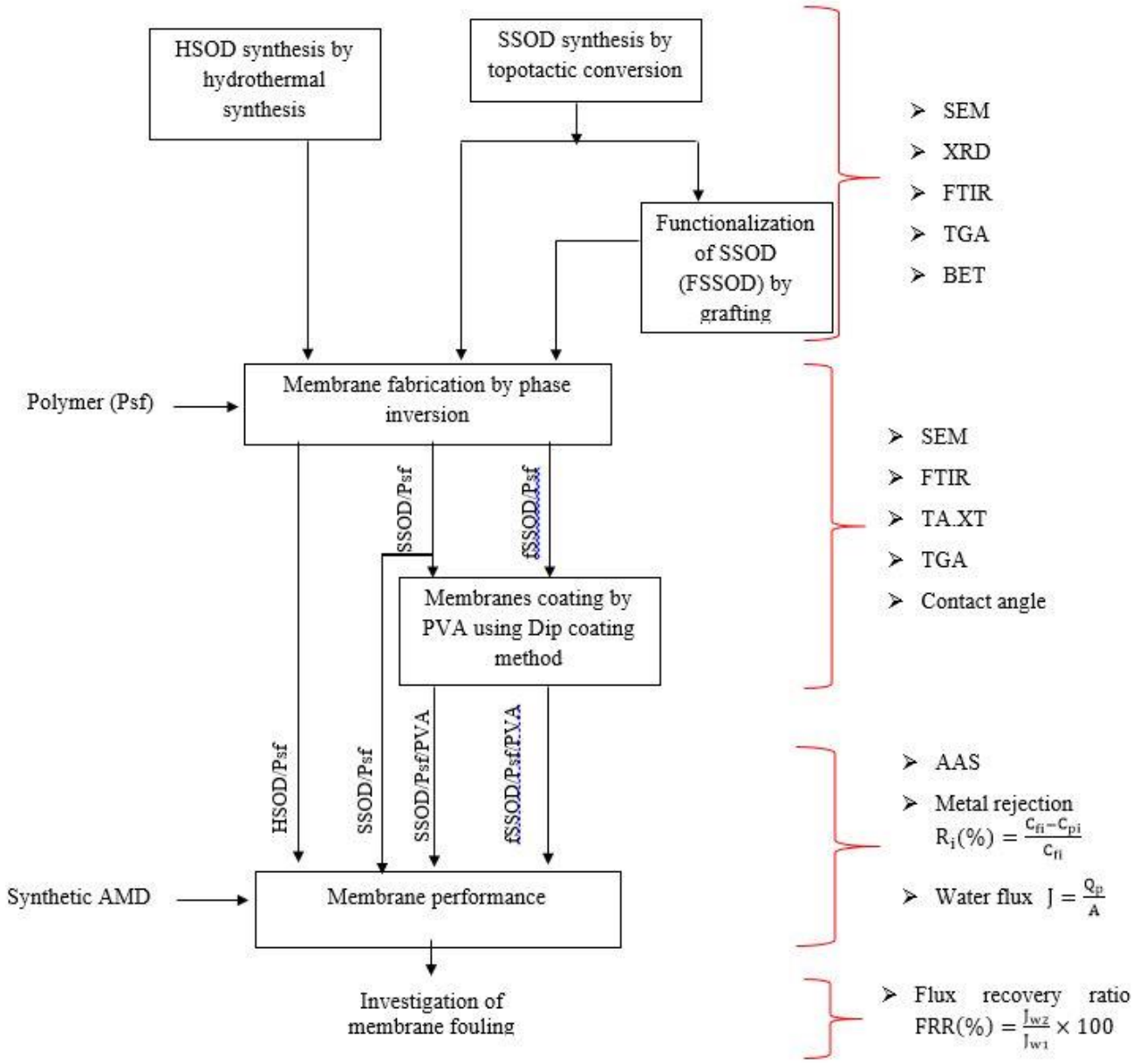


Figure 3.1: Summary of experimental procedure

3.3.1. Synthesis of sodalite nanoparticles

HSOD was synthesised by hydrothermal synthesis following a method described in literature (Daramola et al., 2015; Khajavi et al., 2010; Khajavi et al., 2009). As represented in Figure 3.2, the precursor solution was prepared by NaOH, H_2O, Na_2SiO_3 and $NaAlO_2$. This solution was stirred for 60 minutes at 1000 rpm to form a homogenous solution. This was poured in a 50 mL teflon-lined autoclave and was subjected to hydrothermal synthesis at 140°C for 3.5 hours. Sample was then centrifuged and washed with deionised water until a pH of 7 was obtained. It was then dried overnight in an oven at 100°C.

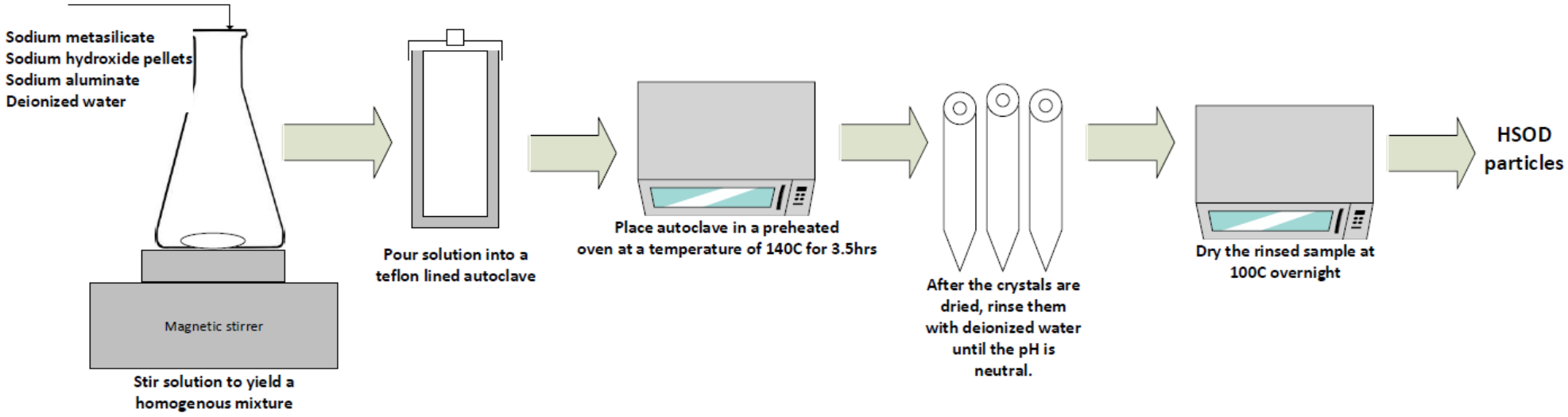


Figure 3.2: Schematic illustration of the synthesis of hydroxy sodalite nanoparticles

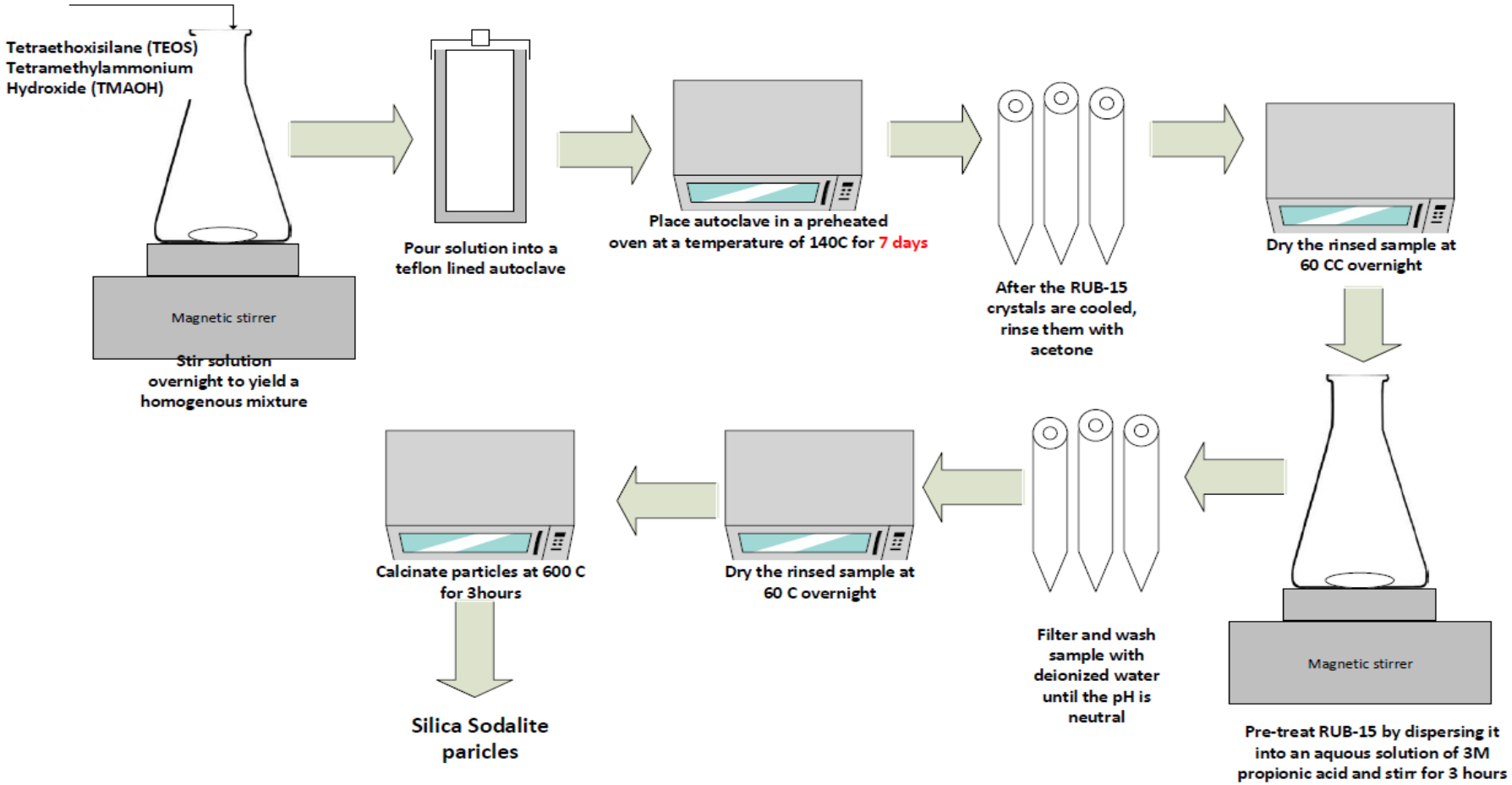


Figure 3.3: Schematic illustration of the synthesis of silica sodalite nanoparticles

SSOD was synthesized by following a procedure (see Figure 3.3) which was described elsewhere (Moteki et al., 2011; Koike et al. 2017). 18.5 g of TEOS was mixed with 32 mL of TMAOH and stirred at 500 rpm overnight to form a homogenous mixture. The solution was then autoclaved at 140°C for seven days. The precipitate was then centrifuged and rinsed with acetone. The particles were then dried at 60°C for 24 hours, producing RUB-15. 0.1 g of the RUB-15 particles were treated with 30 mL of 5M propionic acid. This solution was magnetically stirred at 500 rpm for 180 minutes. Particles were recovered by centrifuge and washed with distilled water to a neutral pH then dried at 60°C for 24 hours. The treated RUB-15 particles were then calcined at 600°C for 3 hours to obtain silica sodalite nanoparticles

3.3.2. Functionalization of SSOD nanoparticles

The surface of the synthesized SSOD nanoparticles was functionalized using carboxylation protocol in order to enhance their dispersion in the polymer matrix (Aberefa et al., 2019). 1 g of the SSOD nanoparticles was dispersed in a mixture of 75 mL H_2SO_4 and 25 mL HNO_3. This was stirred overnight at 40°C to form fSSOD. The produced fSSOD nanoparticles were recovered by centrifugation and were repeatedly washed by deionized water to a neutral pH and dried at 100°C for 24 hours.

3.3.3. Membrane preparation

Polysulfone (10 g) was dissolved in 50 mL of N,N-dimethylacetamide. Varying amounts of the sodalite nanoparticles were added to the mixture to form nanoparticles loadings of 5wt.% and 10wt.% relative to the dry polymer (loading calculated using Equation 3.1). This mixture was sonicated for 10 minutes to uniformly disperse the nanoparticles and stirred on a magnetic stirrer for 24 hours. The solution was hand-cast on a glass-plate using “Dr Blade” and left for 10 seconds to allow the solvent to evaporate. The cast membrane was

then immersed in a bath of deionized water, and the membranes were obtained by phase inversion. The obtained membranes were allowed to soak in deionized water overnight to remove impurities. They were then dried at 60°C overnight.

$$\% \text{ Loading} = \frac{\text{Amount of nanoparticles (g)}}{\text{Amount of Psf (g)+Amount of nanoparticles (g)}} \quad (3.1)$$

3.3.4. Membrane coating

The synthesized membranes were coated by following a procedure reported elsewhere (Ma et al., 2007). 1 g of PVA was dissolved in 100 mL deionised water and stirred at 90°C to form a coating solution. The cross-linking solution was prepared by dissolving 1g maleic acid in deionized water to a total volume of 100 mL. The membranes were immersed in this solution for 3 minutes after which they were cross-linked by immersing into maleic acid solution for a further 3 minutes. The membranes were then dried in an oven overnight.

3.4. Characterization of nanoparticles and membranes

3.4.1. Scanning electron microscopy (SEM)

SEM images of the produced HSOD, SSOD and fSSOD nanoparticles and membranes were obtained using ZEIS scanning electron microscopy (SEM) at an accelerating voltage of 20 kV. Each nanoparticles sample was sprinkled onto an aluminium stub using carbon tapes. Membranes were cut into appropriate size and attached into stubs using carbon tape. All samples were coated with two layers of gold-palladium.

3.4.1. Nitrogen physisorption experiment for surface area

The Micrometrics Tristar 3000 (RS232) was used for surface area and porosity analyses. Prior to the start of recording the surface area and porosity, a precisely weighed 100 mg sample was degassed in an inert environment (nitrogen gas) at 150 °C for 12 hours using a

vacuum pump to remove all adsorbed volatiles. Subsequently, the degassed sample was placed in a liquid nitrogen bath at -195°C and ultra-pure nitrogen gas was passed over the sample and the adsorption was recorded.

3.4.2. X-ray diffraction (XRD)

The crystalline structure of the synthesized nanoparticles HSOD, SSOD and fSSOD was analysed using Bruker XRD D2 Phaser with a CuKα target at a wavelength of 1.54 Å, a tube voltage of 30kV and a tube current of 10mA. The samples were scanned at a stepsize of 0.026° and a rate of 8.5°/min from 5°-90° of 2Θ. The Miller indices (hkl) were obtained from the reference library of Diffrac.Eva software.

3.4.3. Fourier transform infrared (FTIR)

The presence of functional groups on the nanoparticles and membranes was checked by PerkinElmer FTIR spectrometer equipped with a high-performance deuterated triglycine sulfate (DTGS) detector and KBr beam splitter. The spectra of the analysed nanoparticles and membranes was recorded from 4000 to 500 cm^{-1} wavenumbers.

3.4.4. Thermo-gravimetric analysis (TGA)

The thermal behaviour of nanoparticles and membranes was determined by TA instrument SDT Q600 simultaneous DSC/TGA analyzer. The heating rate was 20°C/min from room temperature to 800°C and a nitrogen gas flow of 50 ml/min. The degree of functionalization of the SSOD nanoparticles was determined quantitatively by the thermal stability of the nanoparticles as a function of weight loss with respect to temperature. The thermal stability of the membranes was determined by using the graphs of weight loss against temperature.

3.4.5. Atomic force microscopy (AFM)

The surface topography of the membranes was determined by Veeco Dimension 3100 AFM. The membranes were cut into appropriate size and attached onto a steel disk using a double-sided tape. Sample was mounted onto the instrument and air duster was used to minimise dust on the sample surface. Tapping mode was used as an imaging option. A scan size of $2\ \mu m \times 2\ \mu m$ was used at a scan rate of 1.5 Hz. The AFM nanoscope software was used to process the data and obtain membrane surface images.

3.4.6. Porosity and mean pore size

The membrane porosity (ε) was calculated using Equation 3.2 (Hamid, *et al*., 2011;Ayyaru & Ahn, 2017). The membranes were immersed in water and weight measured (W_w), then dried overnight and dry weight also measured (W_d). This is known as the gravimetric method and was also used to calculate the water uptake of the membranes (equation 3.3).

$$\varepsilon = \frac{W_w - W_d}{\rho . V} \times 100 \quad (3.2)$$

$$EWC\ (\%) = \frac{W_w - W_d}{W_w} \times 100 \quad (3.3)$$

Where: W_w and W_d is the weight (g) of the wet and dry membrane respectively; A is the effective membrane area (cm^2); V is the total volume of the membrane (cm^3) ρ is the water density (0.998 $g.cm^{-3}$); l is the membrane thickness (cm); η is the viscosity of water (8.9×10^{-4} Pa.s); Q is the water flux per unit time ($cm^3.s^{-1}$) and P is the operating pressure (4×10^5 Pa).

3.4.7. Contact angle

The contact angle of the membranes was measured using the sessile drop method (OCA 15 EC GOP, Data physics). Deionized water was used as a probe liquid dispensed at 1 $\mu l/s$.

3.4.8. Mechanical strength (young modulus and tensile strength)

The mechanical properties of the membranes were evaluated using TA.XT plus texture analyzer at ambient temperature to determine the tensile strength (σ) (Equation 3.4) and Young's Modulus (E) (Equation 3.5) of the synthesized membranes. The membranes were cut into 1 cm×3 cm size and fixed into the sample holder of the instrument. Force and time data at a speed of 8.6 mm/s were captured and analysed using integrated Exponent 32-bit software.

$$\text{Tensile strenght} = \frac{\text{Force}}{\text{Area}} \tag{3.4}$$

$$\text{Young Modulus} = \frac{\text{Tensile strenght}}{\text{Strain}} \tag{3.5}$$

Where:

Tensile strength= Uniaxial force × original gauge length

Strain=Cross sectional area of the sample × elongation of the sample

3.5. Membrane performance evaluation

The pH of synthetic AMD was determined by the METTLER TOLEDO pH meter as 2.8. The heavy metal rejection was evaluated by permeating this AMD with ion concentrations shown in Table 3.1 obtained from the Atomic Absorption Spectroscopy (AAS). The synthetic AMD was prepared with reference to metal concentrations of actual AMD collected by Bell et al (2001) from an abandoned coal mine in Witbank, South Africa. The pH of this solution was adjusted by 0.1M H_2SO_4 and NaOH to a pH of 2.8. The heavy metal rejection was obtained by collecting permeate from a dead-end filtration cell as shown in Figure 3.4.

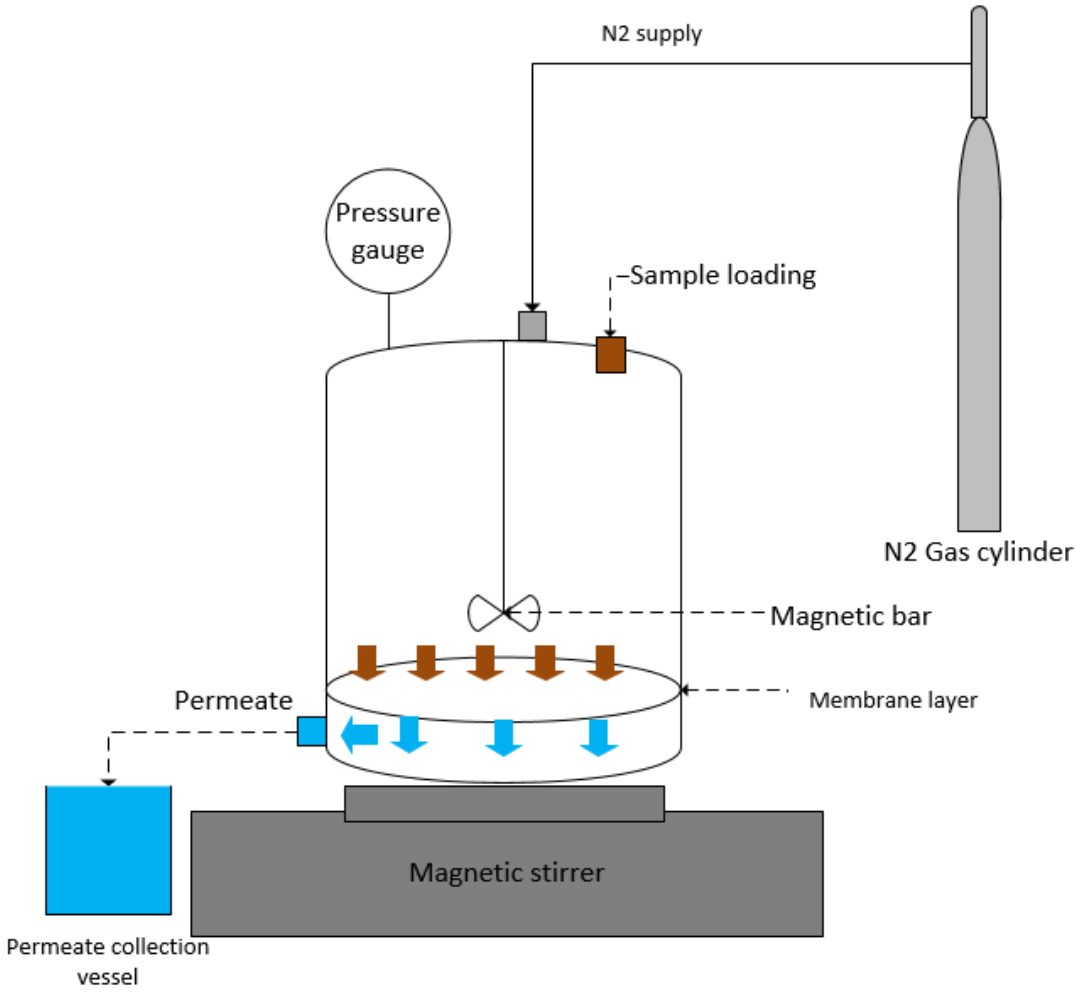


Figure 3.4: Dead-end filtration cell schematic set-up

Table 3.1: Metal composition of synthetic AMD

Cation	Salt	Concentration (mg/L) (Bell et al., 2001)	Sample concentration (mg/L)
Mg^{2+}	$MgCl_2$	15	12.1
Mn^{2+}	$MnCl_2.4H_2O$	5	31.9
Na^{2+}	NaOH pellets	688	624.8
Al^{3+}	$Al(NO_3)_3$	84	89.1
Fe^{3+}	$Fe(NO_3)_3.9H_2O$	111	100.7
Ca^{2+}	Ca_2OH_2	41	59.5
SO_4^{2-}	$NaSO_4$	1108	879.7

The pure water flux of the membranes was evaluated by permeating deionized water through the membrane for two hours. The collected permeate over a period of time at a specific effective membrane area is indicative of the original flux of each membrane. The membrane flux (J_p) was determined by collecting a permeate of the synthetic AMD over a period of time, and it was calculated by Equation 3.6, while the concentration of the permeate was used to calculate the metal rejection (R_i) according to Equation (3.7):

$$J_p = \frac{V_p}{A} \tag{3.6}$$

$$R_i = \frac{C_{fi} - C_{pi}}{C_{fi}} \times 100 \tag{3.7}$$

Where J_p is the water flux $\left(\frac{L}{m^2.h}\right)$, V_p is the permeate volumetric flowrate (L/m^2), A is the effective area of the membrane (0.0032 m^2), R_i is the metal rejection percentage, C_{fi} and C_{pi} are concentrations of metal *i* (mg/L) in the feed and permeate, respectively.

The ability of the membrane to recover from fouling was calculated by the flux recovery ratio (Equation 3.8).

$$FRR = \frac{J_{w2}}{J_{w1}} \times 100 \tag{3.8}$$

Where FRR is the flux recovery ration (%), J_{w1} and J_{w2} are membranes flux $\left(\frac{L}{m^2.h}\right)$ initially and after a cleaning process, respectively.

3.6. References

1. Aberefa, O. A., Daramola, M. O., & Iyuke, S. E. (2019). Production and Functionalization of Carbon nanotubes for Application in Membrane Synthesis for Natural Gas Separation. *Microporous and Mesoporous Materials*, 26-36. doi:10.1016/j.micromeso.2018.12.040

2. Ayyaru, S., & Ahn, Y.-H. (2017). Application of Sulfonic Acid Group Functionalized Graphene Oxide to Improve Hydrophilicity, Permeability, and Nanofiltration of PVDF Nanocomposite Ultrafiltration membranes. *Journal of Membrane Science*, 210-219. doi:10.1016/j.memsci.2016.10.048

3. Bell, F. G., Bullock, S. E., Halbich, T. F., & Lindsay, P. (2001). Environmental Impacts Associated with an Abandoned Mine in the Witbank Coalfield, South Africa. *International Journal of Coal Geology*, 195–216. doi:10.1016/50166-5162(00)00033-1

4. Daramola, M. O., Silinda, B., Masondo, S., & Oluwasina, O. O. (2015). Polyethersulphone-Sodalite (PES-SOD) Mixed-Matrix Membranes: Prospects for Acid Mine Drainage (AMD) Treatment. *Journal of the Southern African Institute of Mining and Metallurgy, 115*(12), 1221-1228. doi:10.17159/2411-9717/2015/v115n12a11

5. Hamid, N. A., Ismail, A. F., Matsuura, T., Zularisam, A. W., Lau, W. J., Yuliwati, E., & Abdullah, M. S. (2011). Morphological and Separation Performance Study of Polysulfone/Titnium Dioxide (PSF/TiO2) Ultrafiltration Membranes for Humic Acid Removal. *Desalination*, 85-92. doi:10.1016/j.desal.2010.12.052

6. Khajavi, S. (2010). *Separation of Process Water Using Hydroxy Sodalite Membrane.* Delft University of Technology. The Netherlands: Unpublished PhD thesis.

7. Khajavi, S., Jansen, J. C., & Kapteijn, F. (2009). Application of Hydroxy Sodalite Films as Novel Water Selective Membranes. *Journal of Membrane Science*, 153–160. doi:10.1016/j.memsci.2008.09.046

8. Koike, M., Asakura, Y., Sugihara, M., Kuroda, Y., Tsuzura, H., Wada, H., & Kuronda, K. (2017). Topotactic Conversion of Layered Silicate RUB-15 to Silica Sodalite through Interlayer Condensation in N-methylformamide. *Royal Society of Chemistry*, 10232–10239. doi:10.1039/c7dt01287j

9. Ma, X., Su, Y., Sun, Q., Wang, Y., & Jiang, Z. (2007). Enhancing the Antifouling Property of Polyethersulfone Ultrafiltration Membranes Through Surface Adsorption-Crosslinking of Poly(Vinyl Alcohol). *Journal of Membrane Science*, 71–78. doi:10.1016/j.memsci.2007.05.008

10. Moteki, T., Chaikittsilp, W., Sakamoto, Y., Shimojima, A., & Okubo, T. (2011). Role of Acidic Pretreatment of Layered Silicate RUB-15 in its Topotactic Conversion into Pure Silica Sodalite. *Chemistry of Materials*, 3564–3570. doi:10.1021/cm201480x

4. Sodalite-Infused Polysulfone Membranes: Characterization and Performance Evaluation

4.1. Introduction

In this chapter, synthesis of silica sodalite (SSOD) nanoparticles and hydroxy sodalite (HSOD) nanoparticles is described. These nanoparticles were used in fabricating polysulfone composite membranes containing 5wt.% and 10wt.% nanoparticles. The synthesized nanoparticles were characterized using SEM, BET, XRD, FTIR, and TGA, and the composite membranes were characterized using SEM, AFM, TGA, FTIR and for mechanical strength. Membranes hydrophilicity was evaluated by determining the membranes contact angle, porosity and mean pore size. Membranes performance was evaluated by permeating synthetic AMD from the synthesized membranes to determine membranes flux and selectivity.

4.2. Nanoparticles characterization

4.2.1. Preparation of sodalite nanoparticles

HSOD was synthesised by hydrothermal synthesis following a method described in literature (Daramola et al., 2015; Khajavi et al., 2009; Khajavi et al., 2010). Precursor solution was prepared by NaOH, H_2O, Na_2SiO_3 and $NaAlO_2$. This solution was stirred for 60 minutes at 1000 rpm to form a homogenous solution. This was then poured in a 50 mL teflon-lined autoclave and was subjected to hydrothermal synthesis at 140°C for 3.5 hours. Sample was then centrifuged and washed with deionised water until a pH of 7 was obtained. It was then dried overnight in an oven at 100°C.

SSOD was synthesized by following a procedure which is described elsewhere (Moteki et al., 2011; Koike et al. 2017). 18.5 g TEOS was mixed with 32 mL TMAOH and stirred at 500 rpm overnight to form a homogenous mixture. The solution was then autoclaved at 140°C for seven days. The precipitate was then centrifuged and rinsed with acetone. The particles were then dried at 60°C for 24 hours, producing RUB-15. 0.1 g of the RUB-15 particles were treated with 30 mL of 5M propionic acid. This solution was magnetically stirred at 500 rpm for 180 minutes. Particles were recovered by centrifuge and washed with distilled water to a neutral pH then dried at 60°C for 24 hours. The treated RUB-15 particles were then calcined at 600°C for 3 hours to obtain silica sodalite nanoparticles.

4.2.2. Morphology and textural properties of synthesized nanoparticles

The SEM images of HSOD, RUB-15, and SSOD are shown in Figure 4.1(a), 4.1(b) and 4.1(c) respectively. The HSOD SEM image depict some thread-ball-like particles and some cubic particles. This confirms the formation of HSOD crystals as reported in literature (Kundu et al., 2010; Daramola et al., 2015). The cubic particles in Figure 4.1(a) depict a form of impurities. These have been identified in literature as A-type zeolites (Eterigho-Ikelegbe et al., 2020). The morphology of RUB-15 shows rectangular shaped sheet-like layers stacked on each other. According to Koike et al. (2017), the lateral size of the RUB-15 plate particle is about 1–10 μm, and its thickness is about 50–100 nm. The RUB-15 morphology is also similar to that of SSOD, which indicates that SSOD was formed in a topotactic manner without collapsing or decomposition of the mother silicate layers (Moteki et al., 2011). It can be observed that the RUB-15 sheets are dense and large in size while those in SSOD are thinner and reduced in size. This is said to be due to the dehydration-condensation that RUB-15 was subjected to where it was pre-treated and calcined to form SSOD, because of the removal of tetramethylammonium (TMA^+) cations and water molecules from the interlayer space of RUB-15 (Moteki et al., 2011).

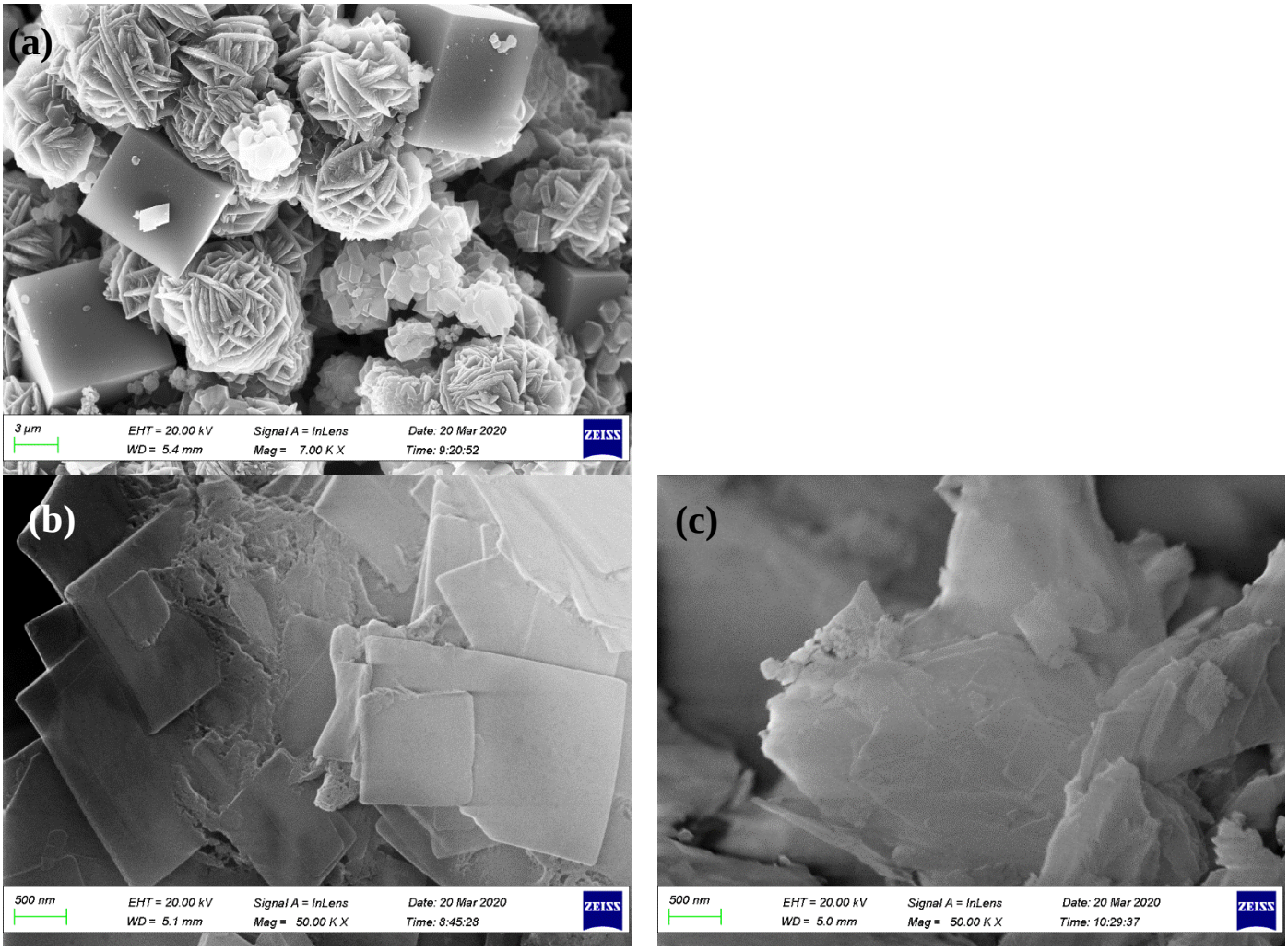


Figure 4.1: SEM images of (a) HSOD, (b) RUB-15 and (c) SSOD

The accessible micropores were evaluated by N_2 physisorption at 77K. The results shown in Table 4.1 indicate that the SSOD nanoparticles have a higher pore volume and pore diameter when compared to the HSOD nanoparticles. The reduced pore volume of HSOD can be attributed to the occlusion of the micropores by water molecules in the HSOD structure (Daramola et al., 2015). The increased pore volume of the SSOD nanoparticles is indicative of the successful topotactic conversion synthesis of SSOD nanoparticles; hence, micropores were unoccluded (Eden and Daramola., 2020).

Table 4.1: BET data of SSOD and HSOD nanoparticles

Nanoparticles type	BET surface area (m^2/g)	Pore volume (cm^3/g)	Pore diameter (nm)
SSOD	200.45	0.242	4.83
HSOD	201.44	0.115	2.29

4.2.3. Crystallinity and purity of synthesized nanoparticles

The formation of pure HSOD crystals was confirmed in Figure 4.2(a) as reported in literature. The major peaks at 15, 25, 32, 35, and 43 2θ are consistent with pure HSOD in literature (Khajavi et al., 2010; Musyoka et al., 2011; Naskar et al., 2011; Nabavi et al., 2014; Daramola et al., 2015; Gobald et al., 2017; Eterigho-Ikelegbe et al., 2020). The reference from the Driffrac.Eva software identified HSOD as Sodium Aluminum Silicate Hydrate ($Na_6(AlSiO_4)_6.4H_2O$). All the peaks of powder XRD in Figure 4.2(b) correspond to those recorderd on the database for SSOD, and to those produced by other researchers without impure crystalline phases (Moteki et al., 2008; Moteki et al., 2011; Koike et al., 2017; Eden and Daramola., 2020). The SSOD pattern waas identified as Silica sodalite, dehydrated (C_2H_7NO)(Si_6O_{12}) by the reference. HSOD exhibit good crystalinity as it has sharp peaks on the XRD patterns while SSOD is a bit amorphous

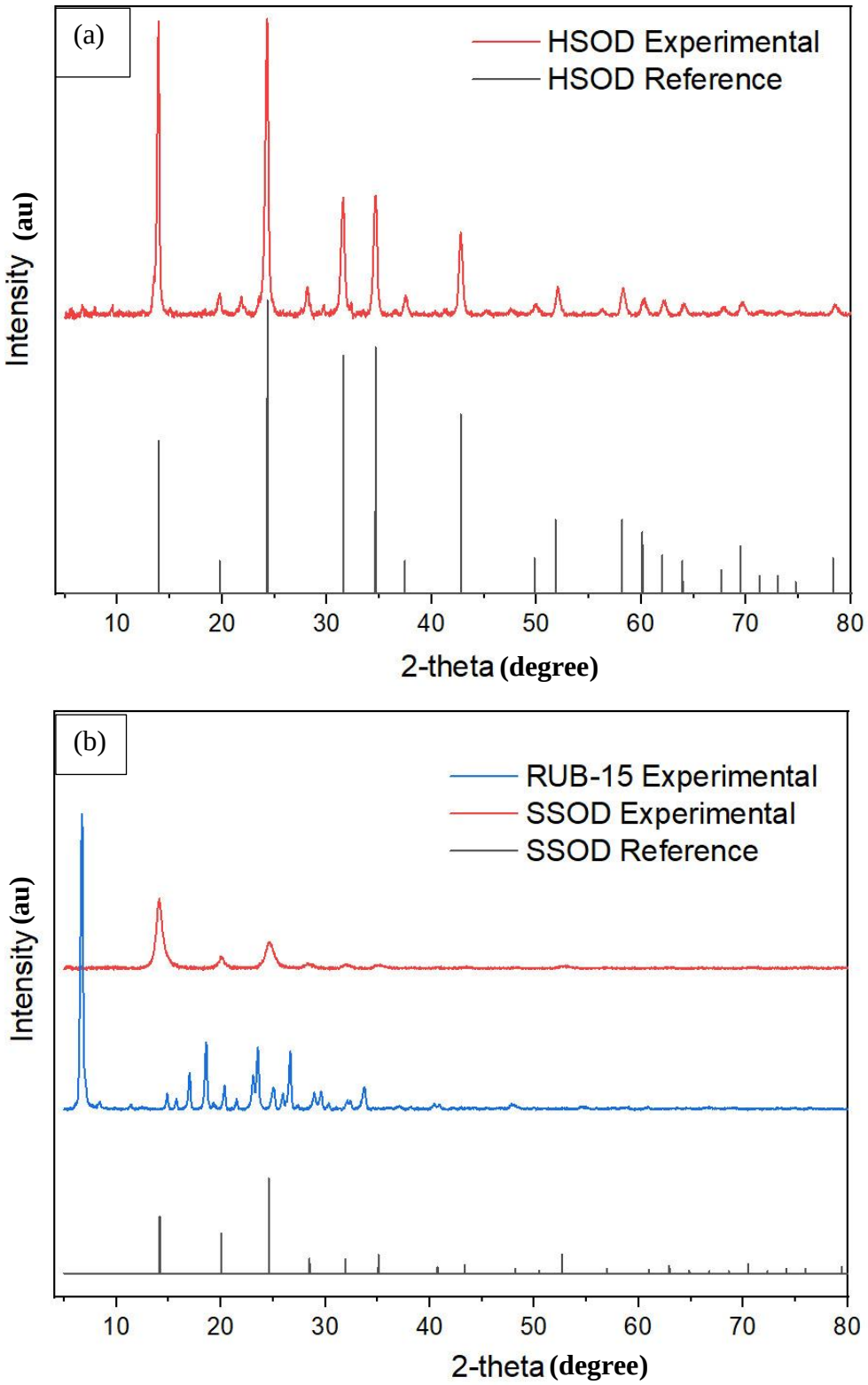


Figure 4.2: XRD patterns for (a) HSOD and (b) RUB-15 and SSOD nanoparticles

FTIR was used to determine the types of bonds and functional groups in the nanoparticles formed. The stretch of the bands indicates the bond lengths. These can be symmetric, where the bonds stretch simultaneously hence achieve similar lengths, and can be asymmetric, where the bonds length are not equal.

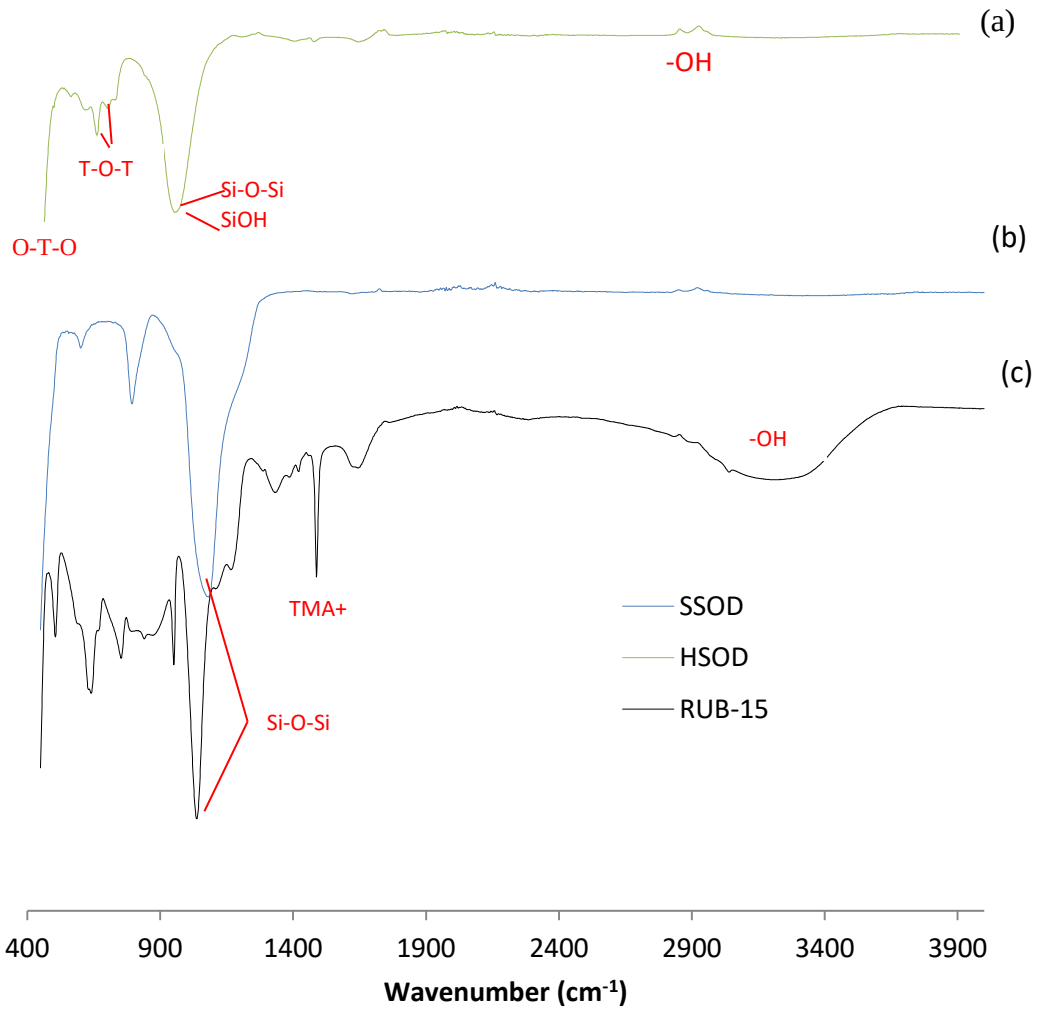


Figure 4.3: FTIR spectra of RUB-15, SSOD, and HSOD nanoparticles

The HSOD spectra (Figure 4.3(a)) shows a sharp absorption band at ~459 cm^{-1}, indicative of the bending vibration of O-T-O (T=Si, Al) (Naskar et al., 2011). The presence of the symmetric stretch band T-O-T at 663 and 734 cm^{-1} can also be observed on the HSOD spectrum (Daramola et al., 2015). The covalent bonds in the 1000-1200 cm^{-1} region (959,

1080 and 1039 cm^{-1} for HSOD, SSOD and RUB-15 respectively) are said to show the existence of a dense silica network where the oxygen atoms play the role of bridges between each two silicon sites, these are asymmetric stretching vibrations of T-O-T (Al-Oweini and El-Rassy, 2009). According to Al-Oweini and El-Rassy (2009), the stretching vibration band centred at ~ 959 cm^{-1} for HSOD is also indicative of the silanol (SiOH) group and that at 1651 cm^{-1} corresponds to the absorbed water molecules.

According to Eden and Daramola (2020), the deformation vibrations at 1488 cm^{-1} and the symmetric and asymmetric stretching vibrations at 3200 cm^{-1} and 3000 cm^{-1} respectively are indicative of the presence of tretramethylammonium cations (TMA^{+}) in the RUB-15 spectra. The -OH band at 3000-3500 cm^{-1} asssigned to the silanol group on the RUB-15 spectra dissappeared on the SSOD spectre due to calcination. This indicates the absence of occluded water molecules, resulting in free porous sodalite cage structures (Eden and Daramola, 2020). These spectres correspond to those reported in literature (Naskar et al., 2011; Daramola et al., 2015) for HSOD while other authors reported for SSOD (Koike et al., 2017; Eden and Daramola, 2020).

4.2.4. Thermal behaviour of nanoparticles (TGA)

The thermal behaviour of the SSOD and HSOD nanoparticles is shown in Figure 4.4. It can be observed that at temperatures below 100°C, there is a rapid weight loss due to the removal of physically adsorbed water. At temperatures above 140°C, there is a gradual weight loss (1.4%), indicating the decomposition of interlayer propionic acid in the SSOD particles (Moteki et al., 2011).

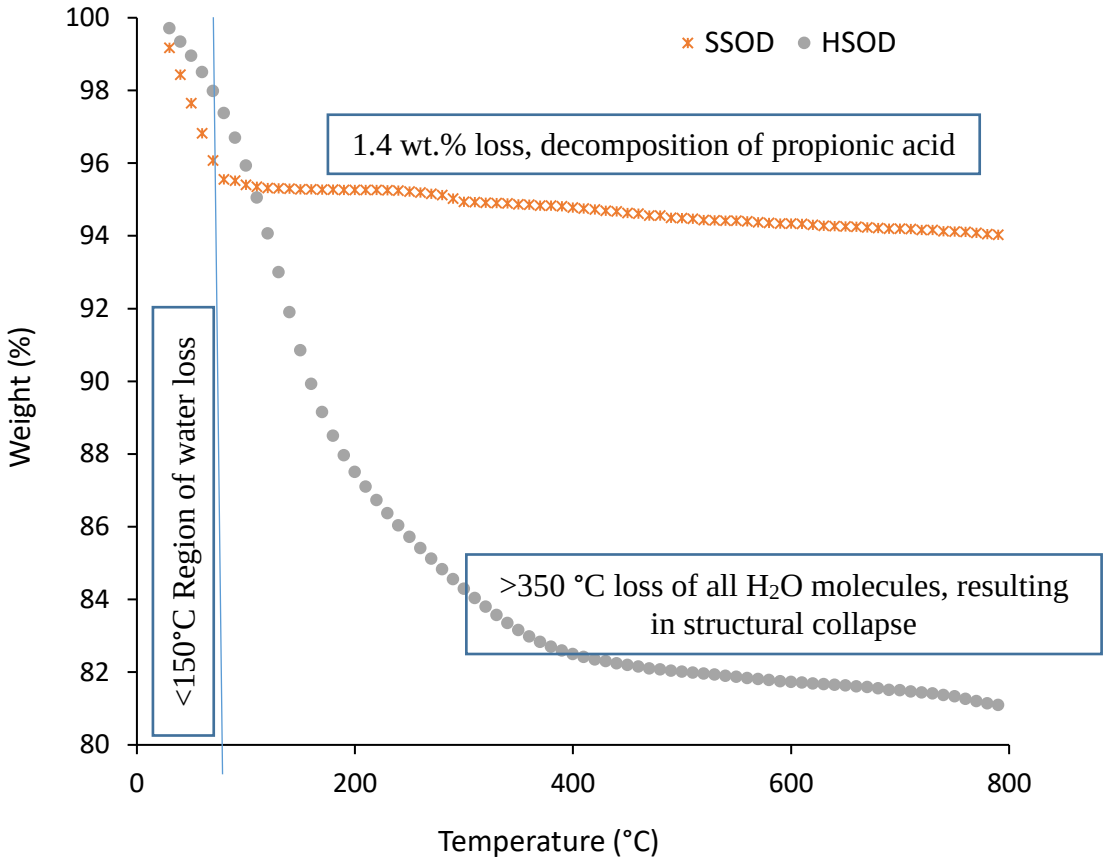


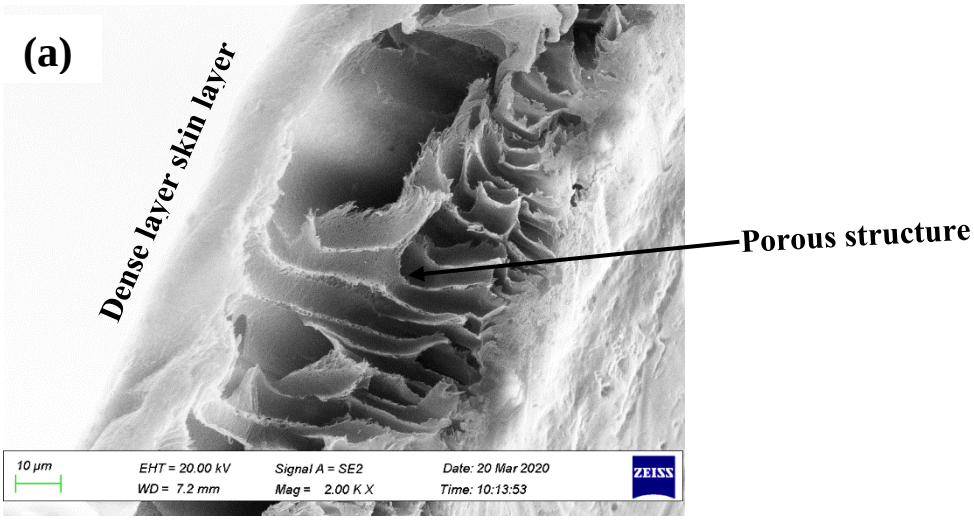
Figure 4.4: SSOD and HSOD Thermo gravimetric weight loss analysis

The hydrophilic HSOD has the molecular formula $Na_6[AlSiO_4]_6(OH)_2.nH_2O$ ($0<n\leq4$) which forms a framework with four and six oxygen membered rings resulting in a cage structure called a β-cage . The TG analysis also shows the two dehydration regions of this molecule as its cages are loaded with water molecules from the synthesis. (1) 9.2% weight loss below 150°C, this is said to correspond to the loss of about one water molecule per β-cage which changes the molecular formula to $Na_8[AlSiO_4]_6(OH)_2.2H_2O$ (Khajavi et al., 2010). (2) Further 7.7% weight loss at 350°C indicates the release of all four hydrate water molecules per unit cell, this changes the molecular formula to $Na_8[AlSiO_4]_6(OH)_2$, which implies the collapse of the molecule framework (Khajavi et al., 2010).

4.3. Membrane characterization

4.3.1. Morphology (SEM) and topology of membrane

The cross-sectional images of the synthesized membranes are shown in Figure 4.5(a-e). Figure 4.5(a) shows the porous structure of Psf with a dense skin layer. The successful loading of nanoparticles is shown in Figure 4.5 (b-e) for 5%HSOD/Psf, 5%SSOD/Psf, 10%HSOD/Psf and 10%SSOD/Psf, respectively. It must be acknowledged that there is an uneven distribution of the nanoparticles within the polymer matrix (clearly visible in Figure 4.5(b)). This is explained by Daramola et al. (2015) as an attribute of ineffective dispersion method used during the synthesis of the membranes. These images indicate that the nanoparticles were successfully infused into Psf to form Psf/*x*SOD matrix membranes (x=H or S).



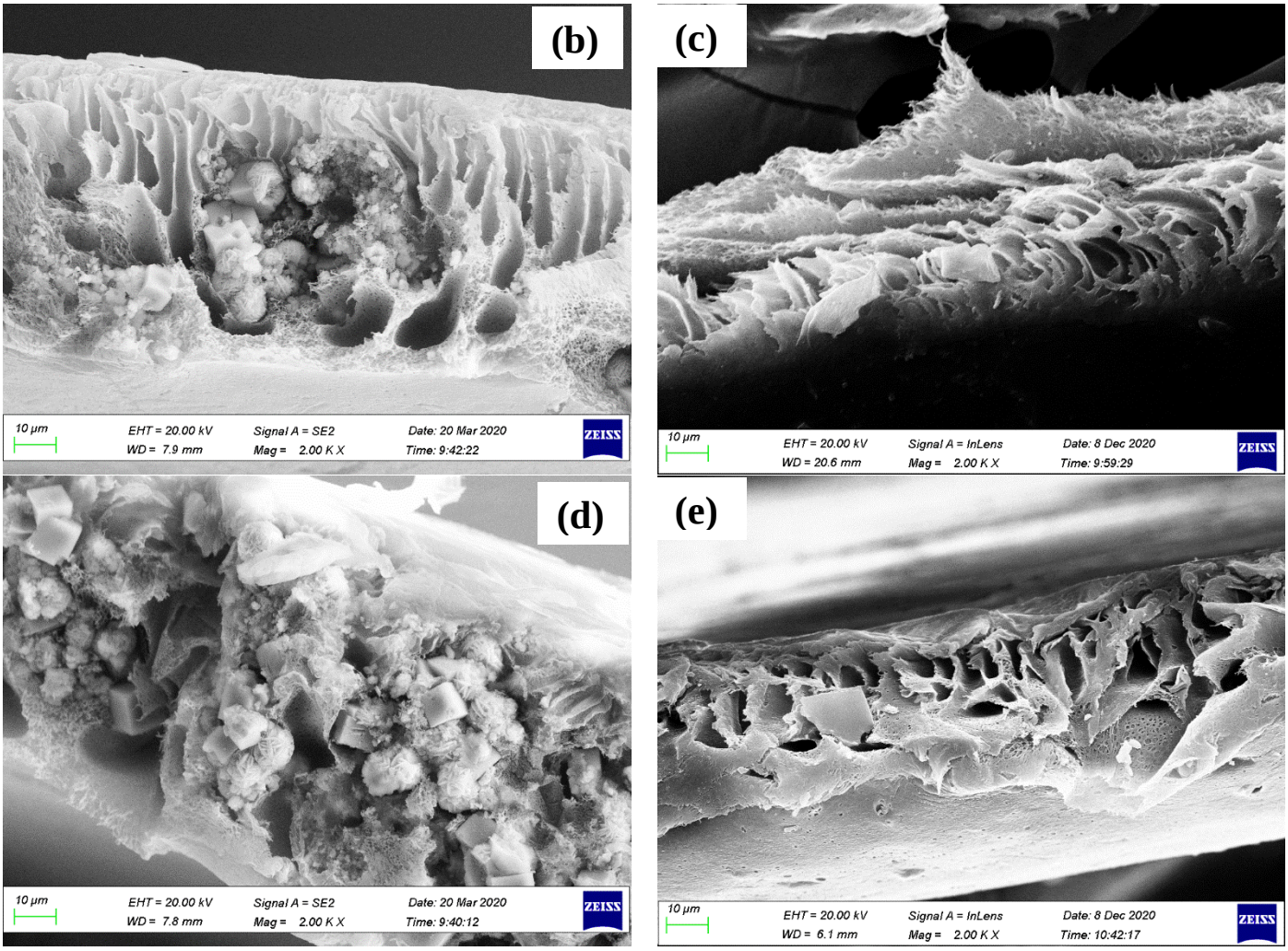


Figure 4.5: Cross sectional SEM images of (a) Psf, (b) 5%HSOD/Psf, (c) 5%SSOD/Psf, (d) 10%HSOD/Psf, and 10%SSOD/Psf.

The surface roughness of the membranes was evaluated by the contact mode Atomic Force Microscopy (AFM). An area of 2×2 μm^2 was analysed as shown in Figure 4.6 and surface roughness parameters obtained as depicted in Figure 4.7. The root mean square (R_{ms}) is the standard deviation of all the vertical distances within the enclosed area and the average roughness (R_a) of the membrane is the mean roughness of the surface relative to the centre plane (Singh et al., 1998). When these parameters are low, they imply that the surface is smooth and less susceptible to fouling; hence, it is expected that there will be a reduced ability of contaminants to accummulate on the membrane surface (Hoek et al., 2003; Rameetse et al., 2020).

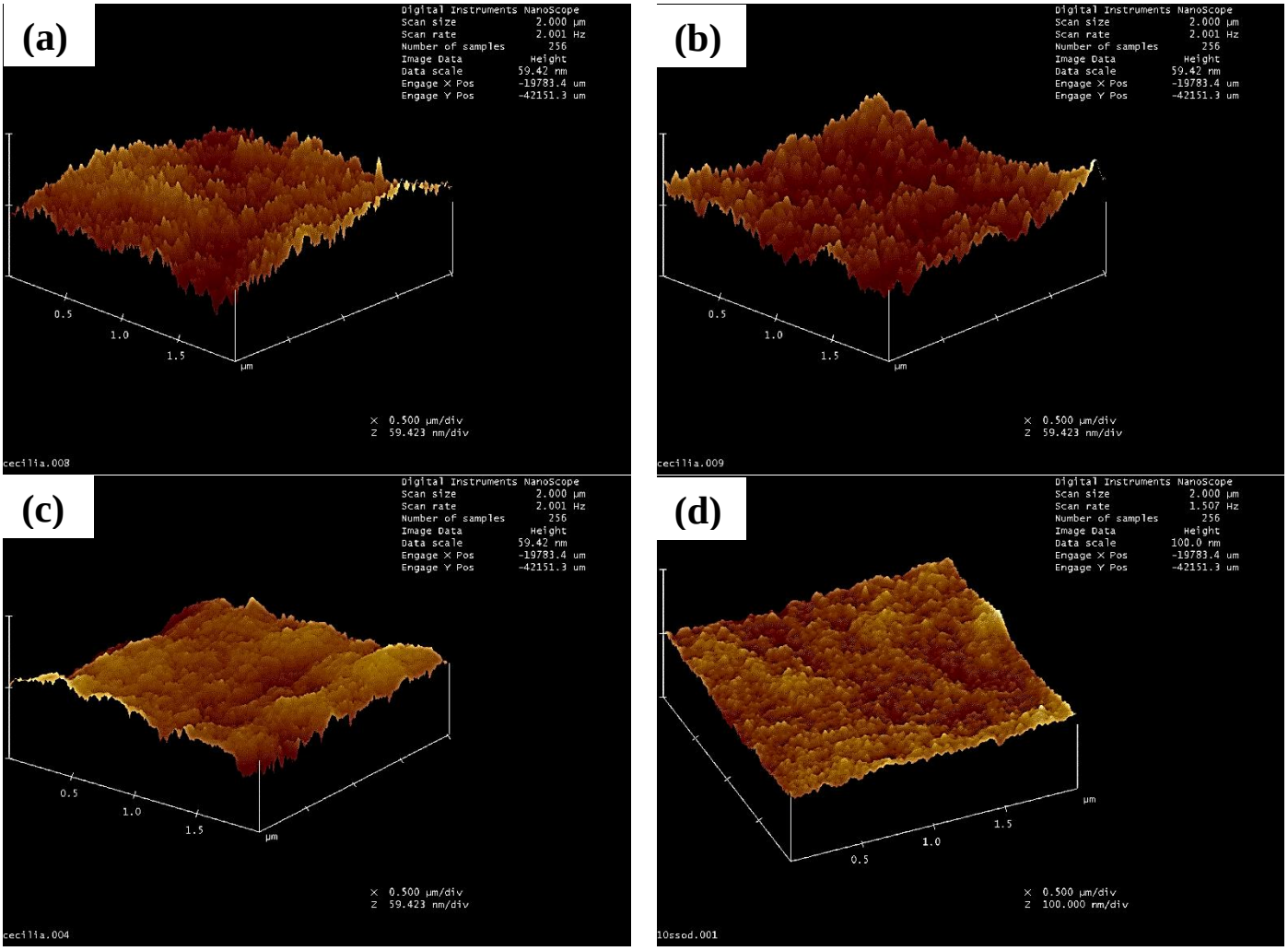


Figure 4.6: AFM images of (a) 5%HSOD/Psf, (b) 10%HSOD/Psf, (c) 5%SSOD/Psf and (d) 10%SSOD/Psf

It can be observed that the HSOD loaded membranes have high roughness parameters with 5%HSOD/Psf having the highest at R_{ms} of 7.94 nm and R_a of 6.29 nm. These results show that the SSOD loaded membranes are less susceptible to fouling when compared to HSOD loaded membranes as they have low roughness parameters.

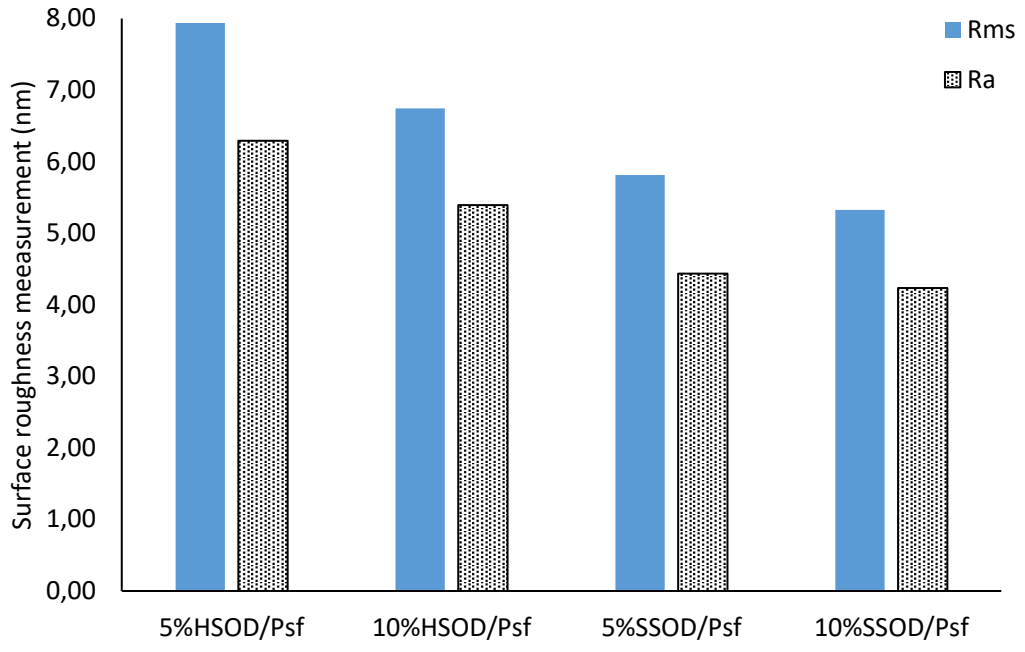


Figure 4.7: Membranes surface roughness evaluation

4.3.2. Membrane thermostability (TGA)

Figure 4.8 shows the thermogravimetric analysis (TGA) of the synthesized membranes, representing regions of weight loss. In the temperature range 20-200 °C, the weight (%) lost by the membranes in the descending order is 1.45%, 1.25%, 0.81%, 0.68%, and 0.45% for Psf, 10%HSOD/Psf, 5%HSOD/Psf, 10%SSOD/Psf and 5%SSOD/Psf respectively. This is said to be due to the water that was absorbed during the phase inversion (Li et al., 2009). The HSOD loaded membranes lost more weight in this region when compared to the SSOD loaded membranes. This is because, at temperatures around 150°C, the HSOD nanoparticles begin to lose about one water molecule per β-cage which changes the molecular formula to $Na_6[AlSiO_4]_6(OH)_2.2H_2O$ (Khajavi et al., 2010).

The solvent (N,N dimethylacetamide) with a boiling point of 165°C is also lost in this temperature range. At this region, the HSOD loaded membranes appear to have lost a lot of weight when compared to the SSOD loaded membranes. This can be attributed to HSOD

being more hydrophilic (Li et al., 2009). This is in agreement with Figure 4.4 which showed that HSOD loses more water content in this region. Second region between 200-500°C indicates the membranes stable region.

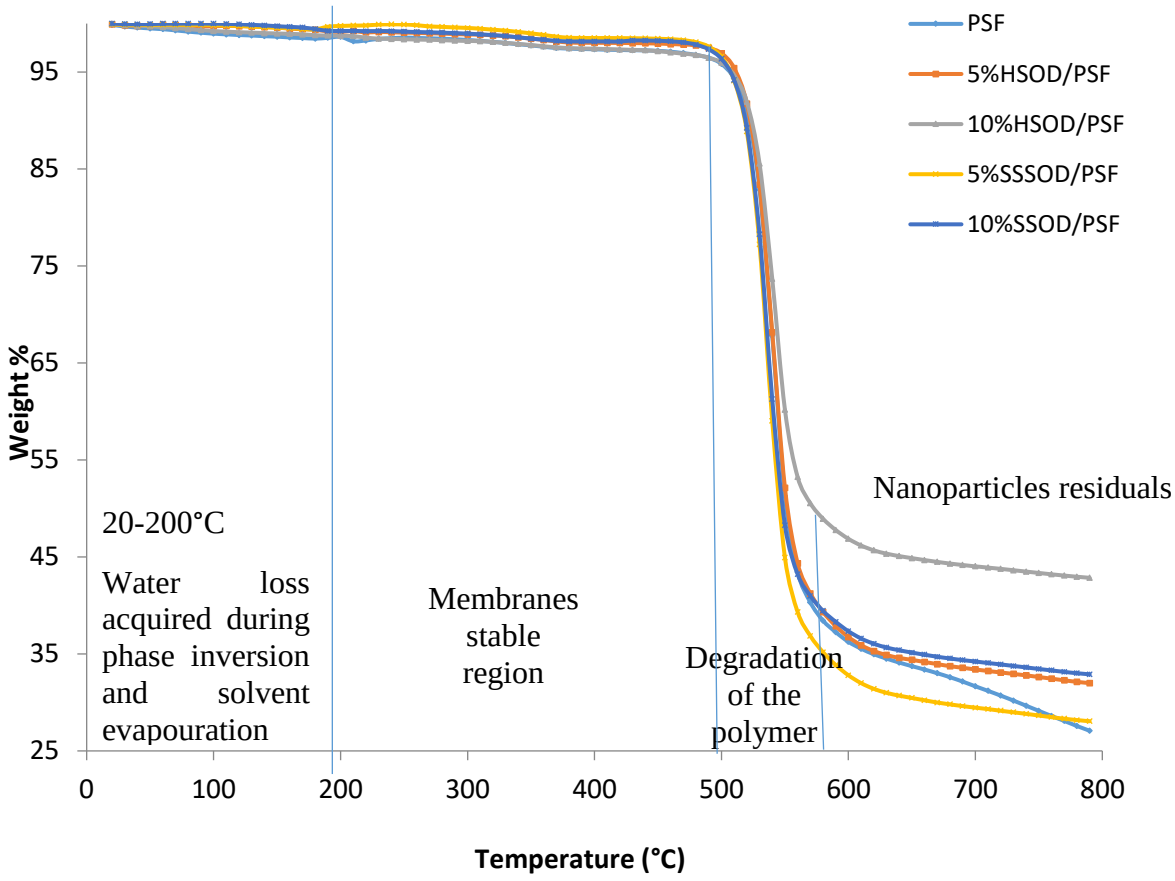


Figure 4.8: Thermogravimetric analysis curve for the sodalite loaded membranes

The third region at 500-600°C, indicates the total decomposition of the membranes. The residuals for 10%HSOD/Psf, 10%SSOD/Psf, 5%HSOD/Psf and 5%SSOD/Psf of 42.85, 32.90, 31.99, and 28.06%, respectively, as depicted in the fourth region (600-800°C) can be assigned to the sodalite crystals (Li et al., 2009). This is in agreement to the amount of nanoparticles loaded on the polymer, hence 10wt.% loaded membranes had more residual when compared to 5wt.% loaded membranes. Despite SSOD being able to withstand high temperatures more than HSOD as was depicted in Figure 4.4, it appears to have been degraded more than HSOD. This can be accounted by the uneven dispersion of SSOD in

the polymer matrix due to the formation of agglomerates. Hence it is possible that the analysed pieces of the membrane contained less nanoparticles than anticipated.

It can be observed that the loading of nanoparticles in the polymer matrix enhances the thermostability of the membranes. On the loaded membranes, the most stable membrane is 10%HSOD/Psf membrane being able to withstand high temperatures up to 800°C with 57.85% weight loss while the least thermostable membrane was Psf with a total weight loss of 72.92%.

4.3.3. Porosity, mean pore size and contact angle

The EWC is said to have a close relation to the pure water flux as flux relies on the number of pores on the surface of the membrane (Rameetse et al., 2019). Table 4.2 shows an enhanced porosity and water uptake on membranes loaded with HSOD nanoparticles when compared to the unloaded Psf membrane. This can be attributed to the hydrophilic HSOD nanoparticles which are able to attract water molecules to their structure. SSOD loaded membranes have a more reduced water uptake and porosity. This is because the loading of SSOD nanorpaticles onto Psf makes the membrane to be more hydrophobic; hence it cannot absorb enough water.

Table 4.2: Porosity (%) and EWC (%) of the membranes

Membrane	EWC (%)	Porosity (%)
Psf	21.51	16.45
5%HSOD/Psf	29.96	17.85
5%SSOD/Psf	6.02	3.84
10%HSOD/Psf	40.45	39.93
10%SSOD/Psf	15.06	9.61

Futhermore, the HSOD loaded membranes appear to be more porous than the SSOD membranes. This is corroborated by the results obtained for the textural properties of the nanoparticles as HSOD was found to have larger pore volume. An increase in mean pore size can also be observed when SOD loading is increased, similar results were observed in literature (Ahmad et al., 2011).

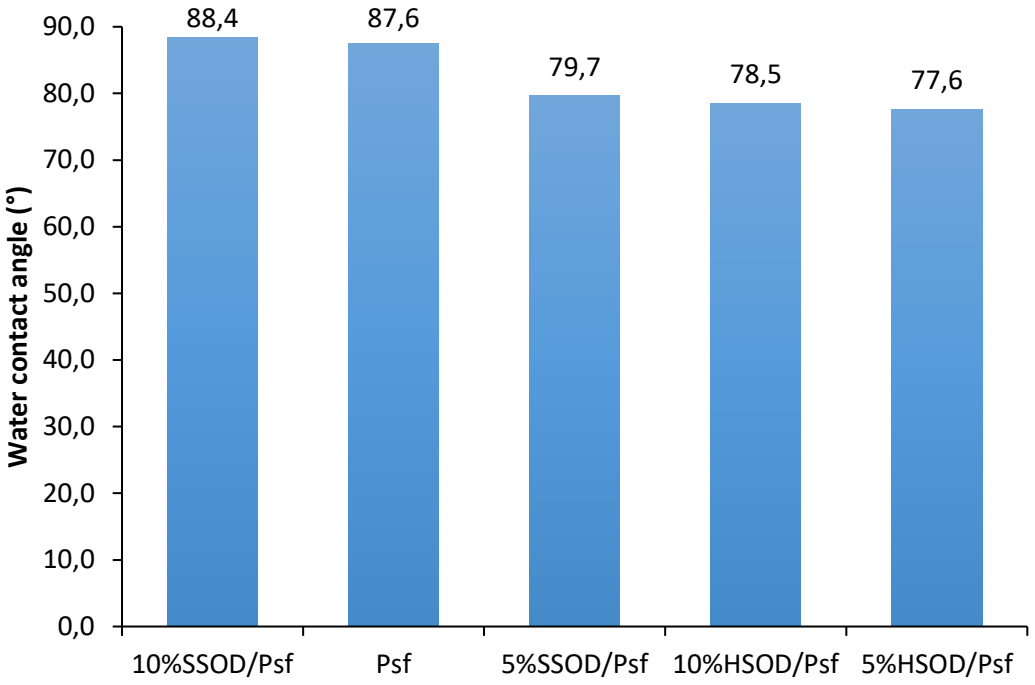


Figure 4.9: Contact angles of sodalite infused polysulfone composite

The contact angle of the synthesized membranes was measured by the sessile drop method. A high contact angle value is said to indicate a hydrophobic surface while hydrophilic surfaces are characterized by small contact angle values (Sun et al., 2010). Figure 4.9 shows the contact angles of the synthesized membranes. The SSOD loaded membrane had the highest contact angle, this indicates that loading SSOD onto the Psf matrix further increases the hydrophobic nature of Psf as SSOD nanoparticles are naturally hydrophobic. The HSOD membranes shows the smallest contact angle as HSOD introduces its hydrophilicity into Psf, hence the reduced contact angles. It can be concluded that HSOD loaded membranes are more hydrophilic when compared to SSOD loaded membranes.

4.3.4. Mechanical strength (young modulus and tensile strength)

TA.XT plus texture analyser was used to measure the breaking strength (tensile strength) and the breaking strain. Figure 4.10 shows a 25% and 10% reduction in young modulus and tensile strength, respectively, for 10%HSOD/Psf when compared to pure Psf membrane. This deviates from what has been reported in literature (Daramola et al., 2015). This can be attributed to the uneven distribution of nanoparticles. In the contrary, infusing Psf with the SSOD nanoparticles resulted in 18% increase of the young modulus of Psf whereas the tensile strength was reduced by 9%. Similar trend was observed by Eden and Daramola (2020), which was explained as being caused by the restriction of polymer chain movement by the increased formation of hydrogen bonds between the polymer and large agglomerates

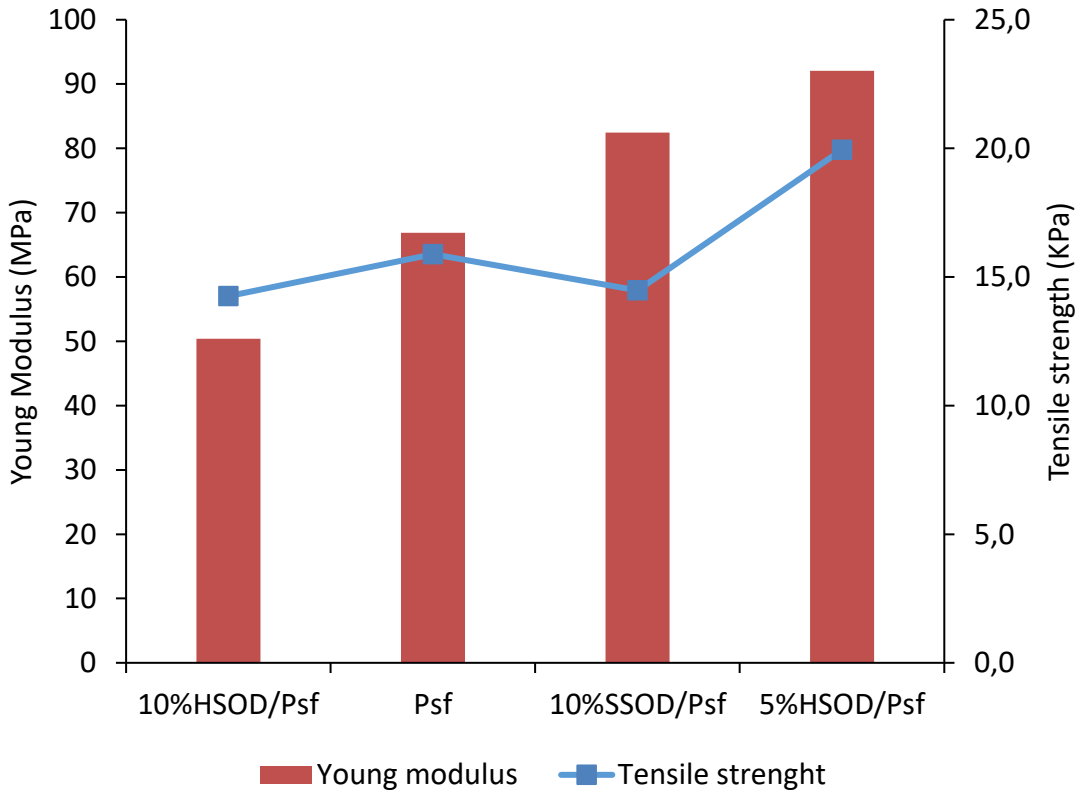


Figure 4.10: Tensile strengths and Young Modulus of the sodalite infused polysulfone membranes

4.3.5. Surface chemistry (FTIR)

Figure 4.11 shows the FTIR spectra of the pure Psf membrane and the sodalite loaded membranes. All the sodalite loaded membranes have a spectrum similar to that of Psf, implying that the presence of sodalite has no significant impact on the Psf surface chemistry. Similar results were observed by Mathaba and Daramola (2020) in PES/Chitosan membranes. The Psf spectra is consistent with previous studies (Rafiq et al., 2012; Nadour et al., 2017).

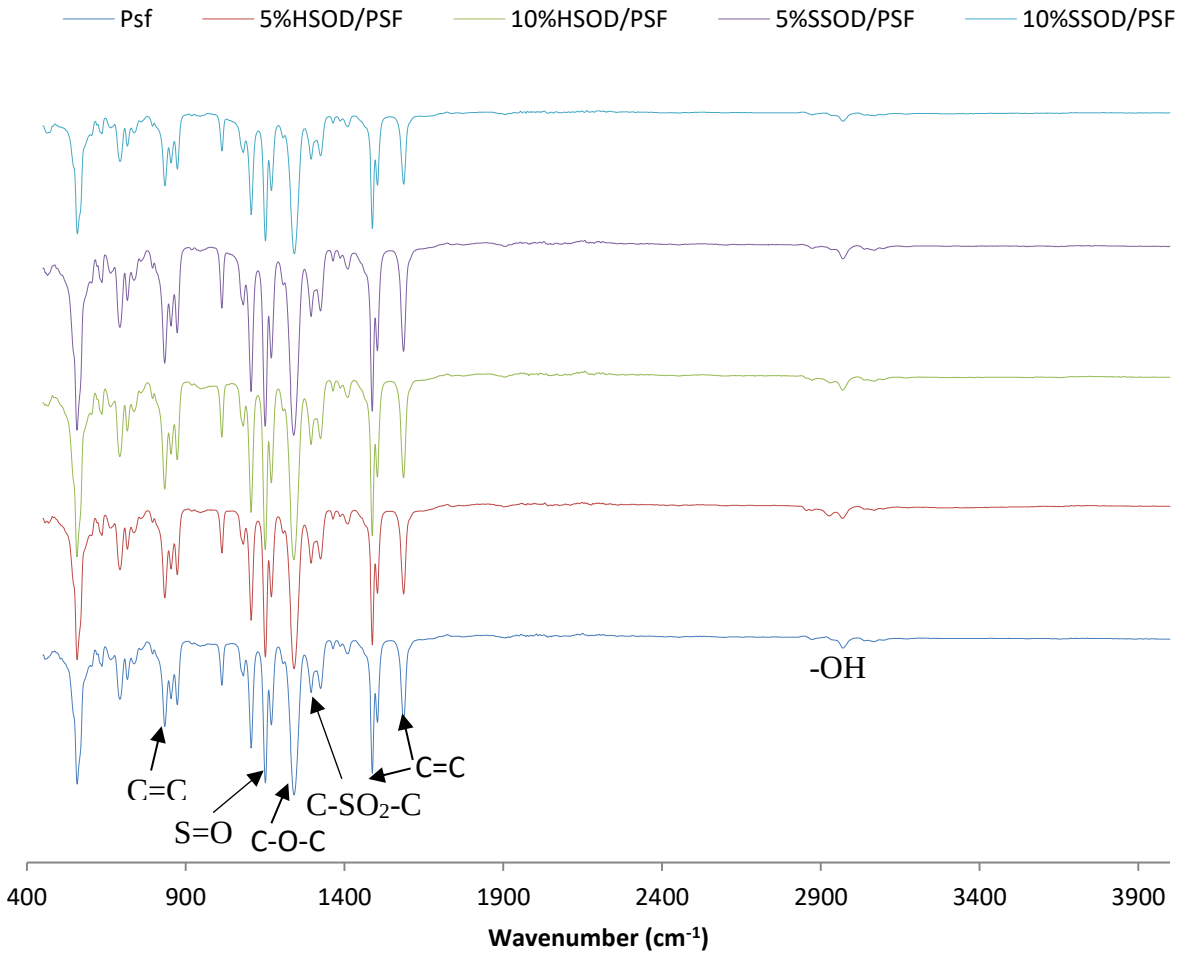


Figure 4.11: FTIR spectra of the synthesized membranes

4.4. Performance evaluation of membrane

4.4.1. Pure water flux

Deionized water was permeated on a membrane at a specific pressure for a duration of one hour in a dead-end filtration cell. A volume of collected permeate after one hour was recorded, and flux was calculated according to Equation 3.6. Figure 4.12 shows the pure water flux for the different membranes at specific pressures. It shows that increasing the transmembrane pressure and the nanoparticles loading also increases the water flux, similar results were observed in literature (Zhong et al. 2007; Vatanpour et al., 2011).

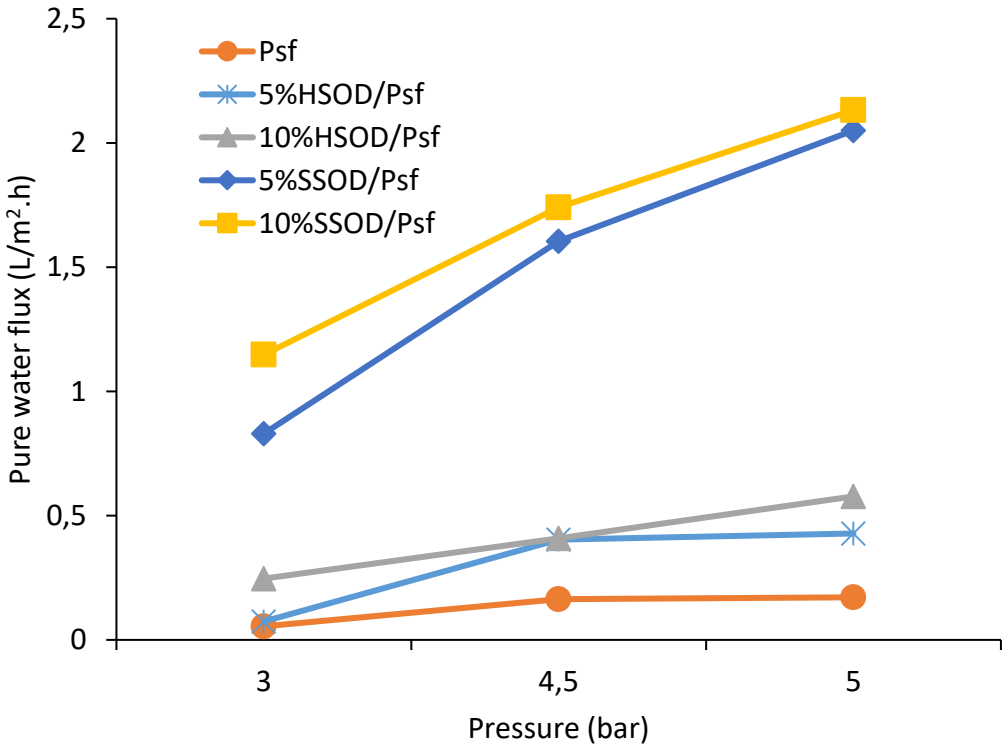


Figure 4.12: Membranes pure water flux at different transmembrane pressures

Membrane permeability is influenced by hydrophilicity, the pore size and structure of the membrane (Vatanpour et al., 2011). Hence the permeability of these membranes correspond to the increased pore size of 4.83 nm and 2.29 nm pore diameter for SSOD and HSOD as discussed in section 4.2.1. The hydrophilic groups of HSOD (Figure 4.3)

improved the hydrophilicity of the Psf membrane by ~60% and ~71% when loaded by 5% HSOD and 10% HSOD, respectively. The enhanced permeability of HSOD membranes when compared to the Psf membrane is also attributed to the increased permeation channels created by the HSOD nanoparticles with cage diameter of ~2.6 $\dot{A}$ which allow the water molecules (kinetic diameter ~2.65$\dot{A}$) to pass easily (Daramola et al., 2015). It is also evident that membranes loaded with SSOD had high water permeation compared to membranes loaded with HSOD, this can be attributed to the size of the nanoparticles as SSOD has large particle size compared to HSOD. Although the 10%SSOD loaded membrane was expected to be less hydrophilic as it had higher contact angle of 88.4°, the permeability was enhanced by the SSOD nanoparticles size which is 53% more than that of HSOD.

4.4.2. Separation performance

4.4.2.1. Membrane flux

Figure 4.13 shows the AMD sample flux collected for the different fabricated membranes in a continuous period of 3 hours at a pressure of 4 bar. It can be observed that the amount collected over time decreases as the membrane remains in operation; a similar trend was observed in literature (Ayyaru & Ahn, 2017). This can be attributed to the metal ions (retentate) that are being deposited over time on the surface of the membrane as permeate leaves the system. These ions are said to block the pores of the membrane surface in one of four mechanisms (complete blocking of pores, intermediate blocking of pores, constriction of pores, and cake layer formation), hence reduced membrane performance (Aly, 2015; Abbasi et al., 2012). Another trait that can be observed is that the Psf membrane had a high flux initially (5.2 $L.m^{-2}.h^{-1}$) which then dropped drastically (93%) within a period of 2 hours. This shows that the non-loaded membrane is more susceptible to fouling, as it is hydrophobic hence the hydrophobic foulant molecules are driven to the membrane surface

(Ahmad et al., 2011; Kumar & Ismail, 2015). The increase in water flux with increasing loading of nanoparticles is also observed in this case as in pure water flux.

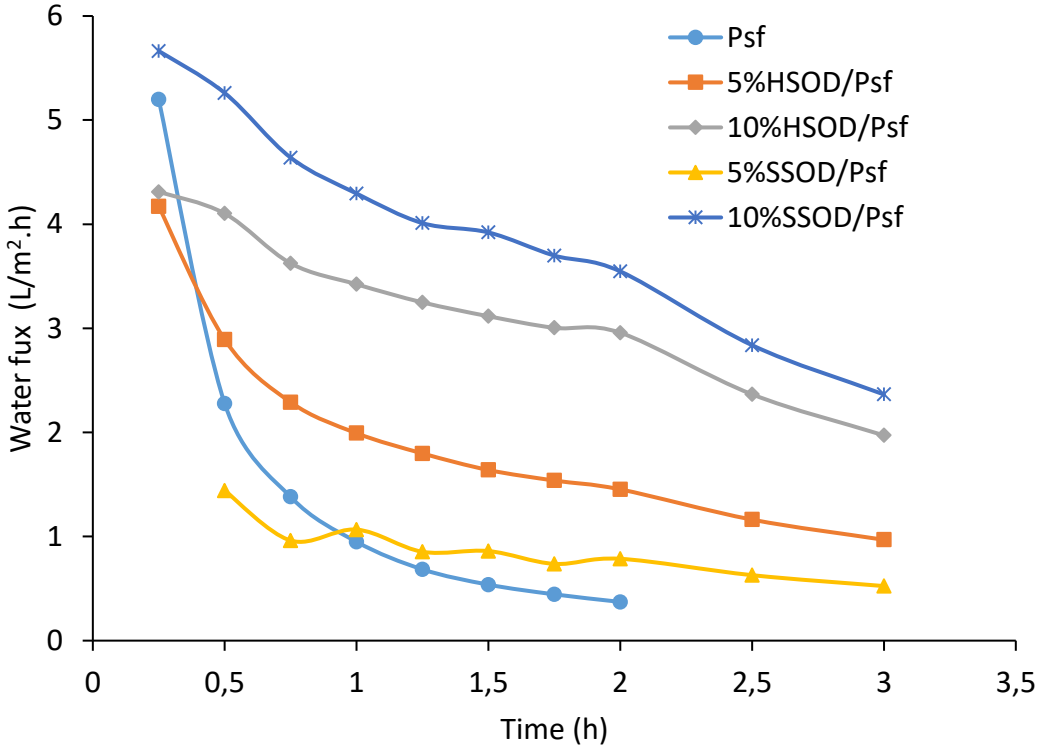


Figure 4.13: Water flux from different membranes

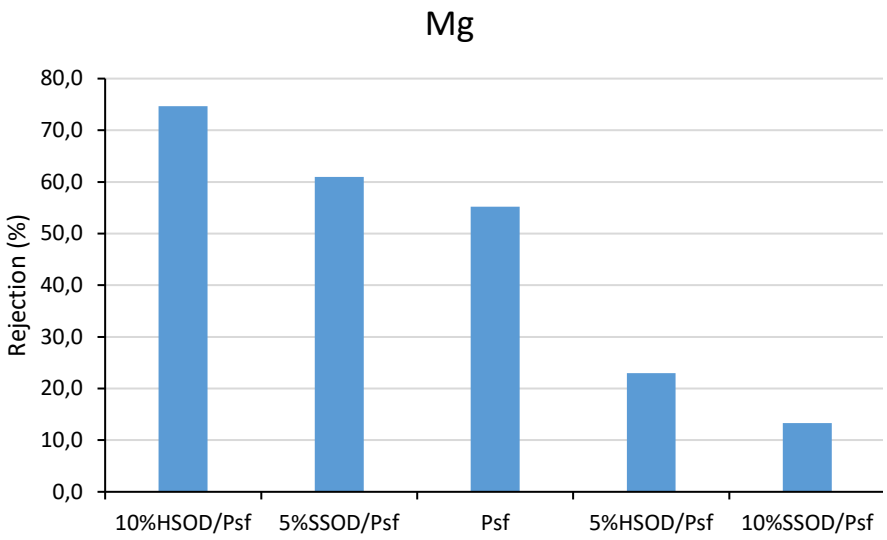
4.4.2.2. Membrane selectivity

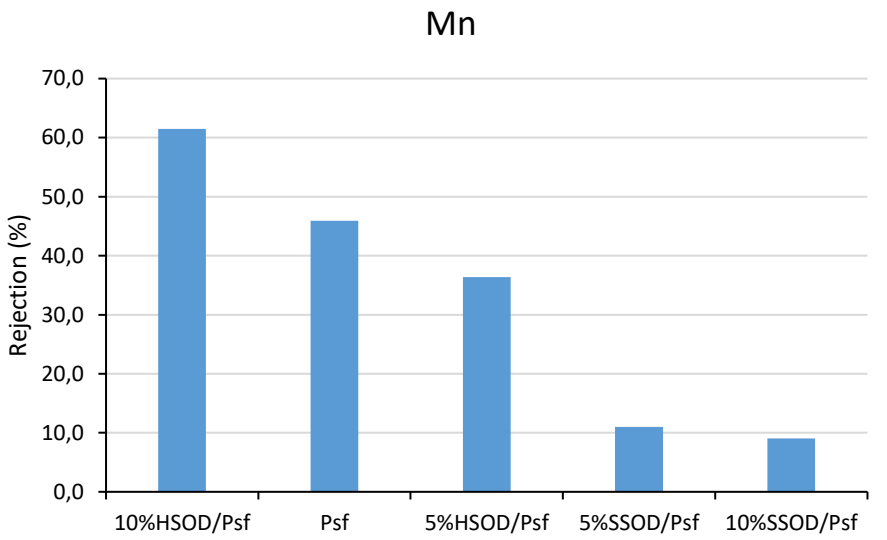
The percentage metal rejection was obtained as shown in Figure 4.14. The pore size of the membranes and cage diameters of the nanoparticles allow the water to be preferentially filtered through by the sorption-diffusion mechanism and preferential sorption capillary flow (PSCF) model (Sourirajan, 1963; Daramola et al., 2015). This explain how the water molecules are preferentially adsorbed to the hydrophilic membrane surface and transported through the membrane pores, then be released as permeate while leaving the retentate behind (Daramola et al., 2015).

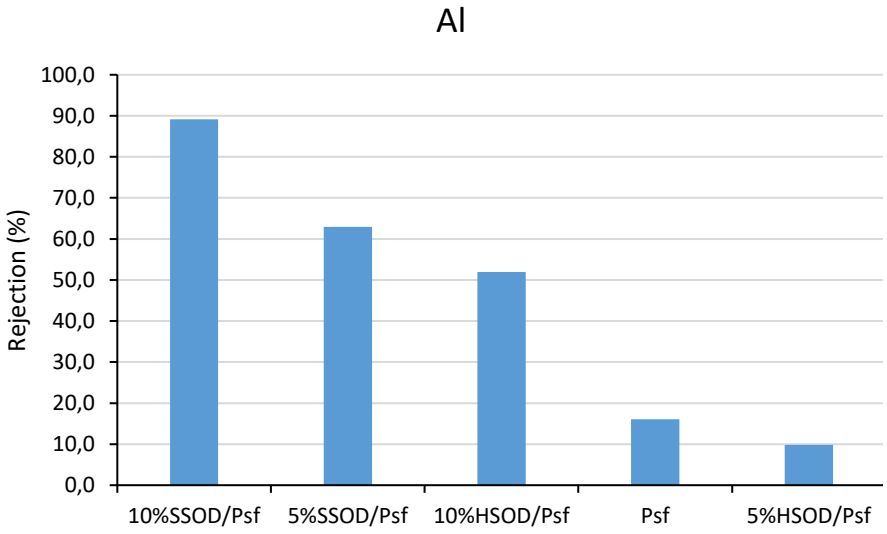
A maximum rejection of 89.1%, 74.7%, 65.8%, 61.5%, 57.4% and 37.7% for Al^{3+}, Mg^{2+}, Fe^{3+}, Mn^{2+}, Ca^{2+}, and Na^{2+}, respectively, was obtained as shown in Figure 4.14. These

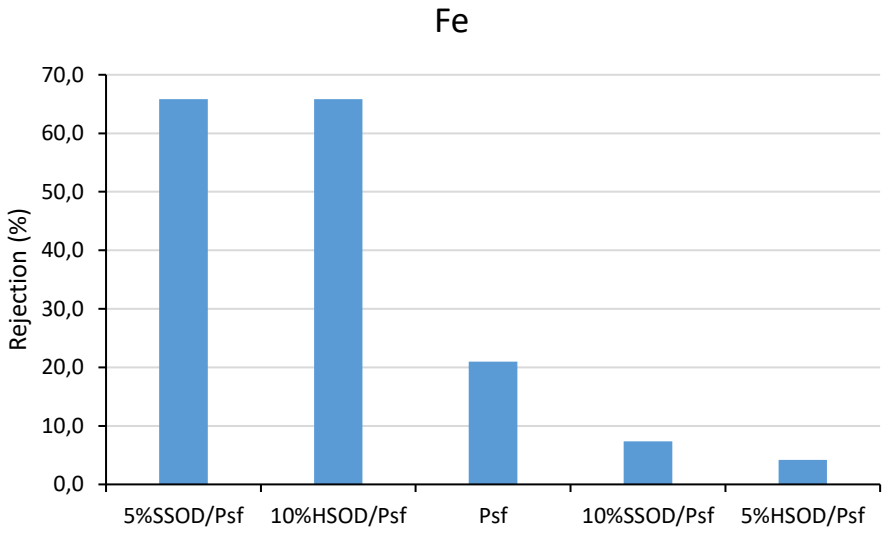
results are higher than results that have been reported in literature for HSOD infused membranes by Daramola et al. (2015). This is likely because the sample concentration used in this study had low concentrations. The maximum rejection was generally obtained from membranes with 10% nanoparticles loading except for Fe^{3+}. This can be attributed to the increased surface area of nanoparticles on highly loaded membranes, hence increased active sites.

The maximum rejection was obtained mostly from 10%HSOD/Psf membrane. This can be attributed to the small BET pore diameter (2.29 nm) when compared to that of SSOD (4.83 nm). Smaller particles size are favourable as they can provide a more polymer/particle interfacial area hence improved separation (Chung et al., 2007; Bose et al., 2004). The 10%SSOD/Psf membrane produced some of the lowest rejection at 10.8% for Ca^{2+} 9.1% for Mn^{2+} and 13.3% for Mg^{2+}. Nevertheless, the 5%SSOD/Psf membrane showed some promising results as it had the second highest rejections following 10%HSOD/Psf in most metal ion. The reduced rejection in 10%SSOD/Psf is likely due to the increased agglomeration of the SSOD nanoparticles resulting in pore blocking, hence an increase in mass transfer resistance (Eden and Daramola, 2020).


Mg
Rejection (%)
80,0
70,0
60,0
50,0
40,0
30,0
20,0
10,0
0,0
10%HSOD/Psf
5%SSOD/Psf
Psf
5%HSOD/Psf
10%SSOD/Psf


Mn
Rejection (%)
70,0
60,0
50,0
40,0
30,0
20,0
10,0
0,0
10%HSOD/Psf
Psf
5%HSOD/Psf
5%SSOD/Psf
10%SSOD/Psf


Al
Rejection (%)
100,0
90,0
80,0
70,0
60,0
50,0
40,0
30,0
20,0
10,0
0,0
10%SSOD/Psf
5%SSOD/Psf
10%HSOD/Psf
Psf
5%HSOD/Psf


Fe
Rejection (%)
70,0
60,0
50,0
40,0
30,0
20,0
10,0
0,0
5%SSOD/Psf
10%HSOD/Psf
Psf
10%SSOD/Psf
5%HSOD/Psf

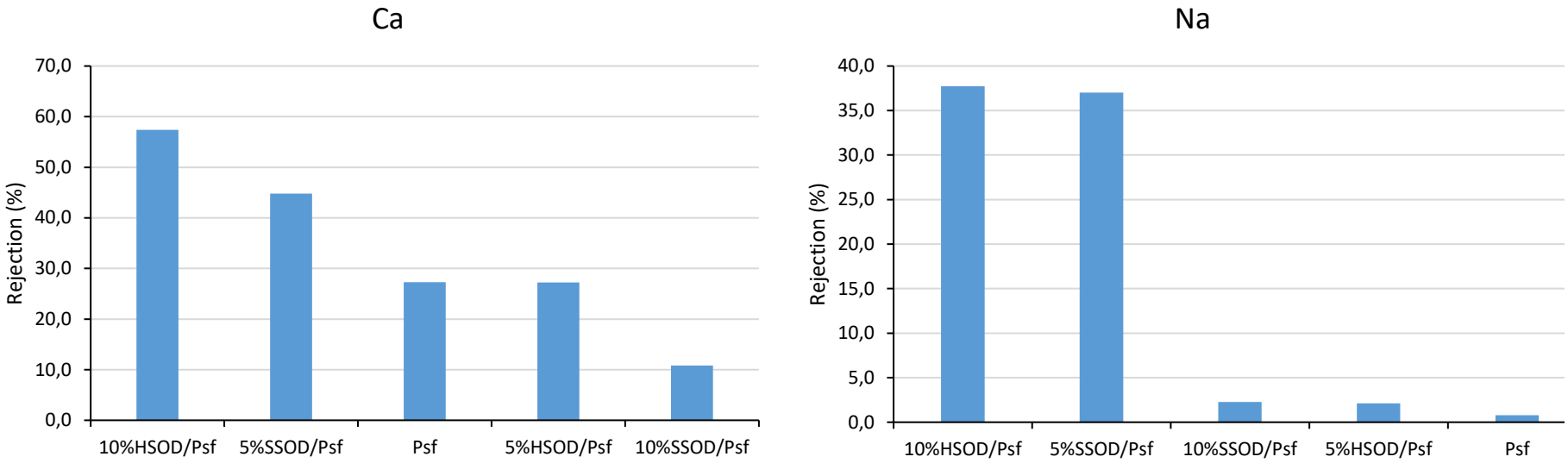


Figure 4.14: Heavy metal rejection from the different membranes

4.5. Summary

In this chapter, HSOD and SSOD nanoparticles were successfully synthesized using hydrothermal synthesis and topotactic conversion, respectively, and were also successfully infused into Psf. The HSOD/Psf and SSOD/Psf composite membranes were successfully synthesized using phase inversion. Synthesized nanoparticles were characterized by SEM, BET, XRD, FTIR, and TGA. While the membranes were characterized by SEM, AFM, TGA, porosity and pore size, mechanical strength, contact angle, and FTIR. The membrane performance was evaluated by membrane water flux and heavy metal rejection. From the results, it was noticed that infusing nanoparticles into Psf enhanced the membrane performance. SSOD loaded membranes showed improved permeability (2.1L/m^2.h for 10%SSOD/Psf at 5 bar) with poor selectivity, while HSOD loaded membranes showed poor permeability (0.60 L/m^2.h for 10%HSOD/Psf at 5 bar) with improved selectivity. As the SSOD loaded membranes show the potential of increased water flux, the following chapter will look at increasing the selectivity of the membranes by modifying the surface of the nanoparticles to be more hydrophilic.

4.6. References

1. Abbasi, M., Sebzari, M. R., Salahi, A., & Mirza, B. (2012). Modelling of Membrane Fouling and Flux Decline in Microfiltration of Oily Wastewater using Ceramic Membranes. *Chemical Engineering Communications*, 78-93. doi:10.1080/00986445.2011.570391

2. Ahmad, A. L., Majid, M. A., & Ooi, B. S. (2011). Functionalized Psf/SiO2 Nanocomposite Membrane for Oil-in-Water Emulsion Separation. *Desalination*, 266-269. doi:10.1016/j.desal.2010.10.017

3. Al-Oweini, R., & El-Rassy, H. (2009). Synthesis and Characterization by FTIR Spectroscopy of Silica Aerogels Prepared Using Several Si(OR)4 and R"Si(OR')3 Precursors. *Journal of Molecular Structure*, 140145. doi:10.1016/j.molstruc.2008.08.025

4. Aly, S. (2015). *PhD Thesis: Pre-Treatment Evaluation Prior to Ultrafiltration in Secondary Effluent Treatment for Water Reuse.* Waterloo: University of Waterloo

5. Ayyaru, S., & Ahn, Y.-H. (2017). Application of Sulfonic Acid Group Functionalized Graphene Oxide to Improve Hydrophilicity, Permeability, and Nanofiltration of PVDF Nanocomposite Ultrafiltration membranes. *Journal of Membrane Science*, 210-219. doi:10.1016/j.memsci.2016.10.048

6. Bose, S., & Mahanwar, P. A. (2004). Effect of Particle Size of Filler on Properties of Nylon-6. *Journal of Minerals & Materials Characterization & Engineering*, 23-31. doi:10.4236/jmmce.2004.31003

7. Chung, T.-S., Jiang, L. Y., & Kulprathipanja, S. (2007). Mixed Matrix Membranes (MMMs) Comprising Organic Polymers with Dispersed Inorganic Fillers for Gas

Separation. *Progress in Polymer Science*, 483-507. doi:10.1016/j.progpolymsci.2007.01.008

8. Daramola, M. O., Silinda, B., Masondo, S., & Oluwasina, O. O. (2015). Polyethersulphone-Sodalite (PES-SOD) Mixed-Matrix Membranes: Prospects for Acid Mine Drainage (AMD) Treatment. *Journal of the Southern African Institute of Mining and Metallurgy, 115*(12), 1221-1228. doi:10.17159/2411-9717/2015/v115n12a11

9. Eden, C. L., & Daramola, M. O. (2020). Evaluation of Silica Sodalite Infused Polysulfone Mixed Matrix membranes during H2/CO2 Separation. *Materials Today: Proceedings*. doi:10.1016/j.matpr.2020.02.393

10. Eterigho-Ikelegbe, O., Bada, S., Daramola, M. O., & Falcon, R. (2020). Synthesis of High Purity Hydroxy Sodalite Nanoparticles via Pore-Plugging Hydrothermal Method for Inorganic Membrane Development: Effect of Synthesis Variables on Crystallinity, Crystal Size and Morphology. *Materials Today: Proceedings*. doi:10.1016/jmatpr.2020.03.639

11. Gobald, S., Khoshnoud, P., & Abu-Zahra, N. (2017). Hydrothermal synhesis of Hydoxy Sodalite from Fly Ash for the Removal of Lead Ions from Water. *International Journal of Scientific and Industrial Technology*, 135-142. doi:10.1007/s13762-016-1133-x

12. Hoek, E. M., Bhattacharjee, S., & Elimelech, M. (2003). Effect of Membrane Surface Roughness on Colloid-Membrane DVLO Interaction. *Langmuir*, 4836-4847. doi:10.1012/la027083c

13. Khajavi, S., Sartipi, S., Gascon, J., Jansen, J. C., & Kapteijn, F. (2010). Thermostability of Hydroxy Sodalite in View of Membrane Applications.

Microporous and Mesoporous Materials, 510-517. doi:10.1016/j.micromeso.2010.03.035

14. Koike, M., Asakura, Y., Sugihara, M., Kuroda, Y., Tsuzura, H., Wada, H., & Kuronda, K. (2017). Topotactic Conversion of Layered Silicate RUB-15 to Silica Sodalite through Interlayer Condensation in N-methylformamide. *Royal Society of Chemistry*, 10232–10239. doi:10.1039/c7dt01287j

15. Kumar, R., & Ismail, A. F. (2015). Fouling Control on Microfiltration/Ultrafiltration Membranes: Effects of Morphology, Hydrophilicity. *Journal of Applied Polymer Science*, 42042-42053. doi:10.1002/app/42042

16. Kundu, D., Dey, B., Naskar, M. K., & Chatterjee, M. (2010). Emulsion-Derived Urchin-Shaped Hydroxy Sodalite Particles. *Materials Letters*, 1630-1633. doi:10.1016/j.matlet.2010.04.015

17. Li, D., Zhu, H. Y., Ratinac, K. R., Ringer, S. P., & Wang, H. (2009). Synthesis and Characterization of Sodalite-Polyimide Nanocomposite Memnbranes. *Microporous and Mesoporous Materials*, 14-19. doi:10.1016/j.micromeso.2009.05.014

18. Mathaba, M., & Daramola, M. O. (2020). Effect of Chitosan's Degree of Deacetylation on the Performance of PES Membrane Infused with Chotosan during AMD Treatment. *Membranes*. doi:10.3390/membranes10030052

19. Moteki, T., Chaikittisilp, W., Shimojima, A., & Okubo, T. (2008). Silica Sodalite without Occluded Organic matters by Topotactic Conversion of Lamellar Precursor.*Journal of the American Chemical Society*,15780. doi:10.1021/ja806930h

20. Moteki, T., Chaikittsilp, W., Sakamoto, Y., Shimojima, A., & Okubo, T. (2011). Role of Acidic Pretreatment of Layered Silicate RUB-15 in its Topotactic Conversion into Pure Silica Sodalite. *Chemistry of Materials*, 3564–3570. doi:10.1021/cm201480x

21. Musyoka, N. M., Petrik, L. F., Balfour, G., Gitari, W. M., & Hums, E. (2011). Synthesis of Hydroxy Sodalite from Coal Fly Ash Using Waste Industrial Brine Solution. *Journal of Environmental Science and Health, Part A*, 1699–1707. doi:10.1080/10934529.2011.623961

22. Nabavi, M. S., Mohammadi, T., & Kazemimoghadam, M. (2014). Hydrothermal Synthesis of Hydroxy Sodalite Zeolite Membrane: Separation of H2/CH4. *Ceramics International*, 5889–5896. doi:10.1016/j.ceramint.2013.11.033

23. Nadour, M., Boukraa, F., Ouradi, A., & Benaboura, A. (2017). Effects of Methylcellulose on the Properties and Morphology of Polysulfone Membranes Prepared by Phase Inversion. *Materials Research*, 339-348. doi:10.1590/1980-5373-mr-2016-0544

24. Naskar, M. K., Kundu, D., & Chatterjee, M. (2011). Effect of Process Parameters on Surfactant Based Synthesis of Hydroxy Sodalite. *Materials Letters*, 463 438. doi:10.1016/j.matlet.2010.11.008

25. Rafiq, S., Man, Z., Maitra, S., Muhhamad, N., & Ahmad, F. (2012). Kinetics of Thermal Degradation of Polysulfone/Polyimide Blended Polymeric Membranes. *Applied Polymer*, 3755-3763. doi:10.1002/app.34862

26. Rameetse, M. S., Aberefa, O. A., & Daramola, M. O. (2019). Synthesis and Characterization of PSF/PES Composite Membranes for Use in Oily Wastewater

Treatment. *Journal of Physics: Conference Series*, (p. 1378). doi:10.1088/1742-6596/1378/2/022013

27. Rameetse, M. S., Aberefa, O., & Daramola, M. O. (2020). Effect of Loading and Functionalization of Carbon Nanotube on the Performance of Blended Polysulfone/Polyethersulfone Membrane during Treatment of Wastewater Containing Phenol and Benzene. *Membranes*, 1-13. doi:10.3390/membranes10030054

28. Singh, S., Khulbe, K. C., Matsuura, T., & Ramamurthy, P. (1998). Membrane Charecterization by Solute Transport and Atomic Force Microscopy. *Journal of Membrane Science*, 111-127. doi:10.1016/S0376-7388(97)00329-3

29. Sourirajan, S. (1963). The Mechanism of Demineralization of Aqueous Sodium Chloride Solutions by Flow, under Pressure, through Porous Membranes. *Industrial Engineering and Chemistry Fundamentals*, 51-55. doi:10.1021/i160005a010

30. Sun, M., Su, Y., Mu, C., & Jiang, Z. (2010). Improved Antifouling Property of PES Ultrafiltration Membrane Using Additive of Silica-PVP Nanocomposite. *Industrial and Engineering Chemistry Research*, 790-796. doi:10.1021/ie900560e

31. Vatanpour, V., Madaeni, S. S., Moradian, R., Zinadini, S., & Astinchap, B. (2011). Fabrication and Characterization of Novel Antifouling Nanofiltration Membrane Prepared from Oxide Multiwalled Carbon Nanotube/ Polyethersulfone Nanocomposite. *Journal of Membrane Science*, 284-294. doi:10.1016/j.memsci.2011.03.055

32. Zhong, C.-M., Xu, Z.-L., Fang, X.-H., & Cheng, L. (2007). Treatment of Acid Mine Drainage (AMD) by Ultra-Low-Pressure Reverse Osmosis and Nanofiltration. *Environmental Engineering Science*, 1297-1306. doi:10.1089/ees.2006.0245

5. Functionalized Silica-Sodalite Infused Polysulfone Composite Membrane

5.1. Introduction

Functionalization is the modification of the materials surface by introducing new functional groups. This is performed to enhance the performance of the specific material. The performance is enhanced by high loading of functional groups, but this may result to poor structural ordering, hence a suitable method must be used (Yokoi et al., 2012). Functionalization can be performed by two methods (1) direct co-condensation or (2) post-synthesis grafting method. Although there are limited studies if any on the functionalization of SSOD nanoparticles, there is evidence that the functionalization of nanoparticles can improve their dispersion on polymer matrix hence improve membrane performance (Li, et al., 2007).

In assessing the HSOD and SSOD loaded membranes performance, it was determined that although the SSOD loaded membranes had low metal rejections, they present a reasonable permeate flux and a reduced rate of fouling. This chapter considers functionalization of SSOD nanoparticles using the post-synthesis grafting method. The functionalized SSOD (fSSOD) was characterized by SEM, BET, FTIR, TGA and XRD. They were infused into Psf to form MMMs which was characterized by SEM, AFM, texture analyzer, and contact angle. The performance of these membranes was evaluated by considering membrane permeability and selectivity. These were used to assess if the functionalization process was able to enhance the dispersion of SSOD particles in polysulfone, and consequently the membrane performance.

5.2. Experimental

5.2.1. Functionalization techniques

The co-condensation method is performed by adding the functionalization agent during the synthesis process, whereas in the grafting method the material is synthesized, calcined to remove surfactant and then the functionalization agent is added (Yokoi et al., 2012). Table 5.1 compares the grafting and co-condensation method. The grafting process occurs by reacting the alkoxyl group of the alkoxysilane with the hydroxyl group of the silica material, hence it produces the organo-organic hybrid (Wamba et al., 2018). The functionalization process produces a better interaction and dispersion of the silica particles in the polymeric matrix, and consequently an improvement in the composite properties (Bracho et al., 2012). The grafting method is recommended for the modification of the chemical structure of polymer membranes to enhance membrane selectivity (Daramola et al., 2019).

Table 5.1: Comparison of functionalization methods (grafting and co-condensation) (Sae-ung & Boonamnuayvitaya, 2008; Yokoi et al., 2012; Da'na, 2017)

Grafting method	Co-condensation method
Functional groups introduced after synthesis	Functional groups introduced before synthesis
Non-uniform and uncontrollable distribution of functional groups	Uniform distribution of functional groups
High loading of functional groups	Low loading of functional groups
Structure of material is maintained	Structure of material is sometimes not maintained
Characteristics of material are influenced by their structural properties and chemical composition	Functionalizing agent influences the materials structure
Reduced pore size of the modified material	Does not affect material pore size
Higher thermal stability of the material	Does not affect material thermal stability
Functional groups are positioned on exterior surface and pore openings	Functional groups are positioned on the interior

5.2.2. Characterization of the functionalized nanoparticles

The plate-like morphology obtained for SSOD is maintained in the functionalized nanoparticles (fSSOD) as shown in Figure 5.1 indicating that the functionalization process did not affect the physical structure of the nanoparticles. The BET surface area was obtained as shown in Table 5.2. The functionalization of SSOD to fSSOD resulted in a slight decrease in BET surface area, an increase in pore diameter, and a relatively unchanged pore volume indicating an increased porosity for fSSOD. An increase in surface pore sizes or the number of pores in the membrane has been reported in other studies (Aberefa et al., 2019; Yang et al., 2016). This has been explained as being caused by the

blockage of pore entrances due to the formation of functional groups on the surface of the nanoparticles (Babaei et al., 2006).

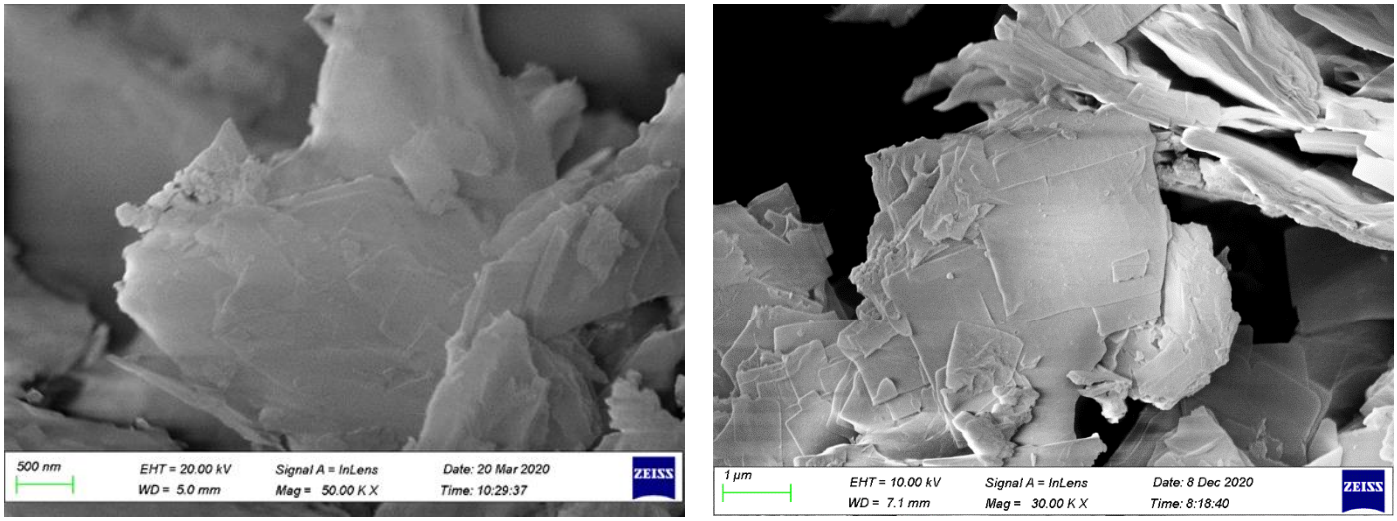


Figure 5.1: SEM images of SSOD (left) and the functionalized SSOD (right) nanoparticles

Table 5.2: fSSOD and SSOD BET analysis data

Nanoparticle type	BET surface area (m^2/g)	Pore volume (cm^3/g)	Pore diameter (nm)
fSSOD	187.76	0.240	5.12
SSOD	200.45	0.242	4.83

The FTIR spectra of fSSOD and SSOD is shown in Figure 5.2. The SSOD material was functionalized using the carboxylation protocol. The SSOD characteristic peaks as were discussed in Chapter 4 are also present in the fSSOD spectra in the fingerprint region (400-1500cm^{-1}). This indicates that the chemical structure of the sodalite nanoparticles was retained. Although not too defined, the fSSOD spectra has a broad band at 2800-3000 cm^{-1} which can be attributed to the –OH vibrations from COOH, and a C=O stretch from COOH at 1724 cm^{-1} (Aberefa et al., 2019). It can also be observed that the SSOD peaks are

more intense when compared to the fSSOD peaks. This is because SSOD is the purest form of the sodalite material. There is also a shift in the SSOD wavenumber to fSSOD. This can be attributed to the additional functional groups that have been introduced into fSSOD.

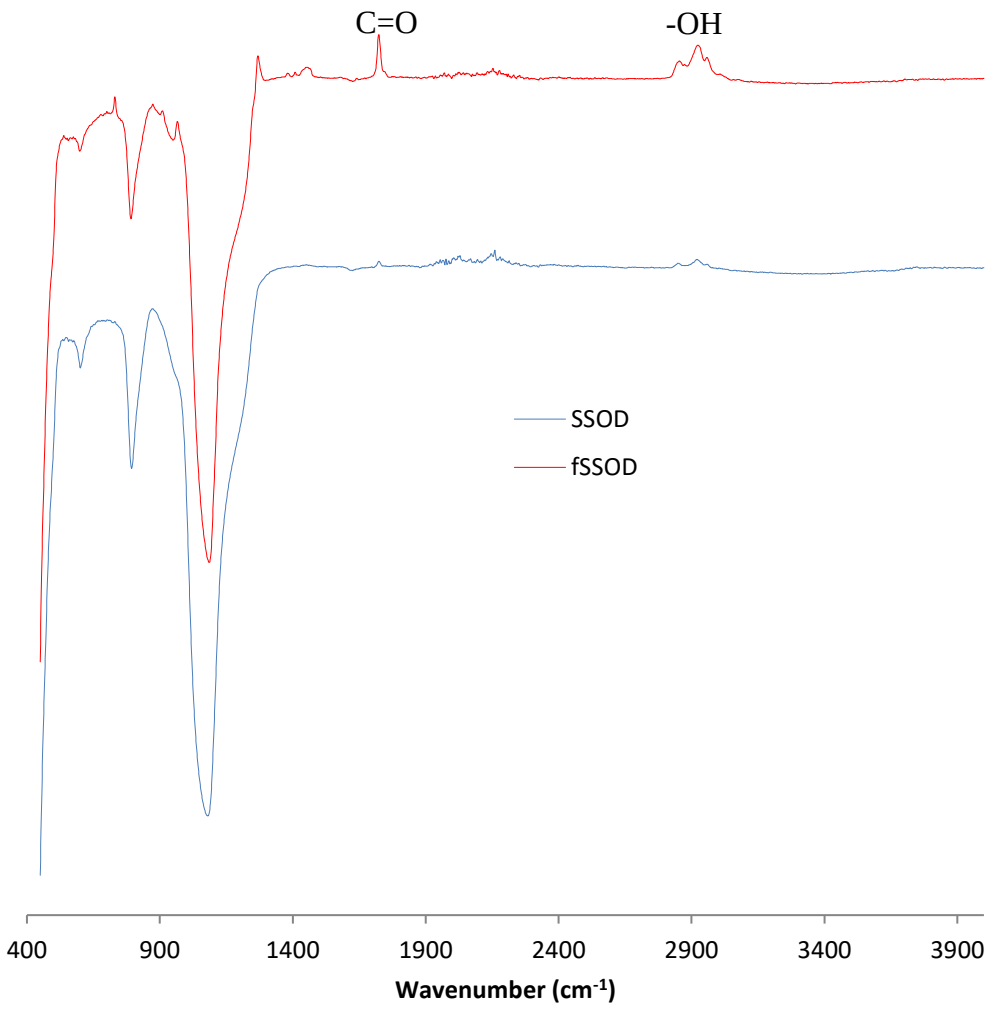


Figure 5.2: FTIR spectra of SSOD and fSSOD nanoparticles

These results can be further supported by the TG analysis shown in Figure 5.3. There is a weight loss of 5% for both SSOD and fSSOD at temperatures below 110°C due to the removal of moisture in the sodalite. There is a further weight loss of 3.6% for fSSOD at temperatures above 110°C due to the decomposition of the –COOH functional group

(Wang et al., 2005; Li et al., 2007). The total mass loss was 5.97% and 8.14% for SSOD and fSSOD, respectively. The increased weight loss in fSSOD is a confirmation of the presence of additional functional groups (Aberefa et al. 2019).

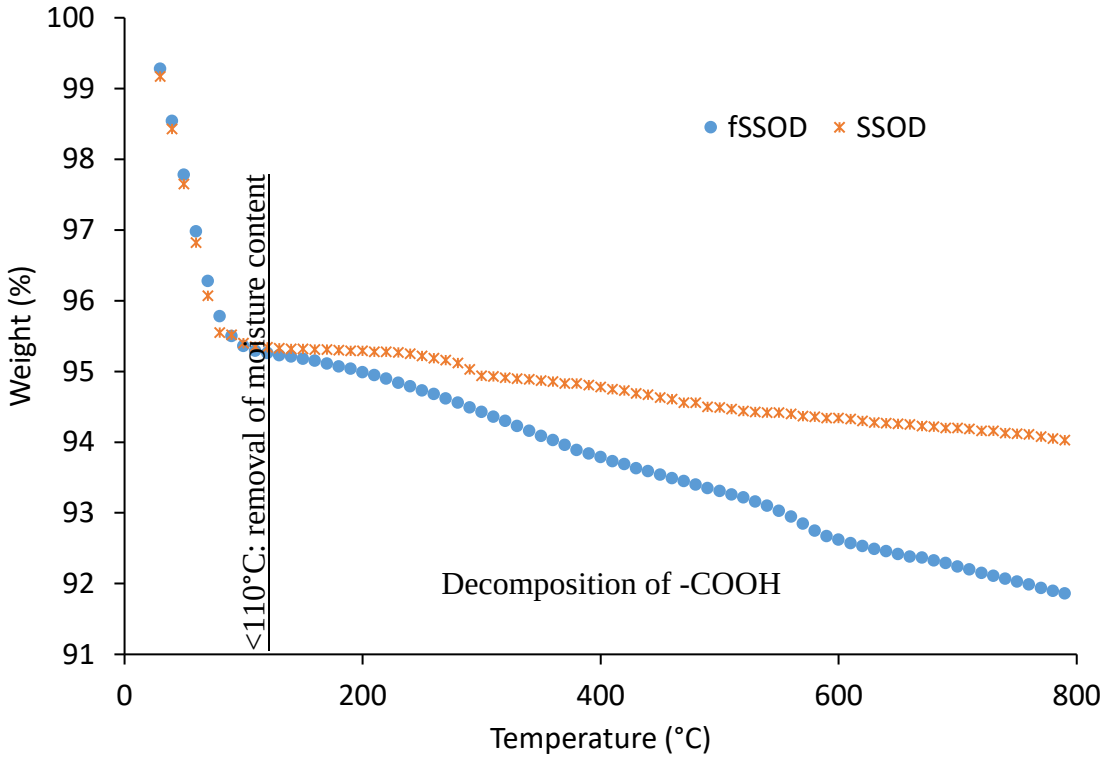


Figure 5.3: TG analysis of fSSOD and SSOD nanoparticles

The XRD pattern in Figure 5.4 shows that sodalite was successfully formed as all the required peaks appear. However, the diffraction intensities increased, confirming the modification with additional functional groups (Liu et al., 2018). Nevertheless, it can be observed that this material (fSSOD) is amorphous as it has wide peaks when compared to the SSOD pattern.

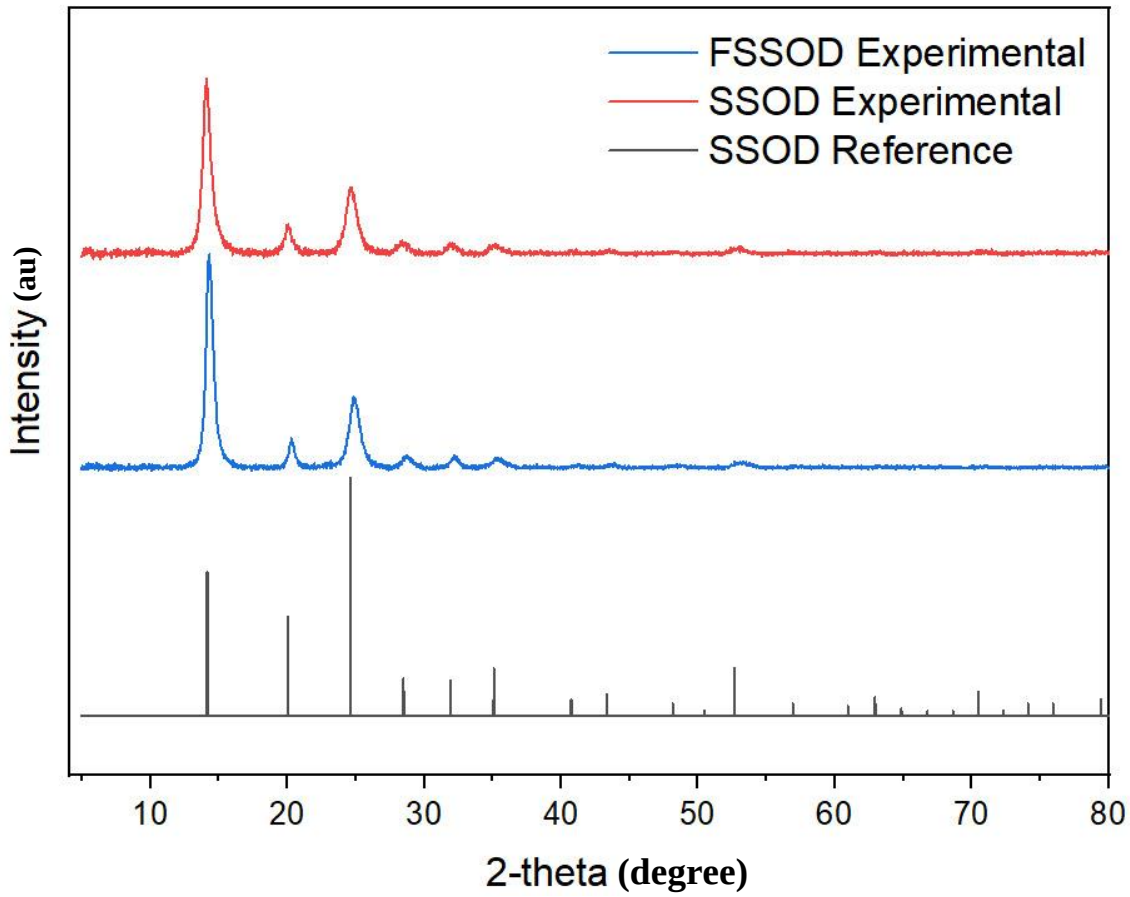


Figure 5.4: XRD pattern of SSOD and fSSOD

5.2.3. Membrane morphology (SEM) and topology (AFM)

Figure 5.5 shows the cross-section images of the 10%SSOD/Psf and 10%fSSOD/Psf membranes. It shows the successful infusion of the SSOD and fSSOD nanoparticles on the Psf polymer matrix. The distribution of nanoparticles can be observed with a visible agglomeration of nanoparticles in the un-functionalized SSOD loaded membranes as there is a localization of nanoparticles marked with *A* in the 10%SSOD/Psf image. The 10%fSSOD/Psf membrane shows an improved distribution of nanoparticles on the membrane surface. This can be attributed to the functionalization of nanoparticles which have been proven to improve the dispersion of nanoparticles on polymer matrix hence improve membrane performance (Li et al., 2007).

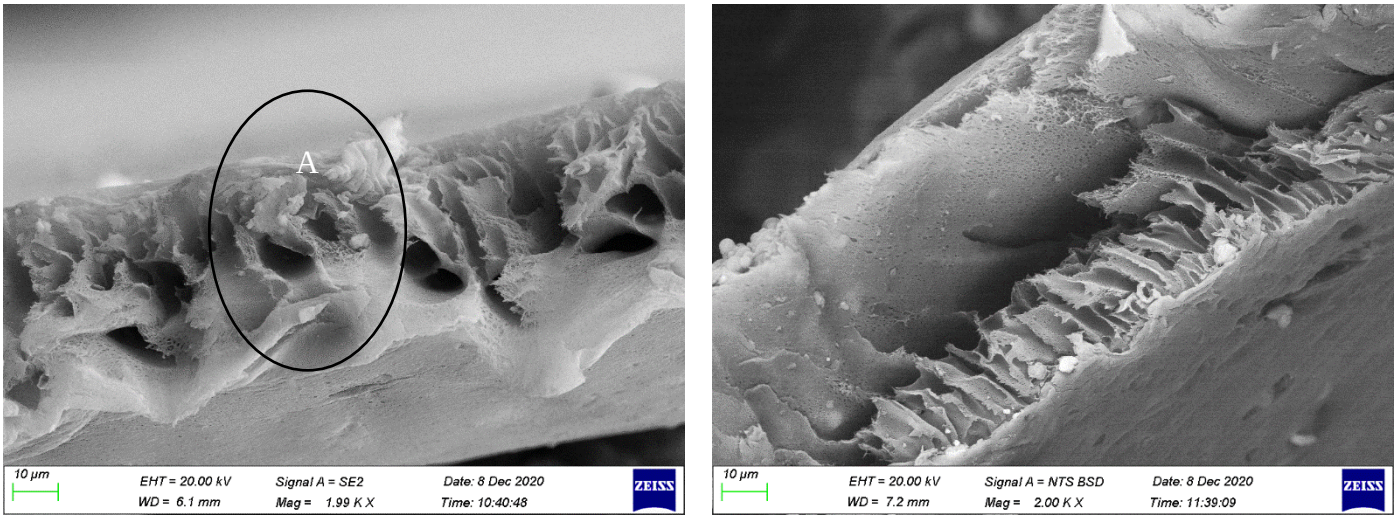


Figure 5.5: SEM cross sectional images 10%SSOD/Psf (left) and 10%fSSOD/Psf (right)

The membrane surface roughness was determined by AFM and images are shown in Figure 5.6 while the roughness parameters are shown in Figure 5.7. It can be observed that the infusion of fSSOD nanoparticles into Psf increased the surface roughness by almost double (40% for Rms and 39.5% for Ra) when compared to the SSOD loaded membrane. This indicates that the presence of fSSOD adds to the roughness of the membrane. This deviates from what has been observed by other researchers after functionalization of nanoparticles (Rameetse et al. 2020). This can be an indication of the even dispersion of the hydrophobic fSSOD.

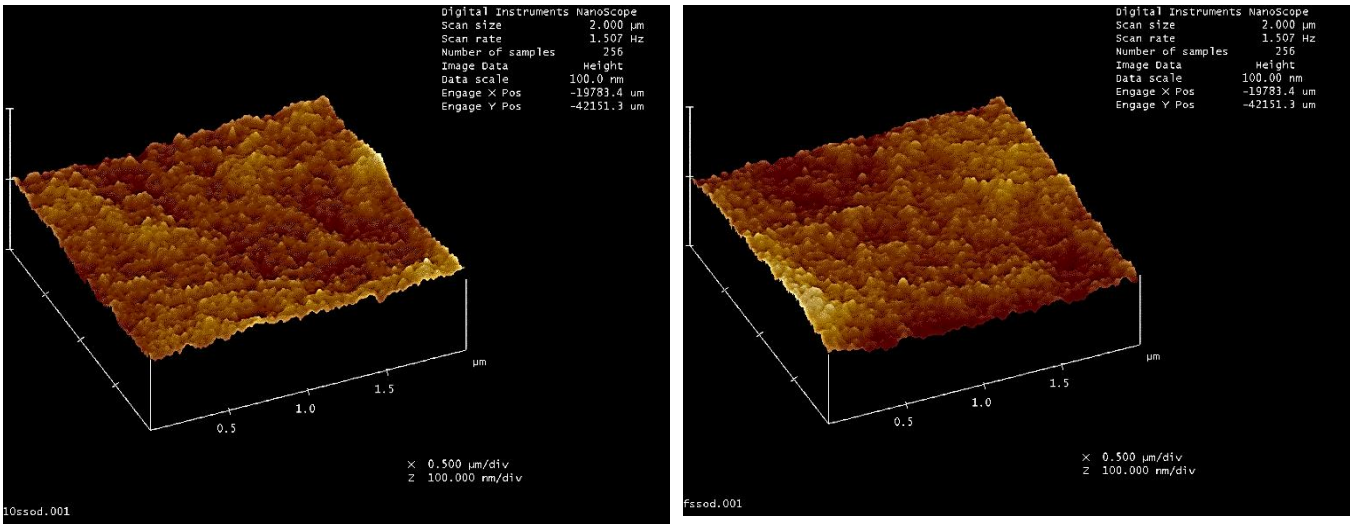


Figure 5.6: AFM images of 10%SSOD/Psf (left) and 10%fSSOD/Psf (right)

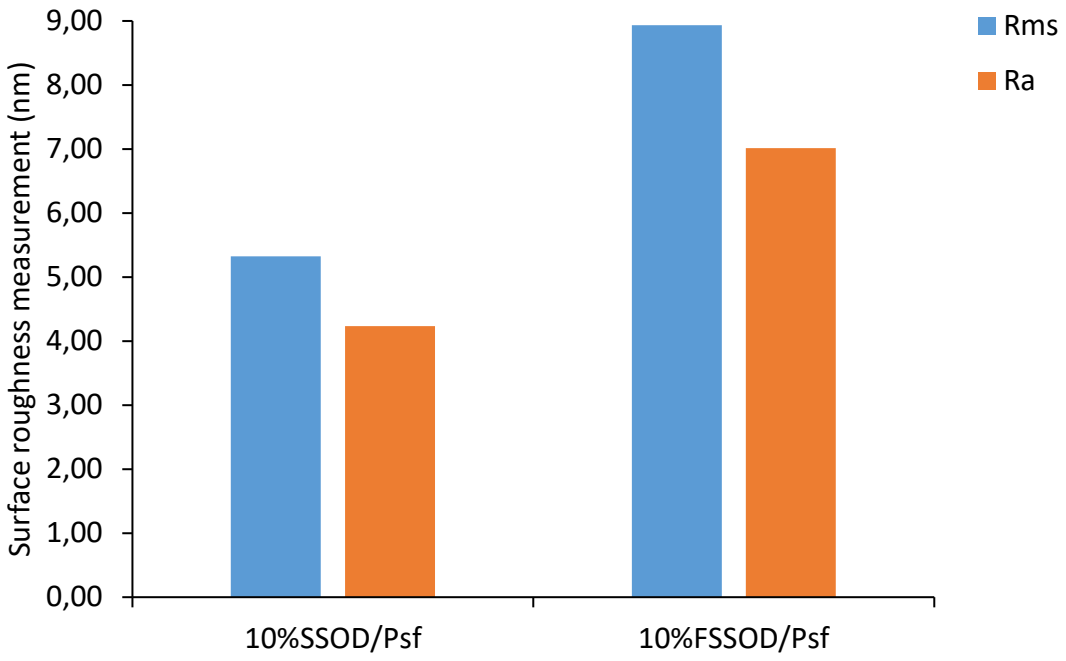


Figure 5.7: Surface roughness measurements of 10%SSOD/Psf and 10%fSSOD/Psf membranes

5.2.4. Mechanical strength of the membranes

Figure 5.8 shows the mechanical testing results of Psf, 10%fSSOD/Psf and 10%SSOD/Psf membranes. It can be observed that infusing the SSOD nanoparticles improved the membranes tensile strength. Nevertheless, the fSSOD infused membrane reduced the tensile strength to 13.6 KPa when compared to that of the SSOD infused membrane (14.5 KPa) and Psf membrane (14.3 KPa). The Young modulus was also reduced by 3% in SSOD loaded membrane when compared to the fSSOD loaded membrane. This reduced mechanical strength of the 10%fSSOD/Psf membrane can be attributed to the high loading of functional groups, which is said to result to poor structural ordering (Yokoi et al., 2012). The SSOD nanoparticles have a smaller particle size when compared to fSSOD. Particles with smaller size are said to be more favourable as they can provide improved mechanical properties (Klaysom et al., 2011; Chung et al., 2007; Bose et al., 2004).

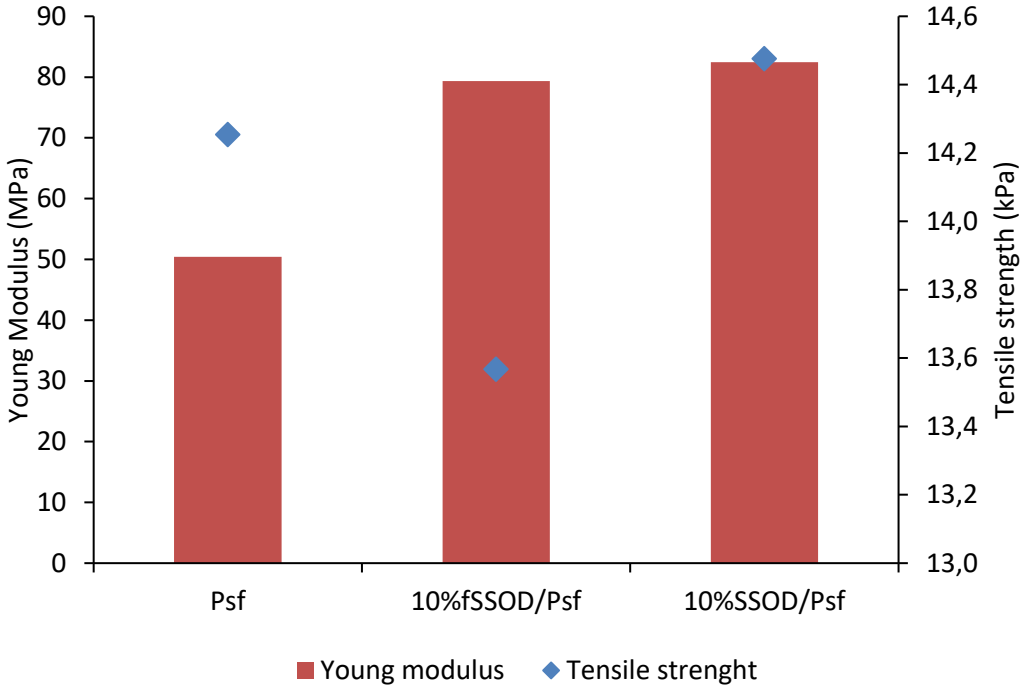


Figure 5.8: Comparison of mechanical strength measures of Psf, 10%fSSOD/Psf and 10%SSOD/Psf

5.2.5. Membranes hydrophilicity (contact angle and porosity)

Figure 5.9 compares the contact angle of the 10%fSSOD/Psf membrane to that of Psf and 10%SSOD/Psf membranes. It can be observed that infusing 10wt.%SSOD into Psf increases the contact angle making the membrane more hydrophobic. This can be attributed to the hydrophobic nature of SSOD. Adding 10wt.%fSSOD into Psf reduces the contact angle by 14.4% indicating improved hydrophilicity. This is further supported by the increased water uptake calculated by Equation 3.3 and porosity from Equation 3.2 of 10%fSSOD/Psf as shown in Table 5.3. This increased porosity can be attributed to the increased pore size of fSSOD as was shown from the BET analysis.

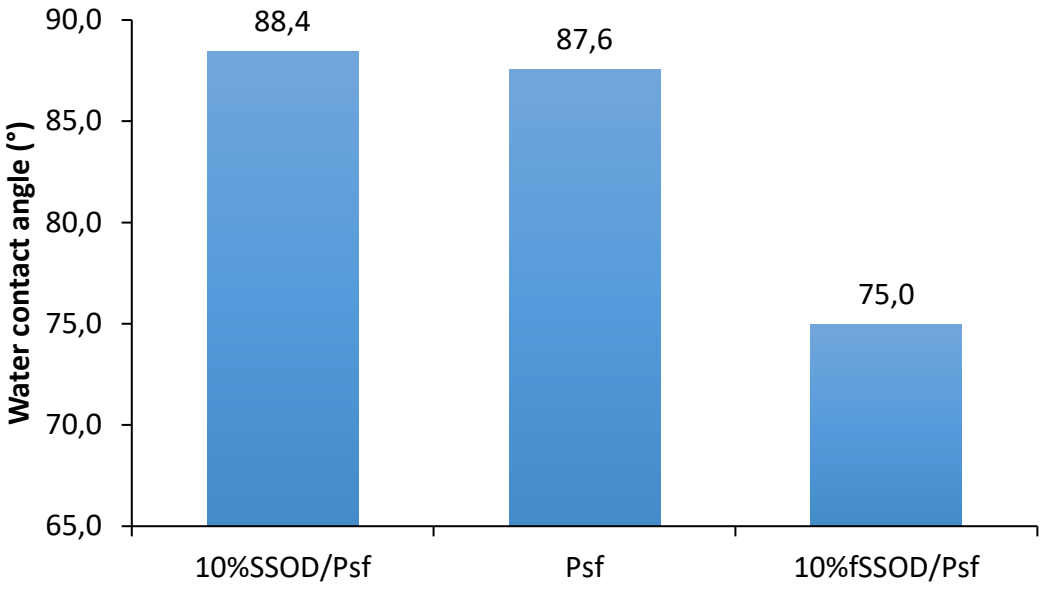


Figure 5.9: Membranes contact angle

Table 5.3: EWC and porosity

Membrane	EWC (%)	Porosity (%)
Psf	21.51	16.45
10%SSOD/Psf	15.06	9.61
10%fSSOD/Psf	25.27	19.88

5.3. Performance evaluation of fSSOD infused membrane

5.3.1. Membrane permeability

The membranes were pre-pressed with deionized water overnight to ensure complete immersion of water in the membrane so that a steady flux can be obtained. Generally, Figure 5.10 shows an increase in pure water flux when the transmembrane pressure is increased. This can be attributed to the increased driving force, which raises the capillary

pressure of the membrane hence the pores (Rameetse et al., 2020). The highest pure water flux was measured at the maximum pressure of 5 bar as 2.3 L/cm^2.h for 10%SSOD/Psf while at the same pressure, the lowest water flux was measured as 0.5 g/cm^2.h for Psf membrane. The membranes loaded with nanoparticles have an increased pure water flux when compared to the Psf membrane. This is because of the presence of nanoparticles which are known to increase the pore size of the membrane (Feng et al., 2015).

An unexpected trend is observed where the 10%fSSOD/Psf membrane shows a rather unaffected flux when compared to 10%SSOD/Psf; whereas, it had high porosity and a small contact angle. The small amount of additional functional groups that was determined as 3.6% from the TG curve can be a possible explanation for this behaviour. It is likely that these small amounts of functional groups do not have a noticeable effect on the flux rate, hence an increase in functional groups loading can be recommended.

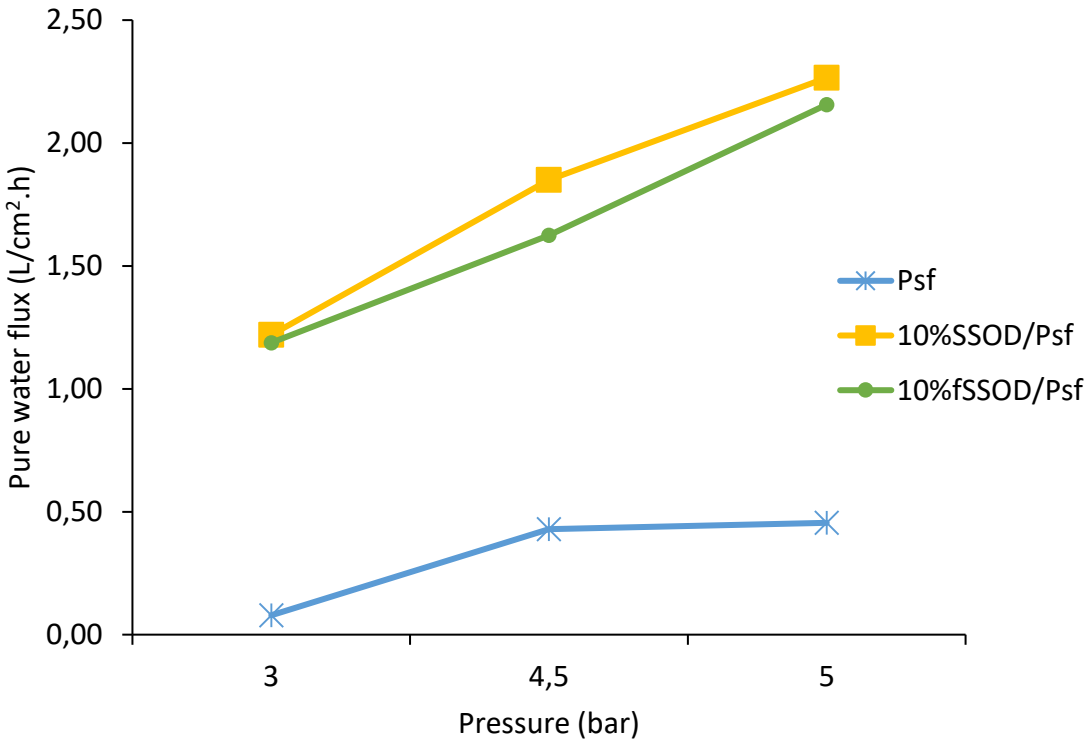


Figure 5.10: Membranes water flux with increasing transmembrane pressure

The permeate flux of the sample over a 3 hour period is shown in Figure 5.11. It can be observed that the flux is reduced over time, indicating fouling or concentration polarization and competitive sorption between heavy metal ions and water. It was noticed that the initial 10%fSSOD/Psf permeate flux was lower than the 10%SSOD/Psf permeate flux. This can be attributed to the possible SSOD nanoparticles agglomeration, which could leave parts of the 10%SSOD/Psf membrane to behave like a Psf membrane.

It can be observed that the Psf and 10%SSOD/Psf membranes had a total flux reduction of 87.7% and 90.8% when compared to the 78.7% reduction of the 10%fSSOD/Psf membrane. This indicates a reduced fouling rate for the fSSOD infused membrane. The possible good dispersion of fSSOD nanoparticles could be an explanation to the reduced fouling rate and reduced permeate flux. The surface area of the filler material is also said to play an important role as it influences the hydraulic retention time where large particles promote the permeability of the material, hence water particles are held within the membrane for an increased time (Westholm et al., 2014).

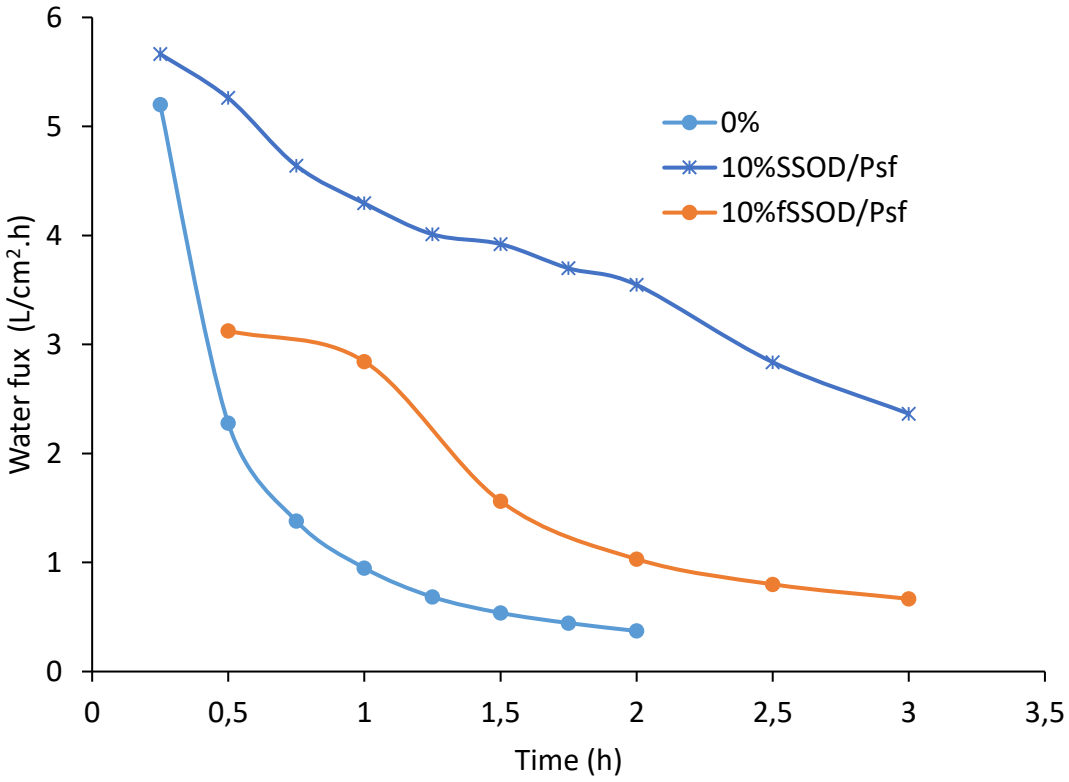


Figure 5.11: Comparison of permeate flux for Psf, 10%fSSOD/Psf and 10%SSOD/Psf membranes

5.3.2. Membrane selectivity

Figure 5.12 shows the metal rejection of the Psf, 10%fSSOD/Psf and 10%SSOD/Psf membranes. The observed low rejection of the heavy metals on SSOD loaded membranes can be attributed to the poor dispersion of nanoparticles on the membrane surface. This is because the agglomeration of nanoparticles is said to result in increased macro voids hence allowing large molecules to pass through (Rameetse et al., 2020). However, metal rejection is drastically improved in the 10%fSSOD/Psf membrane, with rejections in the range of 51.5%-74.2%. The general observed rejection percentage trend is Fe^{3+} > Ca^{2+}>Al^{3+}>Mn^{2+}>Mg^{2+} > Na^{2+} . The improved rejection is associated with the successful functionalization.

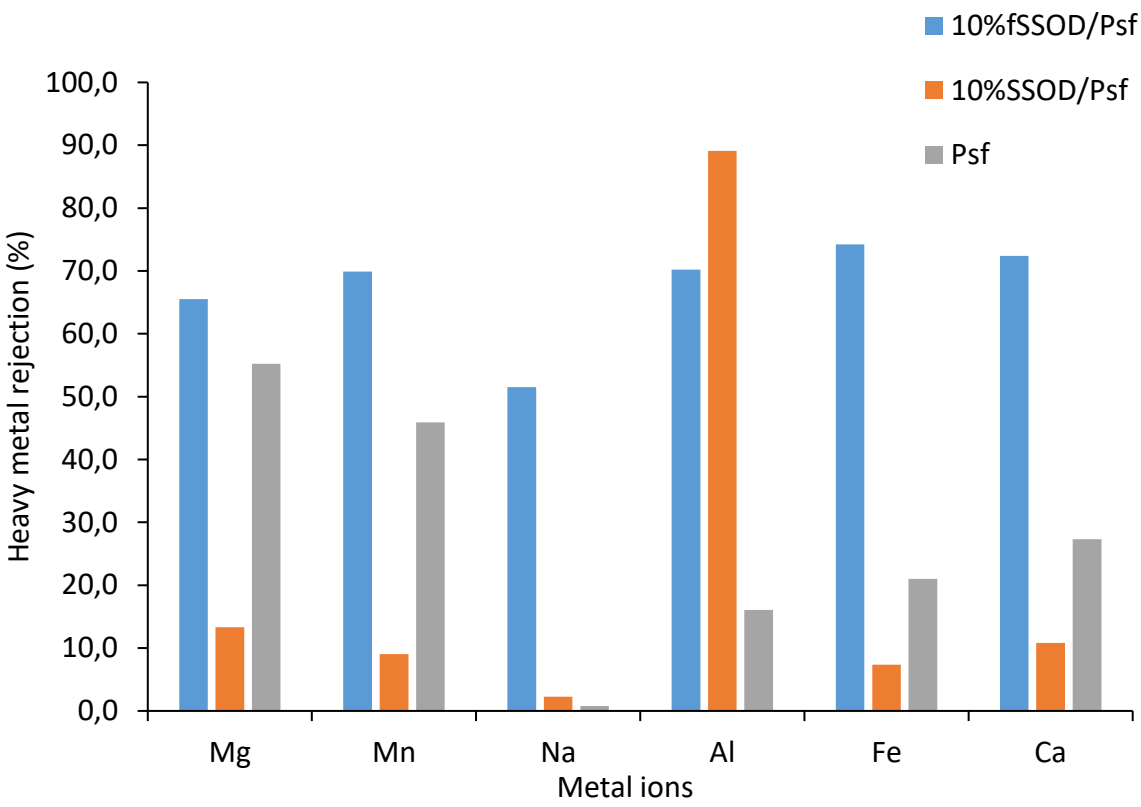


Figure 5.12: Metal rejections from Psf, 10%fSSOD/Psf and 10%SSOD/Psf

5.4. Summary

The successful functionalization of SSOD to fSSOD have been confirmed by the presence of C=O and –OH functional groups from FTIR and the 8% weight loss from the TG analysis. The introduction of new functional groups had negligible effect on the nanoparticles physical structure and crystallinity as was observed from the SEM images and XRD patterns of the nanoparticles. An improvement in nanoparticles dispersion was observed from the membranes SEM images, while there was an improvement in surface roughness and reduction in Young Modulus and tensile strength. The functionalization process was able to improve nanoparticles dispersion as was evidenced by improved membrane performance. 10%fSSOD/Psf showed a reduced fouling rate (78.7% flux reduction) and an improved selectivity with rejections above 50% for all evaluated heavy

metals. The following chapter will look at coating the membranes with a PVA layer in order to enhance the anti-fouling property of the membranes.

5.5. References

1. Aberefa, O. A., Daramola, M. O., & Iyuke, S. E. (2019). Production and Functionalization of Carbon nanotubes for Application in Membrane Synthesis for Natural Gas Separation. *Microporous and Mesoporous Materials*, 26-36. doi:10.1016/j.micromeso.2018.12.040

2. Babaei, M., Anbia, M., & Kazemipour, M. (2006). Surface Area Measurement of Functionalized Single-Walled Carbon Nanotubes. *Journal of Phys Chem*, 24812-24815. doi:10.1021/jp065044u

3. Bose, S., & Mahanwar, P. A. (2004). Effect of Particle Size of Filler on Properties of Nylon-6. *Journal of Minerals & Materials Characterization & Engineering*, 23-31. doi:10.4236/jmmce.2004.31003

4. Bracho, D., Dougnac, V. N., Palza, H., & Quijada, R. (2012). Functionalization of Silica Nanoparticles for Polypropylene Nanocomposite Applications. *Journal of Nanomaterials*. doi:10.1155/2012/263915

5. Chung, T.-S., Jiang, L. Y., & Kulprathipanja, S. (2007). Mixed Matrix Membranes (MMMs) Comprising Organic Polymers with Dispersed Inorganic Fillers for Gas Separation. *Progress in Polymer Science*, 483-507. doi:10.1016/j.progpolymsci.2007.01.008

6. Da'na, E. (2017). Adsorption of Heavy Metals on Functionalized-Mesoporous Silica: A Review. *Microporous and Mesoporous Materials*, 145-157. doi:10.1016/j.micromeso.2017.03.050

7. Daramola, M. O., Sadare, O. O., Oluwasina, O. O., & Iyuke, S. E. (2019). Synthesis and Application of Functionalizaed Carbon Nanotube Infused Polymer Membrane (fCNT/PSF/PVA) for Treatment of Phenol-Containing Wastewater. *Journal of Membrane Science & Research*, 310-316. doi:10.22079/jmsr.2019.98343.1235

8. Feng, Y., Shamsaei, E., Davies, C. H., & Wang, H. (2015). Inorganic Particle Enhanced Polymer Hollow Fiber Membranes with High Mechanical Properties. *Materials Chemistry and Physics*, 209-218. doi:10.1016/j.matchemphys.2015.10.034

9. Klaysom, C., Moon, S.-H., Ladewig, B. P., Max Lu, G. Q., & Wang, L. (2011). The Influence of Inorganic Filler Particle Size on Composite Ion-exchange membranes for Desalination. *The Journal of Physical Chemistry*, 15124-15132. doi:10.1021/jp112157z

10. Li, D., Yao, J., Wang, H., Hao, N., Zhao, D., Ratinac, K. R., & Ringer, S. P. (2007). Organic-Functionalized Sodalite Crystals and their Dispersion in Solvents. *Microporous and Mesoporous Material*, 145-157. doi:10.1016/j.micromeso.2007.03.006

11. Liu, W., Zhu, Y., Wang, F., Li, X., Liu, X., Pang, J., & Pan, W. (2018). Galactosylated Chitosan-Functionalized Mesoporous Silica Nanoparticles for Efficient Colon Cancer Cell-Targeted Drug Delivery. *Royal Society Open Science*. 181027. doi:10.1098/rsos.181027

12. Mathaba, M., & Daramola, M. O. (2020). Effect of Chitosan's Degree of Deacetylation on the Performance of PES Membrane Infused with Chitosan during AMD Treatment. *Membranes, 52*. doi:10.3390/membranes10030052

13. Rameetse, M. S., Aberefa, O., & Daramola, M. O. (2020). Effect of Loading and Functionalization of Carbon Nanotube on the Performance of Blended Polysulfone/Polyethersulfone Membrane during Treatment of Wastewater Containing Phenol and Benzene. *Membranes*, 54. doi:10.3390/membranes10030054

14. Sae-ung, S., & Boonamnuayvitaya, V. (2008). Direct Synthesis and Charecterization of Amine-Functionalized mesoporous Silica Materials and their Applications as Formaldehyde Adsorbents. *Environmental Engineering Science*, 1477-1485. doi:10.1089/ees.2007.0237

15. Wamba, A. G., Kofa, G. P., Koungou, S. N., Thue, P. S., Lima, E. C., dos Reis, G. S., & Kayem, J. G. (2018). Grafting of Amine Functional Group on Silicate Based Material as Adsorbent for Water Purification. *Journal of Environmental Chemical Engineering*, 3192-3203. doi:10.1016/j.jece.2018.04.062

16. Wang, X., Lin, K. S., Chan, J. C., & Cheng, S. (2005). Direct Synthesis and Catalytic Application of Ordered Large Pore Aminopropyl-Functionalized SBA-15 Mesoporous Materials. *Journal of Physical Chemistry*, 1763-1769. doi:10.1021/jp045798d

17. Westholm, L. J., Repo, E., & Sillanpaa, M. (2014). Filter Mateials for Metal Removal from Mine Drainage- A Review. *Environmental Science and Pollution Research*, 9109-9128. doi:10.1007/s11356-014-2903-y

18. Yang, Y., Nie, C., Deng, Y., Cheng, C., He, C., Ma, L., & Zhao, C. (2016). Improving Antifouling and Antimicrobial Efficiency of Ultrafiltration Membranes with Functional Carbon Nanotubes. *RSC Advances*, 88265-88276. doi:10.1039/C6RA18706D

19. Yokoi, T., Kubota, Y., & Tatsumi, T. (2012). Amino-Functionalized Mesoporous Silica as Base catalyst and Adsorbent. *Applied Catalysis A: General*, 14-37. doi:10.1016/j.apcata.2012.02.004

6. Investigation of the Fouling Behaviour of Poly(Vinyl Alcohol) Coated Psf/SSOD and Psf/f-SSOD Membranes

6.1. Introduction

The increasing interest in membranes for wastewater treatment is mainly due to its simplicity, effectiveness and inexpensiveness. Nevertheless, the application of membranes is limited by fouling due to accumulation and deposition of contaminants on the membrane surface and within the pores (Mathaba & Daramola, 2020). Furthermore, several studies have investigated the modification of membrane surfaces or embedding nanoparticles in the polymer matrix to limit membrane fouling (Daramola et al., 2019). In this study, the performance of HSOD, SSOD and fSSOD loaded Psf membranes in the treatment of AMD has been evaluated. Polysulfone membranes are known to be hydrophobic, which results in an increased fouling rate and reduced mechanical strength (Rameetse et al., 2020). Nevertheless, they are favoured in water treatment because of their low cost, superior film forming ability, good mechanical properties, strong chemical and thermal stability (Ahmad et al., 2011). It has been observed from the previous chapters that the performance of the Psf membrane can be improved by infusing filler nanoparticles. Although the membrane permeability and selectivity were improved, one major challenge still remain which limits membrane application in industries as it increases maintenance cost, that is membrane fouling. The objective of this chapter is to coat the SSOD and fSSOD infused Psf membranes with Poly(vinyl alcohol) PVA in order to investigate the fouling behaviour of the membrane during AMD treatment

6.2. Membrane coating

Polysulfone is a hydrophobic polymer as it has been shown in the previous chapters where it displayed low permeation and high contact angle. With this comes a challenge of membrane fouling which has been shown by the reduction in permeate flux over time. This phenomenon is defined as a deposition of unwanted particles on the surface or in the pores of the membrane, hence resulting in a decline of the membrane performance (Akbari et al., 2015). Studies have been conducted to modify the surface of the hydrophobic membranes (Daramola et al., 2019; Saraf et al., 2014; Park et al., 2018). The increase of membrane hydrophilicity is said to reduce fouling (Richards et al., 2012).

Above the membrane surface modification by embedding filler particles (Chapter 4 and 5), hydrophilic groups can be introduced by membrane coating of the polymer structure resulting in an overall hydrophilic membrane. PVA has been mostly used for this purpose as it is a hydrophilic polymer with good film forming characteristics, hence it is a good candidate to enhance the hydrophilicity of a hydrophobic polymer (Daramola et al., 2019).

6.3. Physico-chemical characterization of membrane (SEM & Contact angle)

The 10%SSOD/Psf and 10%fSSOD/Psf membranes were dip-coated by 1 %v/v PVA and cross-linked by 1 %v/v maleic acid. Figure 6.1 compares the cross-sectional images of PVA coated and uncoated 10%fSSOD/Psf membranes. There are no visible separate layers on the 10%fSSOD/Psf/PVA membrane. This shows that there was a good bond formation between the Psf and PVA layers (Barona et al., 2012).

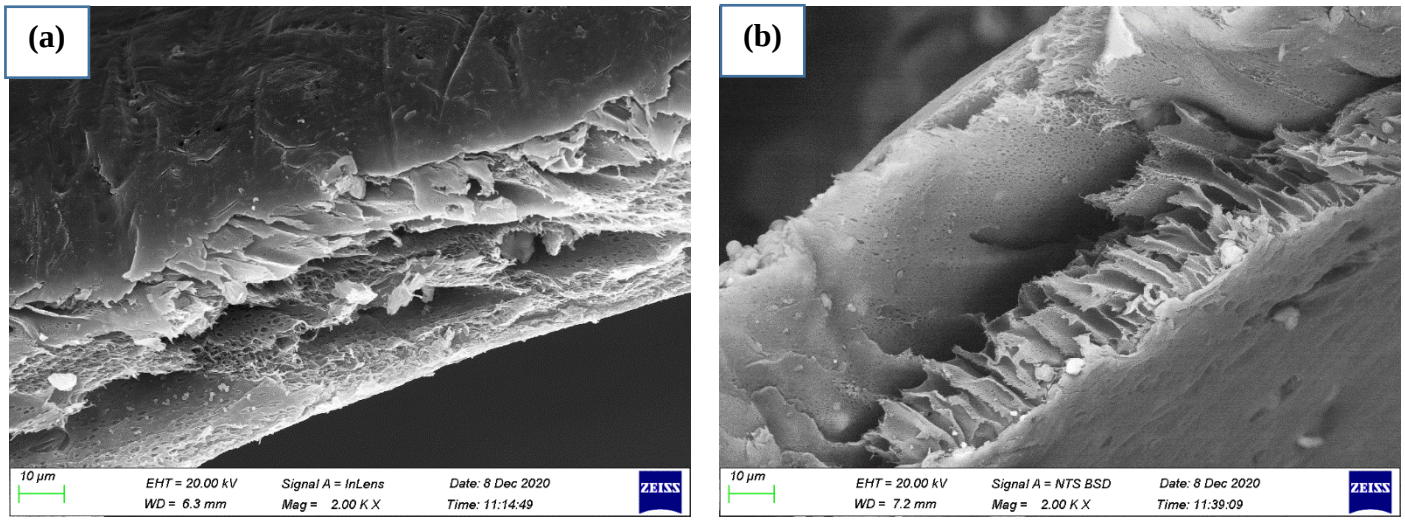


Figure 6.1: Cross sectional images of (a) 10%fSSOD/Psf/PVA and (b) 10%fSSOD/Psf membranes

The contact angle of the 10%fSSOD/Psf/PVA membrane was 72.6° and that of the Psf membrane was 87.6° as shown in Figure 6.2. This indicates that coating the membranes with the PVA layer had enhanced the hydrophilicity of the membranes (Daramola et al., 2019). The surface roughness measurements parameters also show that coating the fSSOD loaded membrane smoothens the membrane surface while coating the SSOD loaded membrane have no significance impact on the membrane surface roughness. The mechanical strength of the membranes is improved between 12.2 - 40.6% by the PVA coat as shown in Figure 6.3.

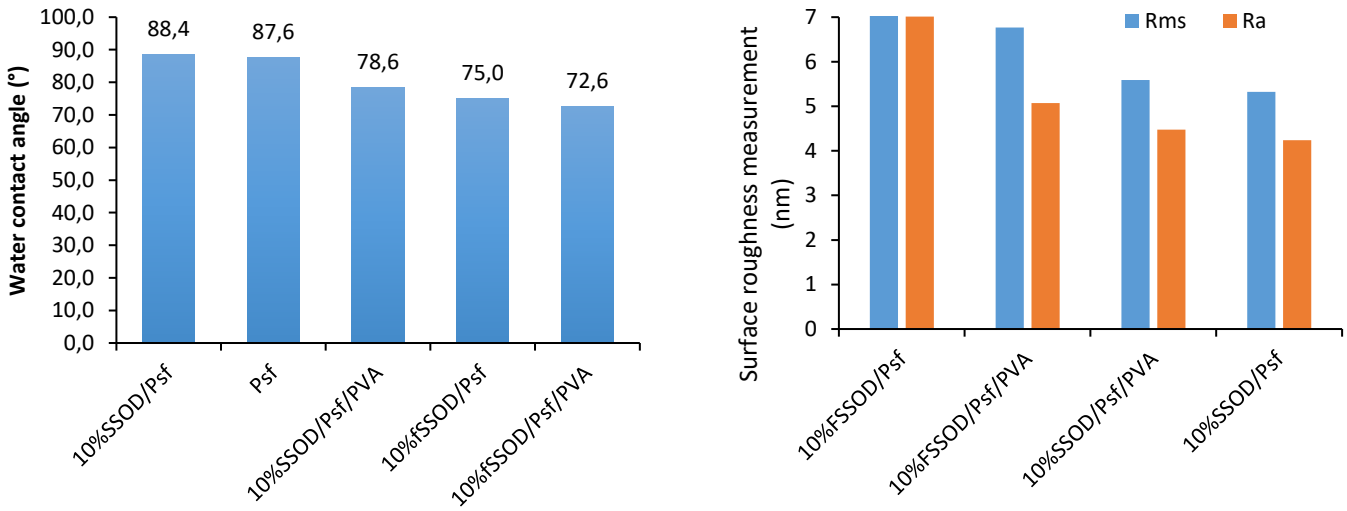


Figure 6.2: Membranes water contact angle (left) and surface roughness measurement (right)

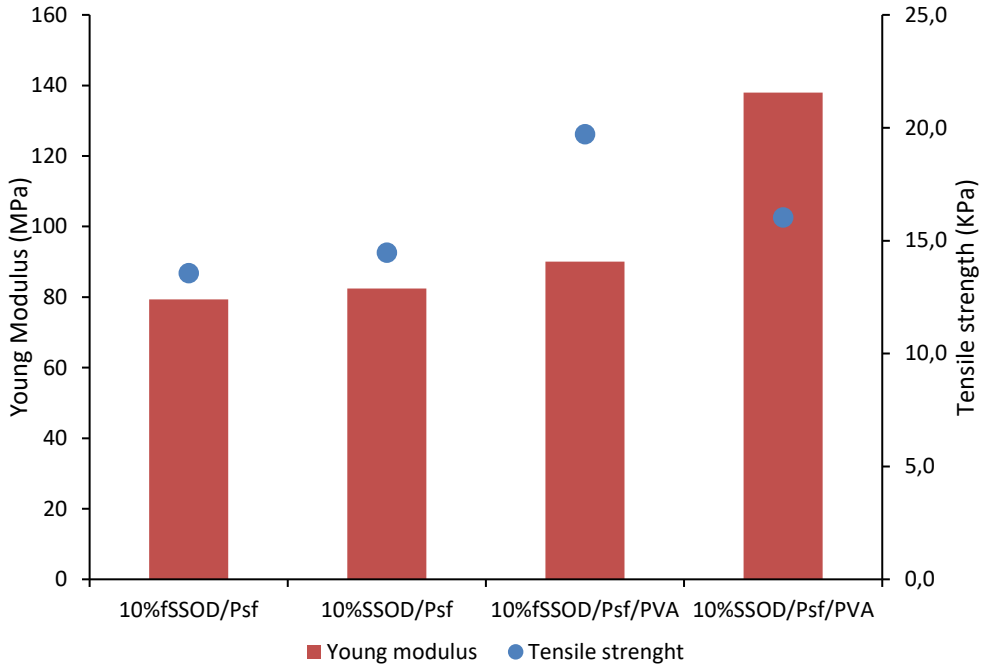


Figure 6.3: Mechanical strength of the PVA coated and the uncoated membranes

6.4. Performance evaluation of fSSOD/Psf/PVA membrane

The performance of the 10%SSOD/Psf/PVA and 10%fSSOD/Psf/PVA membranes was evaluated by permeating synthetic AMD on the membranes in a dead-end filtration cell.

6.4.1. Membranes selectivity

Figure 6.4 shows heavy metal rejections from the PVA coated and non-coated membranes. There is very poor rejection in the 10%SSOD/Psf membrane which was attributed to nanoparticles agglomeration while the improved rejection in 10%fSSOD/Psf was attributed to the improved dispersion of the functionalized nanoparticles.

Coating the 10%fSSOD/Psf membrane with PVA to 10%fSSOD/Psf/PVA membrane results to negligible difference in heavy metal rejections except for Mn^{2+} and Ca^{2+} which displayed a decline of 49.6% and 46.7%, respectively. The unchanged rejection is likely an

indication of successful coating without interference of the membrane as permeation and fouling rate were improved without affecting the rejection.

On the contrary the 10%SSOD/Psf/PVA membrane showed a noticeable increase in selectivity when compared to the 10%SSOD/Psf membrane. Initially the poor rejection by 10%SSOD/Psf membrane was attributed to the agglomeration of nanoparticles which could have resulted in increased pore sizes hence allowing unwanted nanoparticles to pass through. The observed increased rejection is likely an indication of a good PVA film formation on the surface of the membrane, hence closing the surface pores (Ma et al., 2007).

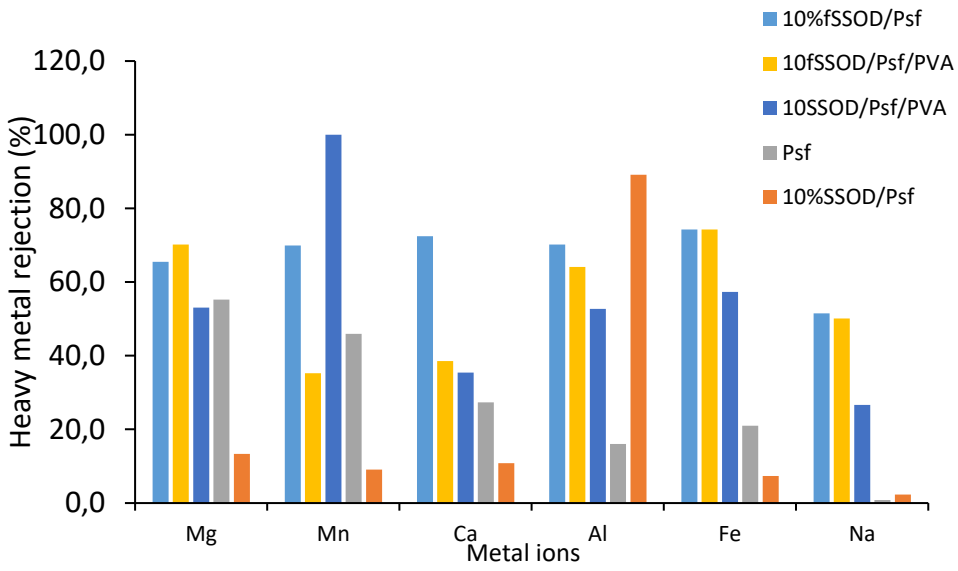


Figure 6.4: Comparison of heavy metal rejection between PVA coated and uncoated membranes

6.4.2. Effects of transmembrane pressure on the selectivity

A reasonably acceptable rejections were obtained at constant pressure of 4 bars. The membranes performance was then evaluated at different pressures (2, 4, and 5 bars) as shown in Figure 6.5. An improved rejection was obtained at low pressure of 2 bars as shown in Figure 6.5(a). When pressure is increased, there is a high presence of heavy metals in the permeate stream. An increase in heavy metal rejection was obtained when pressure was increased in other studies (Zhong et al., 2007; Al-Zoubi et al., 2010). The observed

reduction in rejection at increasing pressure in this study is likely an indication of the presence membrane surface defects.

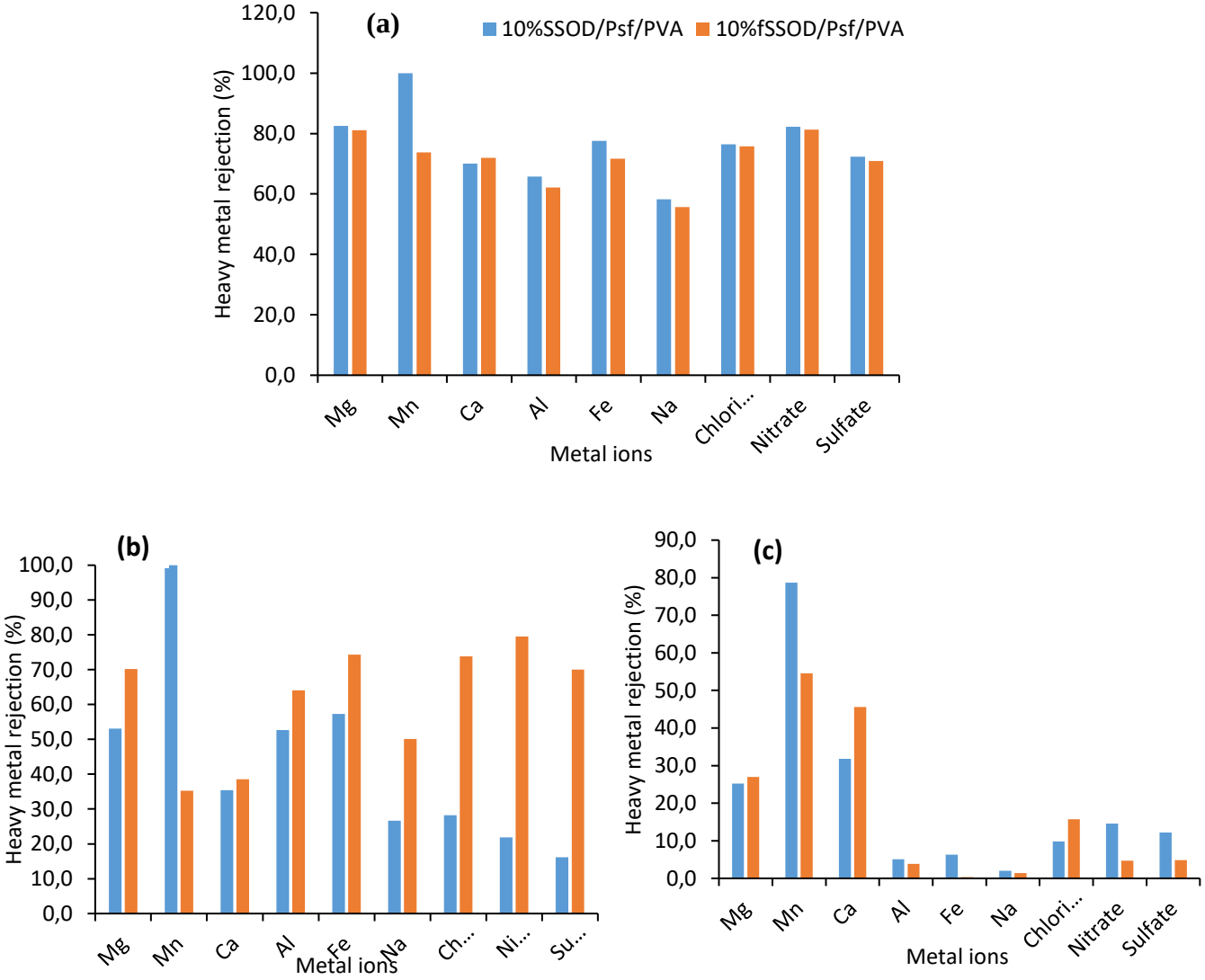


Figure 6.5: Heavy metal rejection of PVA coated membranes at different transmembrane pressures (a) 2 bar, (b) 4 bar, and (c) 5 bar

6.4.3. Fouling behaviour of fSSOD/Psf/PVA membrane

Fouling is classified as organic, inorganic and biofouling which can be reversible or irreversible depending on the type of foulants present (Arnal et al., 2011). In this study, the membranes fouling behaviour was evaluated by measurement of permeate collected over a 3 hour period. Figure 6.6 shows the decline in flux over a period of time which can be attributed to membrane fouling and/or concentration polarization. A 90.8% reduction in

flux was observed for 10%SSOD/Psf, 87.8% for Psf and 68.2% for the PVA coated membranes. The pronounced flux reduction in Psf and 10%SSOD/Psf membranes can be attributed to the hydrophobic nature of the membranes as hydrophobic foulants are said to be more driven to these types of membranes surfaces (Ahmad et al., 2011; Kumar & Ismail, 2015).

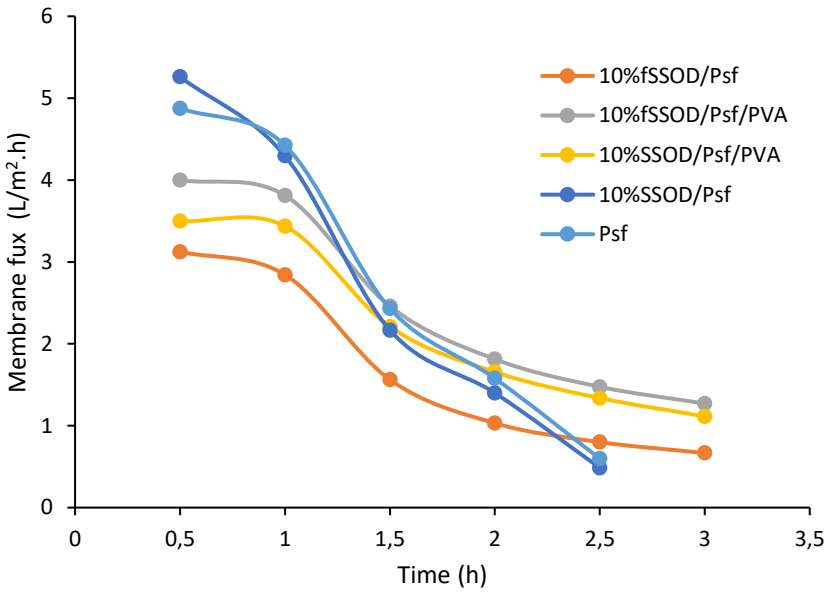


Figure 6.6: Membranes flux reduction over time

According to Arnal et al. (2011), the extent of fouling in membranes can be minimised by feed pre-treatment, operation conditions and membrane cleaning. Nevertheless, feed pre-treatment and optimisation of the operating conditions does not eliminate the problem of membrane fouling, hence, to increase the life of the membrane, cleaning methods have to be applied to reverse fouling in cases where it is reversible. It is important for the type of foulants to be identified in order to determine the type of cleaning method required. Membrane cleaning is recommended for systems where there is a 10-15% decline of permeate flux, 10-15% increase of permeate concentration, and/or 15-20% increase of pressure drop (Arnal et al., 2011). Membranes can be cleaned by either physical, chemical, or physico-chemical cleaning methods. Physical cleaning methods include sponge ball

cleaning, forward and reverse flushing, backwashing, air flushing and CO_2 back permeation, while chemical cleaning methods include the use of general acids, alkaline solutions, metal chelating agents, surfactants and enzymes (Arnal et al., 2011).

Figure 6.7 shows the flux recovery ratio of the PVA coated membranes after a 30 minutes deionized water cleaning. The 10%fSSOD/Psf/PVA membrane was able to recover its initial flux by more than 80% while the 10%SSOD/Psf/PVA was only able to recover about 55% of its initial flux after use. The reduced recovery rate on the 10%SSOD/Psf/PVA is attributed to the possible agglomerates that could have been formed due to poor dispersion. The agglomerates are said to form defects which could entrap the foulants molecules, hence the cleaning process does not become much effective (Rajaeian et al., 2015).

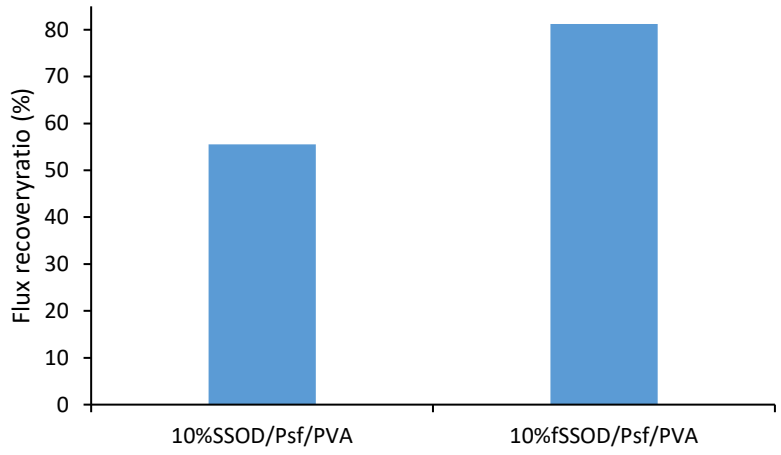


Figure 6.7: Flux recovery ratio of PVA coated membranes

6.5. Summary

The 10%SSOD/Psf and 10%fSSOD/Psf membranes were successfully coated with PVA. The membranes enhanced hydrophilicity was confirmed by the reduced contact angle of the PVA coated membranes. The PVA coat was able to smoothen the membranes surface as confirmed by AFM analysis and membranes mechanical strength was improved by 12.2 - 40.6%. PVA coat had negligible effect on selectivity of the fSSOD loaded membrane

while there was a good improvement on the SSOD loaded membranes. The PVA coat was able to reduce the membranes fouling rate to 68.2% for PVA coated membranes when compared to 90.8%, 87.8% and 78.7% for 10%SSOD/Psf, Psf and 10%fSSOD/Psf membranes respectively. A flux recovery rate of 55.6% and 81.3% was observed for 10%fSSOD/Psf/PVA and 10%SSOD/Psf/PVA respectively.

References

1. Ahmad, A. L., Majid, M. A., & Ooi, B. S. (2011). Functionalized Psf/SiO2 Nanocomposite Membrane for Oil-in-Water Emulsion Separation. *Desalination*, 266-269. doi: 10.1016/j.desal.2010.10.017

2. Akbari, A., Derikvandi, Z., & Rostami, S. M. (2015). Influence of Chitosan Coating on the Separation Performance, Morphology and Anti-Fouling Properties of the Polyamide Nanofiltration Membranes. *Journal of Industrial and Engineering Chemistry*, 268–276. doi:10.1016/j.jiec.2015.03.002

3. Al-Zoubi, H., Rieger, A., Steinberger, P., Pelz, W., Haseneder, R., & Hartel, G. (2010). Optimization Study for Treatment of Acid Mine Drainage Using Membrane Technology. *Separation Science and Technology*, 2004-2016. doi:10.1080/01496395.2010.480963

4. Arnal, J. M., García-Fayos, B., & Sancho, M. (2011). Membrane Cleaning. *Expanding Issues in Desalination* (pp. 3-84). doi:10.5772/19760

5. Barona, G. N., Choi, M., & Jung, B. (2012). High Permeate Flux of PVA/Psf Thin Film Composite Nanofiltration Membrane with Aluminosilicate Single-Walled Nanotubes. *Journal of Colloid and Interface Science*, 189-197. doi: 10.1016/j.jcis.2012.07.049

6. Daramola, M. O., Sadare, O. O., Oluwasina, O. O., & Iyuke, S. E. (2019). Synthesis and Application of Functionalizaed carbon Nanotube Infused Polymer Membrane (fCNT/PSF/PVA) for Treatment of Phenol-Containing Wastewater. *Journal of Membrane Science & Research*, 310-316. doi:10.22079/jmsr.2019.98343.1235

7. Kumar, R., & Ismail, A. F. (2015). Fouling Control on Microfiltration/Ultrafiltration Membranes: Effects of Morphology, Hydrophilicity. *Journal of Applied Polymer Science*, 42042-42053.

8. Ma, X., Su, Y., Sun, Q., Wang, Y., & Jiang, Z. (2007). Enhancing the Antifouling Property of Polyethersulfone Ultrafiltration Membranes Through Surface Adsorption-Crosslinking of Poly(Vinyl Alcohol). *Journal of Membrane Science*, 71–78. doi: 10.1016/j.memsci.2007.05.008

9. Mathaba, M., & Daramola, M. O. (2020). Effect of Chitosan's Degree of Deacetylation on the Performance of PES Membrane Infused with Chitosan during AMD Treatment. *Membranes,* 52. doi:10.3390/membranes10030052

10. Park, M. J., Gonzales, R. R., Wahab, A. A., Phuntsho, S., & Shon, H. K. (2018). Hydrophilic Polyvinyl Alcohol Coating on Hydrophobic Electrospun Nanofiber Membrane for High Performance Thin Film Composite Forward Osmosis Membrane. *Desalination*, 50-59. doi:10.1016/j.desal.2017.10.042

11. Rajaeian, B., Heitz, A., Tade, M. O., & Liu, S. (2015). Improved Separation and Antifouling Performance of PVA Thin Film Nanocomposite membranes Incorporated with Carboxylated TiO2 Nanoparticles. *Journal of Membrane Science*, 48-59. doi: 10.1016/j.m3msci.2015.03.009

12. Rameetse, M. S., Aberefa, O., & Daramola, M. O. (2020). Effect of Loading and Functionalization of Carbon Nanotube on the Performance of Blended Polysulfone/Polyethersulfone Membrane during Treatment of Wastewater

Containing Phenol and Benzene. *Membranes*, 54. doi:10.3390/membranes10030054

13. Richards, H. L., Baker, P. G., & Iwuoha, E. (2012). Metal Nanoparticle Modified Polysulfone Membrane for Use in Wastewater Treatment: A Critical Review. *Journal of Surface Engineered materials and Advanced Technology*, 183-193. doi:10.4236/jsemat.2012.223029

14. Saraf, A., Johnson, K., & Lind, M. L. (2014). Poly(vinyl) Alcohol Coating of the Support Layer of Reverse Osmosis membranes to Enhance Performance in Forward osmosis. *Desalination*, 1-9. doi: 10.1016/j.desal.2013.11.024

15. Zhong, C.-M., Xu, Z.-L., Fang, X.-H., & Cheng, L. (2007). Treatment of Acid Mine Drainage (AMD) by Ultra-Low-Pressure Reverse Osmosis and Nanofiltration. *Environmental Engineering Science*, 1297-1306. doi:10.1089/ees.2006.0245

7. Conclusions and Recommendations

7.1. Conclusions

Water treatment technologies for heavy metal removal in AMD have been explored by many researchers in an attempt to remediate polluted water. This is one of the major concerns in the mining, agricultural, water and environmental protection industries as there is no defined treatment technology that can address this challenge. Nevertheless, nanotechnology-based membranes have shown promising results in the treatment of AMD. To address the objectives outlined in the beginning of this study, the following conclusions have been drawn from this work:

i. HSOD and SSOD nanoparticles were successfully synthesized by hydrothermal synthesis and topotactic conversion, respectively. These were infused into Psf in loadings of 5wt.% and 10wt.%. Characterization of HSOD nanoparticles showed thread-ball-like morphology with a touch of cubic structures and a pore volume of 0.115 cm^3/g from SEM and BET, respectively. SSOD nanoparticles presented a plate-like morphology, pore volume of 0.242 cm^3/g, crystalline structure, good thermal stability and a successful conversion from its mother silicate RUB-15. TG analysis confirmed the occlusion of HSOD pores by water molecules as it had a total weight loss of 19% when compared to a weight loss of 6% by SSOD nanoparticles. The SSOD infused membranes showed good permeability with 10%SSOD/Psf reaching a maximum pure water flux of $2.1L/m^2.h$ while 10%HSOD/Psf membranes showed poor permeability 0.6 $L/m^2.h$. The HSOD loaded membranes presented good selectivity with more than 50% rejections in most metal ions. The 10%SSOD/Psf membrane was then selected to be evaluated further as it presented good permeability.

ii. The successful grafting functionalization of SSOD to fSSOD nanoparticles was confirmed by the introduced functional groups from the FTIR spectra and the visible enhanced dispersion on the polymer matrix. The 10%fSSOD/Psf membrane presented reduced fouling rate with 78.7% reduction in flux over time while the 10%SSOD/Psf membrane showed 90.8% which is even higher than that of pure Psf (87.7%). Functionalization of the nanoparticles was also able to enhance the membranes selectivity, with most rejections in the range of 51.5%-74.2% indicating enhanced nanoparticles dispersion while 10%SSOD/Psf membrane had poor metal ion rejections (2.3-13.3%) due to the formation of agglomerates on the membranes surface.

iii. The 10%SSOD/Psf and 10%fSSOD/Psf membranes were successfully coated with PVA. Coating of 10%fSSOD/Psf to 10%fSSOD/Psf/PVA had negligible effect on membranes selectivity while the 10%SSOD/Psf/PVA membrane presented an improved selectivity when compared to the 10%SSOD/Psf membrane. The successful coating of the membranes was confirmed by the improved reduction of flux over time of 68.2% for PVA coated membranes when compared to 90.8%, 87.8% and 78.7% for 10%SSOD/Psf, Psf and 10%fSSOD/Psf membranes respectively. A flux recovery rate of 55.6% and 81.3% was observed for 10%fSSOD/Psf/PVA and 10%SSOD/Psf/PVA respectively.

The reproducibility and quality of the obtained results was confirmed by a duplicate AMD permeation from membranes produced from different batches, and an average was used. This study has presented the potential of silica sodalite infused polysulfone composite membranes in the treatment of AMD. The performance shown by the 10%fSSOD/Psf/PVA membrane shows that this membrane can be applied in the treatment of AMD as it was able to present good selectivity and permeability.

7.2. Recommendations

There is limited literature on the study of silica sodalite. These nanoparticles presented enormous characteristics which needs to be explored, particularly on the water treatment processes. This study can form base of exploring different types of functionalization for the SSOD to be able to adapt in different wastewater contamination concentrations. Furthermore, the quality of the results dissembled in this study can be improved by evaluating the membrane performance at prolonged period of time to imitate real processes. This could ensure membranes stability and resistance to the harsh conditions from real processes. Membrane performance using a crossflow filtration system can also be explored in the future to evaluate the effectiveness of the as-produced membranes in a different flow regime.

APPENDIX

A.1. Water characteristics

AMD water is differentiated from normal water according to the following aspects:

- Electrical conductivity (EC) which is a useful measure of total dissolved solids (TSD) in water.
- Sulphates (SO_4^{2-}) which is a measure of pyrite oxidation.
- Other metals concentrations (Al, Co, Cu, Mn, Ni, U, and Zn) which depend on each individual mining site.
- pH which is a measure of the hydrogen ions in the solution.
- Alkalinity a measure of the acid- neutralising capacity of the water. Total alkalinity is the sum of HCO_3^-, CO_3^-, and OH^-.
- Chemical oxygen demand (COD) which gives an estimate of the organic matter present in a water body.
- Acid is a measure of hydrogen ions (H^+) and is measured using a pH meter. This is generally calculated according to equation …

  $$pH = -\log_{10}[H^+]$$

  Where the square brackets indicate the concentration in mg/L.
- Acidity is a measure of total hydrogen ions including the ones which can be generated if other metal hydroxides can precipitate at a given pH, it is expressed as $mgCaCO_3/L$. According to (Taylor, Pape, & Murphy, 2005), this can be calculated using equation … for coal mine AMD

  $$Acidity = 50\left(\frac{3}{56}[Fe^{3+} + Fe^{2+}] + \frac{3}{27}[Al^{3+}] + \frac{2}{55}[Mn^{2+}] + 1000 \times 10^{-pH}\right)$$

- Acidity load is the product of the total acidity and flow rate. If flow data is available, it can be calculated using equation…

$$Acidity\ load\ \left(tonne\frac{CaCO_3}{day}\right) = 86400 \times 10^{-9} \times Flow\ rate \times Acidity$$

Copyright Permissions

Permission for reuse of Figure 2.2

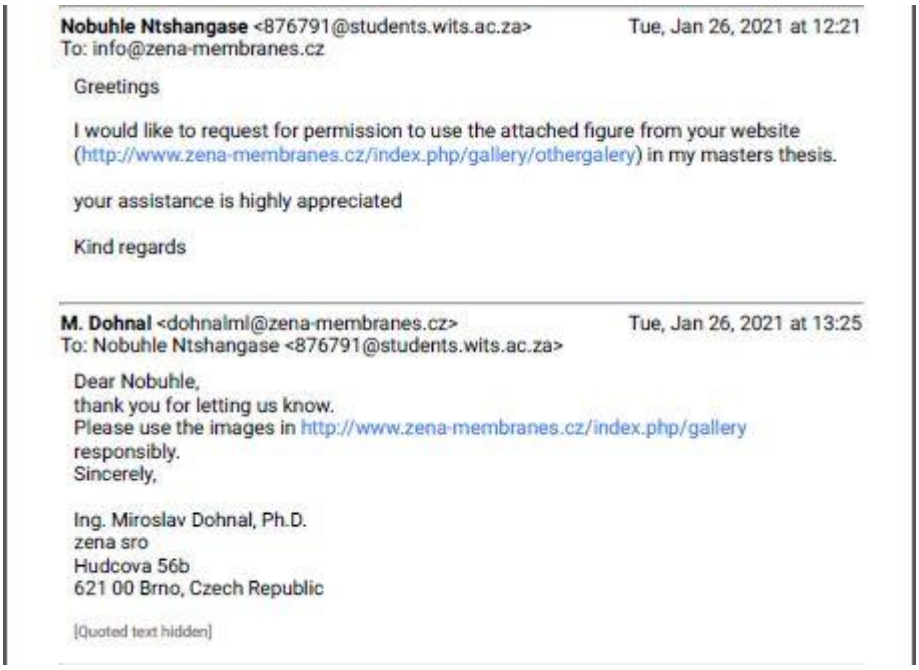
ELSEVIER LICENSE TERMS AND CONDITIONS

Jan 26, 2021

This Agreement between Ms. Nobuhle Ntshangase ("You") and Elsevier ("Elsevier") consists of your license details and the terms and conditions provided by Elsevier and Copyright Clearance Center.

License Number	4996390004315
License date	Jan 26, 2021
Licensed Content Publisher	Elsevier
Licensed Content Publication	Progress in Polymer Science
Licensed Content Title	Mixed matrix membranes (MMMs) comprising organic polymers with dispersed inorganic fillers for gas separation
Licensed Content Author	Tai-Shung Chung,Lan Ying Jiang,Yi Li,Santi Kulprathipanja
Licensed Content Date	Apr 1, 2007
Licensed Content Volume	32
Licensed Content Issue	4
Licensed Content Pages	25
Start Page	483
End Page	507
Type of Use	reuse in a thesis/dissertation
Portion	figures/tables/illustrations
Number of figures/tables/illustrations	1
Format	both print and electronic
Are you the author of this Elsevier article?	No
Will you be translating?	No
Title	Treatment of Acid mine drainage using silica sodalite infused polysulfone composite membrane
Institution name	University of the Witwatersrand
Expected presentation date	Feb 2021
Portions	Figure 2
Requestor Location	Ms. Nobuhle Ntshangase 280 8th Avenue Bezuidenhout valley Johannesburg Johannesburg, Gauteng 2094 South Africa Attn: Ms. Nobuhle Ntshangase
Publisher Tax ID	ZA 4110266048
Total	**0.00 USD**

Permission for reuse of Figure 2.4



Nobuhle Ntshangase <876791@students.wits.ac.za> Tue, Jan 26, 2021 at 12:21
To: info@zena-membranes.cz

Greetings

I would like to request for permission to use the attached figure from your website (http://www.zena-membranes.cz/index.php/gallery/othergalery) in my masters thesis.

your assistance is highly appreciated

Kind regards

M. Dohnal <dohnalml@zena-membranes.cz> Tue, Jan 26, 2021 at 13:25
To: Nobuhle Ntshangase <876791@students.wits.ac.za>

Dear Nobuhle,
thank you for letting us know.
Please use the images in http://www.zena-membranes.cz/index.php/gallery
responsibly.
Sincerely,

Ing. Miroslav Dohnal, Ph.D.
zena sro
Hudcova 56b
621 00 Brno, Czech Republic

[Quoted text hidden]

Permission for reuse of Figure 2.3

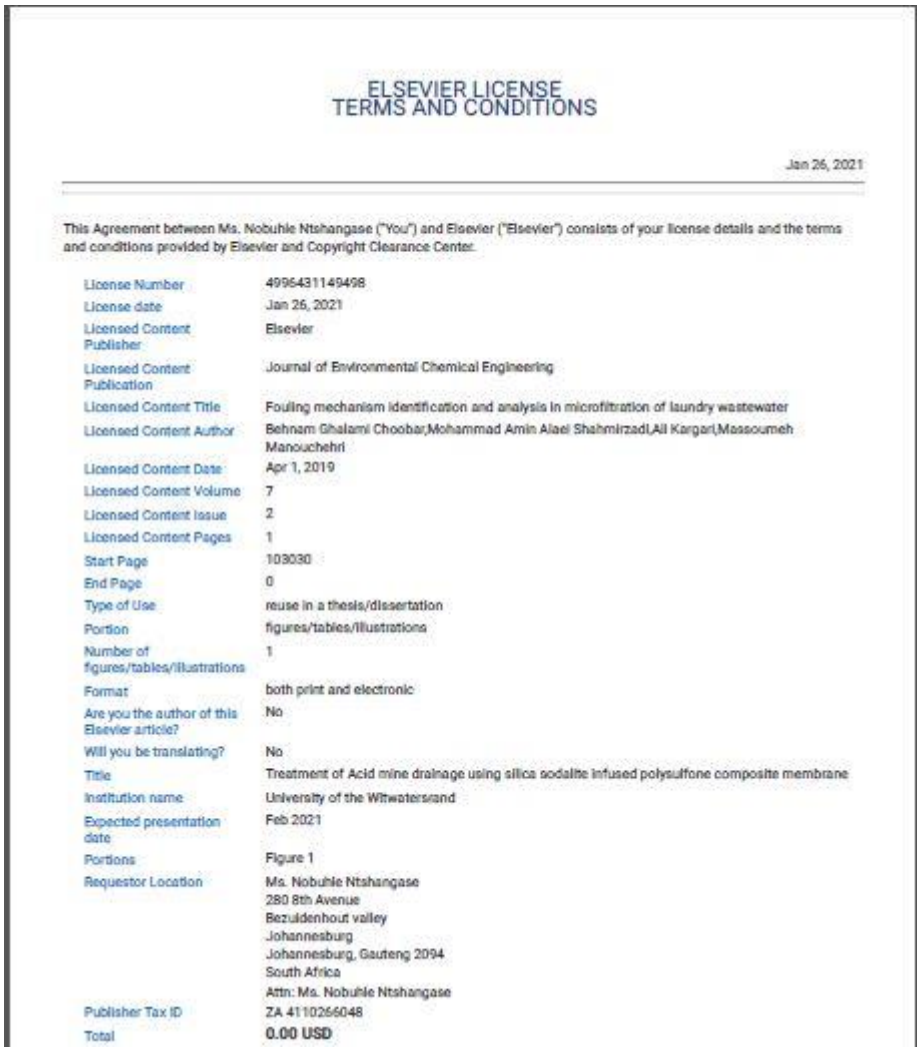
ELSEVIER LICENSE TERMS AND CONDITIONS

Jan 26, 2021

This Agreement between Ms. Nobuhle Ntshangase ("You") and Elsevier ("Elsevier") consists of your license details and the terms and conditions provided by Elsevier and Copyright Clearance Center.

License Number	4996411211139
License date	Jan 26, 2021
Licensed Content Publisher	Elsevier
Licensed Content Publication	Journal of Membrane Science
Licensed Content Title	Application of hydroxy sodalite films as novel water selective membranes
Licensed Content Author	Sheida Khajavi,Jacobus C. Jansen,Freek Kapteijn
Licensed Content Date	Jan 5, 2009
Licensed Content Volume	326
Licensed Content Issue	1
Licensed Content Pages	8
Start Page	153
End Page	160
Type of Use	reuse in a thesis/dissertation
Portion	figures/tables/illustrations
Number of figures/tables/illustrations	1
Format	both print and electronic
Are you the author of this Elsevier article?	No
Will you be translating?	No
Title	Treatment of Acid mine drainage using silica sodalite infused polysulfone composite membrane
Institution name	University of the Witwatersrand
Expected presentation date	Feb 2021
Portions	Figure 1
Requestor Location	Ms. Nobuhle Ntshangase 280 8th Avenue Bezuidenhout valley Johannesburg Johannesburg, Gauteng 2094 South Africa Attn: Ms. Nobuhle Ntshangase
Publisher Tax ID	ZA 4110266048
Total	**0.00 USD**

Permission for reuse of Figure 2.5



ELSEVIER LICENSE
TERMS AND CONDITIONS

Jan 26, 2021

This Agreement between Ms. Nobuhle Ntshangase ("You") and Elsevier ("Elsevier") consists of your license details and the terms and conditions provided by Elsevier and Copyright Clearance Center.

License Number	4996431149498
License date	Jan 26, 2021
Licensed Content Publisher	Elsevier
Licensed Content Publication	Journal of Environmental Chemical Engineering
Licensed Content Title	Fouling mechanism identification and analysis in microfiltration of laundry wastewater
Licensed Content Author	Behnam Ghalami Choobar,Mohammad Amin Alaei Shahmirzadi,Ali Kargari,Massoumeh Manouchehri
Licensed Content Date	Apr 1, 2019
Licensed Content Volume	7
Licensed Content Issue	2
Licensed Content Pages	1
Start Page	103030
End Page	0
Type of Use	reuse in a thesis/dissertation
Portion	figures/tables/illustrations
Number of figures/tables/illustrations	1
Format	both print and electronic
Are you the author of this Elsevier article?	No
Will you be translating?	No
Title	Treatment of Acid mine drainage using silica sodalite infused polysulfone composite membrane
Institution name	University of the Witwatersrand
Expected presentation date	Feb 2021
Portions	Figure 1
Requestor Location	Ms. Nobuhle Ntshangase 280 8th Avenue Bezuidenhout valley Johannesburg Johannesburg, Gauteng 2094 South Africa Attn: Ms. Nobuhle Ntshangase
Publisher Tax ID	ZA 4110266048
Total	0.00 USD